Final Report to

Research Partnership to Secure Energy for America

Improvement of Fracturing for Gas Shales

07122-38.FINAL

August, 2012

Kishore K. Mohanty (PI),

Abhishek Gaurav, Ming Gu

Department of Petroleum & Geosystems Engineering

The University of Texas at Austin

200 E. Dean Keaton

Austin, TX 78712-1587

512-471-3077 (phone), 512-471-9605 (fax)

mohanty@mail.utexas.edu

Dr. Ali Daneshy (Subcontractor)

15995 N. Barkers Landing, Suite 201

Houston, TX 77079

281-584-9444 (phone), alidaneshy@daneshy.com

Disclaimer

This report was prepared by Prof. K. K. Mohanty of The University of Texas as an account of work sponsored by the Research Partnership to Secure Energy for America, RPSEA. Neither RPSEA, members of RPSEA, the National Energy Technology Laboratory, the U.S. Department of Energy, nor any person acting on behalf of any of the entities:

a. MAKES ANY WARRANTY OR REPRESENTATION, EXPRESS OR IMPLIED WITH RESPECT TO ACCURACY, COMPLETENESS, OR USEFULNESS OF THE INFORMATION CONTAINED IN THIS DOCUMENT, OR THAT THE USE OF ANY INFORMATION, APPARATUS, METHOD, OR PROCESS DISCLOSED IN THIS DOCUMENT MAY NOT INFRINGE PRIVATELY OWNED RIGHTS, OR

b. ASSUMES ANY LIABILITY WITH RESPECT TO THE USE OF, OR FOR ANY AND ALL DAMAGES RESULTING FROM THE USE OF, ANY INFORMATION, APPARATUS, METHOD, OR PROCESS DISCLOSED IN THIS DOCUMENT.

THIS IS A FINAL REPORT. THE DATA, CALCULATIONS, INFORMATION, CONCLUSIONS, AND/OR RECOMMENDATIONS REPORTED HEREIN ARE THE PROPERTY OF THE U.S. DEPARTMENT OF ENERGY.

REFERENCE TO TRADE NAMES OR SPECIFIC COMMERCIAL PRODUCTS, COMMODITIES, OR SERVICES IN THIS REPORT DOES NOT REPRESENT OR CONSTIITUTE AND ENDORSEMENT, RECOMMENDATION, OR FAVORING BY RPSEA OR ITS CONTRACTORS OF THE SPECIFIC COMMERCIAL PRODUCT, COMMODITY, OR SERVICE.

Principal Investigator Signature:

Kishore K. Mohanty

Date: August 31, 2012

Abstract

As the global demand for energy rises and the discovery of new hydrocarbon resources drops, the recovery from unconventional resources like shale gas become increasingly important. The shale reservoirs need to be fractured hydraulically to produce at an economic rate. Long propped fractures are needed to maximize productivity. Slick water fracturing with sand produces long fractures, but only the near-wellbore region is propped due to proppant settling. Gels can create long propped fractures, but they damage the fracture surface. The goal of this project is to develop non-damaging fracturing fluids and proppants for gas shale reservoirs that also minimize water use. Lightweight proppants are tested because they settle slowly during fracturing. Foams are evaluated as the fracturing fluid because they minimize water use and decrease proppant settling.

Mechanical properties and chemical compatibility were measured for three ultra light weight (ULW) proppants (ULW1 Polymer, ULW2 Resin-Walnut and ULW3 Resin-Ceramic, supplied by BJ services). Conductivity of proppant packs has been determined as a function of proppant concentration and confining stress. Proppant pack conductivity decreases as the confining stress increases. Conductivity is an increasing function of proppant concentration for ULW3 Resin-Ceramic, the resin-coated ceramic proppant. For ULW1 Polymer and ULW2 Resin-Walnut, the conductivity has a minimum at about 0.1-0.4 lbm/ft^2 concentration. The proppant conductivity is low (of the order of 1-10 mD-ft) at 6000 psi confining stress. The application of light weight proppants in stimulation treatments in shale reservoirs is limited to a net confining stress of 6000 psi.

The stability of foams produced from different surfactants has been studied first in a static column. Proppant settling rate has been measured in slick water and foams. Foams made with anionic surfactants are more stable than those made with nonionic surfactants tested. Half-life of these foams can be more than one hour and increases with the addition of stabilizers. Increasing the temperature reduces the half-life of foams. The settling velocity of proppants (three ULWs and sand) in water does not follow Stokes equation because the Reynolds number is larger than unity. Instead, it agrees well with the Happel correlation, which is valid for Reynolds number between 2 and 500. The use of foam eliminates the gravity settling of even sand proppants. The rheology of three different surfactant as well as their foams was evaluated in a flow loop under high pressure and temperature. All foams show shear thinning behavior at qualities lower than 50% and shear thickening behavior above that. The temperature has less effect on foam rheology at high qualities than at medium and low qualities. The pressure (from 200 psi to 1000 psi) affects the viscosity of foam at qualities higher than 50%. Foams with 50% quality and higher show good suspension and transport of sand and ultra light weight proppants through a slot representing a fracture. The application of gel-free foams would not only eliminate the polymer damage to the fracture face and proppant packs, but also carry proppants deeper into fracture networks than the slickwater.

The effect of proppants, fracturing fluid and injection schedule on the hydraulic fracture creation and on subsequent gas production has been simulated. The results show that a mixture of ULW proppants and sand outperforms all individual ULW proppants or sand. Adding a small amount of ULW1 Polymer to sand can highly improve the fracture conductivity by improving the sand placement. Gel-free foams can increase the propped fracture length compared to slick water and improve gas productivity.

Table of Contents

Executive Summary

As the global demand for energy rises and the discovery of new hydrocarbon resources drops, the recovery from unconventional resources like shale gas become increasingly important. The shale reservoirs need to be fractured hydraulically to produce at an economic rate. Long propped fractures are needed to maximize productivity. Slick water fracturing with sand produces long fractures, but only the near-wellbore region is propped due to proppant settling. Gels can create long propped fractures, but they damage the fracture surface. The goal of this project is to develop non-damaging fracturing fluids and proppants for gas shale reservoirs that also minimize water use. Lightweight proppants are tested because they settle slowly during fracturing. Foams are evaluated as the fracturing fluid because they minimize water use and decrease proppant settling.

Sphericity, size distribution, bulk density, mechanical properties and chemical compatibility were measured for three ultra light weight (ULW) proppants (ULW1 Polymer, ULW2 Resin-Walnut and ULW3 Resin-Ceramic supplied by BJ services). Of the three proppants tested, ULW-1 is the most deformable and ULW-3 is the most brittle. ULW-2 is fairly deformable. All the proppant packs are significantly strong to endure the stresses expected in Barnett shale.

Conductivity of proppant packs has been determined as a function of proppant concentration and confining stress. Proppant pack conductivity decreases as the confining stress increases. Conductivity is a significantly increasing function of proppant concentration for ULW3, the resin-coated ceramic proppant. For ULW1 Polymer and ULW2 Resin-Walnut, the conductivity has a minimum at about 0.1-0.4 lbm/ft^2; the partial monolayer conductivity is not much lower than that of multilayer packs because they are deformable. The proppant conductivity is low (of the order of 1-10 mD-ft) at 6000 psi confining stress. The application of light weight proppants in stimulation treatments in shale reservoirs is limited to a net confining stress of 6000 psi.

The stability of foams produced from different surfactants has been studied first in a static column. Proppant settling rate has been measured in slick water and foams. Foams made with anionic surfactants are more stable than those made with nonionic surfactants tested. Half-life of these foams can be more than one hour and increases with the addition of stabilizers. Increasing the temperature reduces the half-life of foams. The settling velocity of proppants (three ULWs and sand) in water does not follow Stokes equation because the Reynolds number is larger than unity. Instead, it agrees well with the Happel correlation, which is valid for Reynolds number between 2 and 500. The use of foam eliminates the gravity settling of even sand proppants.

The rheology of three different surfactant fluids (Fluid A: 0.5 vol% anionic surfactant fluid, Fluid B: Fluid A + 2 vol% glycerol, Fluid C: 0.5 vol% viscoelastic surfactant fluid) as well as their foams was evaluated in a flow loop under high pressure and temperature. All foams exhibit power-law model behavior in a laminar flow regime. For the same shear rate and quality, the least viscous fluid is fluid A, while the most viscous fluid is fluid C with an apparent viscosity similar to that of guar foams (with 20 lbm/Mgal guar). All foams show shear thinning behavior at qualities lower than 50% and shear thickening behavior above that. The temperature has less effect on foam rheology at high qualities than at medium and low qualities. The back

pressure (from 200 psi to 1000 psi) affects the viscosity of foam at qualities higher than 50%. Foams of fluid A with 50% quality or greater show good proppant suspension and transport through a slot representing a fracture. The application of gel-free foams would not only eliminate the polymer damage to the fracture face and proppant packs, but also carry proppants deeper into fracture networks than the slickwater.

The effect of proppants, fracturing fluid and injection schedule on the hydraulic fracture creation and on subsequent gas production has been simulated. The results show that a mixture of ULW proppants and sand outperforms all individual ULW proppants or sand. Adding a small amount of ULW1 Polymer to sand can highly improve the fracture conductivity by improving the sand placement. Gel-free foams can increase the propped fracture length compared to slick water and improve gas productivity.

Introduction

The Barnett shale is being produced through more than 8,000 wells today (Wang 2008). The success of gas production from Barnett can be attributed to horizontal drilling and hydraulic fracture stimulation. But there were many lessons learned while exploiting Barnett shale gas reserves. Fracture stimulation in shale gas reserves is not the same as fracturing typical gas reservoirs. These shale gas formations have permeability of the order of 10^{-9} Darcies. Therefore, hydraulic fractures need to be thin and long to maximize reservoir contact.

If conventional proppants, like Ottawa sand (specific gravity = 2.65), are used in typical fracturing fluid like slick water, proppants settle during the fracturing process before reaching the end of the long fractures, due to which a lot of producible surface area is lost after stimulation. Re-stimulation is an option, but it makes the process more expensive. The fracturing fluids can carry the conventionally used heavy proppants if they are made more viscous by using polymers in them. This viscosity can be further increased by cross-linking these polymers. However, when the fracturing fluid is very viscous, the resulting fractures are short and thick, and do not reach a major part of the producible area. Also, the large polymer molecules can plug the fracture faces of these extremely low permeability shales.

One way to overcome these problems is to use light weight proppants which can be transported by a less complex fracturing fluid and at the same time, be strong enough to withstand reservoir stresses. These light weight proppants can be used with simpler fracturing fluids, like slick water, effectively. Typical fracturing processes are extremely water intensive. Once the fracturing job is over, there are other issues with the disposal of the fracturing fluids. The proppants being light also gives us an option of using fracturing foams (mixture of gas and liquid phase), thereby reducing the usage of water.

Silica sand has been the most commonly used proppant. The ready availability and lower cost makes it attractive for stimulation treatments. If conventional proppants, like Ottawa sand (specific gravity = 2.65), are used in typical fracturing fluid like slick water, proppants settle during the fracturing process before reaching the end of the long fractures, which results in the loss of a lot of producible surface area after stimulation. Re-stimulation is an option, but it makes the process more expensive.

Sintered bauxite, another commonly used proppant material, is significantly stronger than sand and is used in deeper formations where high fracture closure stresses severely crush sand proppants. The fracturing fluids can carry the conventionally used heavy proppants if they are made more viscous by using polymers. This viscosity can be further increased by cross-linking these polymers. However, when the fracturing fluid is very viscous, the resulting fractures are short and wide, and do not reach a major part of the producible area. Also, the large polymer molecules can plug the fracture faces of these extremely low permeability shales.

One way to overcome these problems is to use light weight proppants which can be transported by a less complex fracturing fluid and at the same time, be strong enough to withstand reservoir stresses. Recent research and development efforts have created a new class of ultra-light weight proppants (ULWP), having both low specific gravity and requisite mechanical strength (Brannon and Starks, 2009). These light weight proppants could effectively be used with simpler fracturing fluids, like slick water. The first generation of ULWPs were resin-impregnated and coated, sized, chemically modified walnut hulls, having a specific gravity of 1.25, less than half of sand density (2.65). These proppant particles could achieve neutral buoyancy in fracturing water. Settling rates for these first generation ULWPs were 24% that of similarly sized sand. Another type of ULWPs developed around the same period were resin coated ceramic proppants, which had a specific gravity of 1.75; much lighter than sand particles. In terms of transportability, these proppants showed more promise with slickwater than conventional sand or sintered bauxite (sp. gr. ~ 3.6).

To make the proppants travel further into the fractures before settling, one can use a more viscous fluid, lighter proppants or a combination. There are usually two ways to increase a fluid viscosity. One way is to add polymers, such as guar and guar derivatives. Common linear gel fluids have Fann viscosities from 10 to 200 cp depending on the polymer concentrations from 20 to 80 lbm/Mgal (Sudhakar, 2004). Cross-linking these polymers can further increase their viscosities by several orders of magnitude. However, the large molecules can plug the small pores of the fracture surface, and decrease the gas flow (Gidley et al. 1989). The second way is to use foam-based fracturing fluids or energized fracturing fluids. The physical structure of foams gives an effective viscosity similar to that of a gelled fluid. Typical foams applied in the field have a quality of 70 to 80%. Foam fracturing has the advantages of minimizing the water use, reducing the leaking-off rate, and improving fluid recovery efficiency. The disadvantages could be high cost, high surface pump pressure, and low proppant load ability (Gidley et al. 1989).

Foams made from a surfactant foamer without such stabilizers as guar, HPG, or Xanthan gums are known as gel-free aqueous foams. They generally yield a half-life of 3-4 minutes (Gidley et al. 1989). The foam rheology is a very important property for fracturing-treatment design. It influences the tubing flow pressure drops, pump pressure head, fracture geometry, propptant transport and fluid loss to the matrix. It is affected by foam quality, texture, viscosity of the aquous phase, pressure and temperature. There are three major rheological measurement systems, which are rotational viscometer, circulating loop and single-pass pipe viscometer. The rheology results obtained from different systems cannot be compared directly because of differences in foam structures. Even for the same measurement method, the differences in the data analysis methods, the equipment used, and the capillary diameter / length can lead to different results. So, only the results from similar systems are comparable. Some typical

circulating loop viscometers are Schlumberger-Chandler foam rheometer (Hutchins 2003), the recirculating foam loop of the Well Construction Technology Center (WCTC) of the University of Oklahoma (Bonill et al. 2000), and the flow loop viscometer in Halliburton (Reidenbach & Harris 1986). Listed below are their major results and conclusions.

Hutchins (2003) investigated the foam dynamic stability and rheology up to 400 F and 2000 psi by using the Schlumberger-Chandler foam rheometer. The tested fluid all contained 20 - 40 lbm/Mgal linear HPG. The dynamic stability was obtained by measuring apparent viscosity changing with the time at a typical fracturing shear rate of 100 s^{-1}. A microscope and camera were used to investigate the foam texture correlated with the foam stability (Hutchins 2003). Bonilla et al. (2000), Sani et al. (2001), and Sudhakar (2002) utilized the same system of WCTC to investigate the rheology of Guar foams or Xanthan foams. They chose the 0.5vol% anionic surfactant solution as the base fluid. The guar gel or Xanthan gum was added to the base fluid at concentrations from 0 to 60 lbm/Mgal. The tests were all under 1000 psi pressure and room temperature to 200 F. Herschel-Bulkley model and power law model were adopted and the rheology correlations as a function of the polymer concentration, temperature, and the quality were developed. Harris (1987) used a very similar foam loop to investigate the foam rheology in the laminar regime. He found foam did not thin as rapidly as gel under high temperature conditions up to 300F and high-temperature dynamic stability depends more on surfactant type and concentrations rather than gelling-agent concentrations (1989). Besides, he developed a technique to measure changes in foam texture against foam viscosity in the recirculating loop and came up with some important conclusions: (1) The foams are shear-history-dependent fluids; (2) The foam texture will adjust to an equilibrium state that depends on the time at a given shear rate; (3) Finer texture come from higher shear rates higher surfactant concentrations and higher pressures. He also pointed out that rheology does not depend on the type of gas: N_2, CO_2, and

mixed-gas. Adding N_2 to CO_2 foams decreases the half-life to that of the pure N_2 foam, which is one fourth of the pure CO_2 foams half-life (Harris 1995).

Harris (1996) has one paper focused on high quality water foam. In this paper, foams with a quality up to 95% were prepared from 2% anionic surfactant solutions. Adding gelling agents reduced the maximum quality. Water foams of 90 and 95 quality had higher viscosities than foams containing gelling agent. Other than water foams and linear gel foams, crosslinked foams were also studied by Harris [1996]. in the circulating loop. He found that viscosity increased by factors of 3 to 10 when polymer was crosslinked in the foam. Since 2005, Harris [2005] measured the rheology of foams containing propping agents in a modified Fann Model 50-type viscometer, which belongs to rotational viscometers. By using the viscometer, the capability of a fracturing fluid to transport proppants, the viscous and elastic components, and the correlation between the crossover frequency G', G'' and settling time of particles in fluids are all investigated [Harris 2005]. In his latest paper (2009), he listed the issues that arise when developing a new fracturing fluid: high retained conductivity, excellent proppant transport, low pipe friction, controllable viscosity, and capacity to be used in produced water. He also mentioned that the potential problem of generating a long, skinny fracture in low permeable reservoirs is the entry width, which may not be enough for proppants passing through if not designed properly.

The goal of this work is to evaluate ultra light weight proppants and gel-free foams to create long propped fractures. This work focuses on three ultra light weight proppants, ULW-1 (polymeric), ULW-2 (resin coated and impregnated ground walnut hull) and ULW-3 (resin coated ceramic), supplied by BJ services. The physical properties of these proppants have been evaluated along with their mechanical properties. These tests are followed up with conductivity

measurements of various concentrations of proppants at different stress levels. The factors affecting foam stability and proppant settling are investigated systematically. Surfactants and temperature are varied for the stability experiment. Proppant density is varied for the settling experiments. The goal of this work is to develop more stable aqueous foams under high temperature and pressure without the use of gels. A simulator is developed to model the bi-wing planar fracture propagation coupled with proppant transport. Then, the simulation results of fracture geometries (width and length) and the proppant distribution are imported into the reservoir simulator CMG to calculate the fractured well productivity. The well performances of the different hydraulic fracturing treatments completed by injecting different fracturing fluids (water and gel free foam) with different kinds of proppants (sand, ULW1 Polymer, ULW2 Resin-Walnut, ULW3 Resin-Ceramic, mixture) are compared. Based on the simulation results, the impacts of foams and ULW proppants are evaluated. Devon had conducted several tests with lightweight proppants. They had shared some of the data of the field tests with Daneshy Consulting which is summarized in Appendix-A.

<center>**Literature Review**</center>

Fracture Conductivity

Various graphical/computerized methods have been developed to estimate the effects of fracture length and fracture conductivity on well productivity increase for both low permeability and high permeability reservoirs. For high permeability reservoirs, where steady-state (or pseudo steady state) flow develops relatively quickly, methods provided by McGuire and Sikora (1960), can be used to estimate the productivity increase from a fracturing treatment. Figure 1 indicates productivity increase as a function of fracturing parameters: relative conductivity $(\sqrt{40/A})wk_F/k$) and fracture penetration (L/r_e). As the fracture penetration increases, the productivity increases. As the relative conductivity increases, the productivity increases to some extent and then does not change. For example, for $(L/r_e)=0.2$, the productivity does not increase much for relative conductivity greater than 10^5. If the permeability is 10^{-5} md and well spacing is 160 acres, then the critical fracture conductivity (wk_F) is 0.2 md-ft.

<center>16</center>
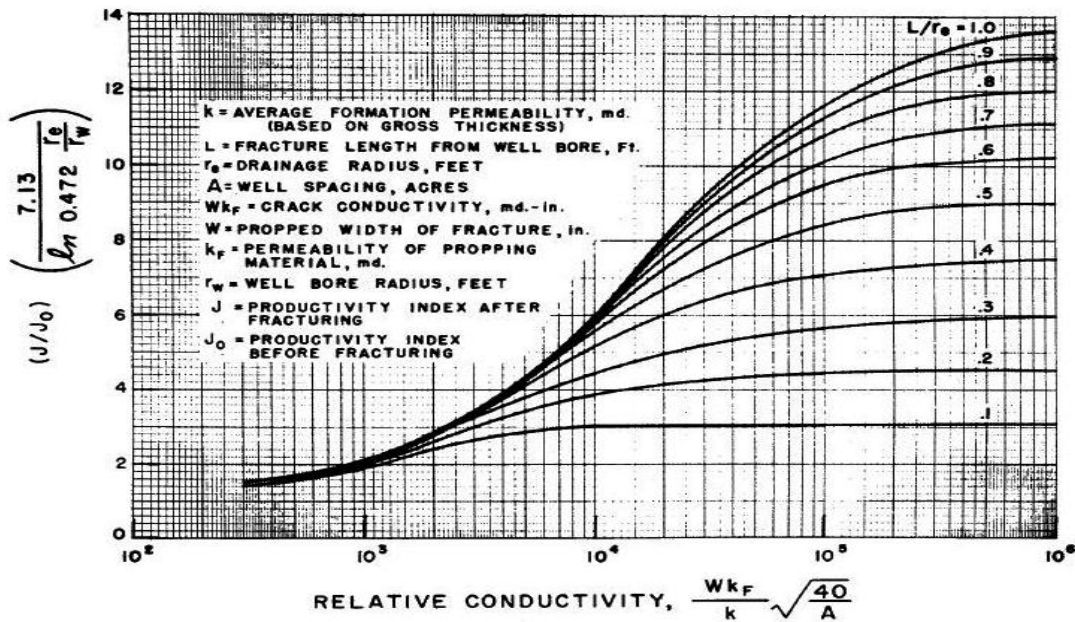
Figure 1. McGuire and Sikora's producing-rate folds-of-increase curves (1960)

Figure 2 shows productivity index ratio to be a function of relative capacity and fracture penetration, similar to Figure 1.

$$X = \left(\frac{k_f \; w_f \; h_f}{200 \; \pi \; k_i h_i}\right) \; \ln(r_e/r_w) \; \sqrt{\frac{10}{S}} \quad \text{RELATIVE CAPACITY (ft)}$$
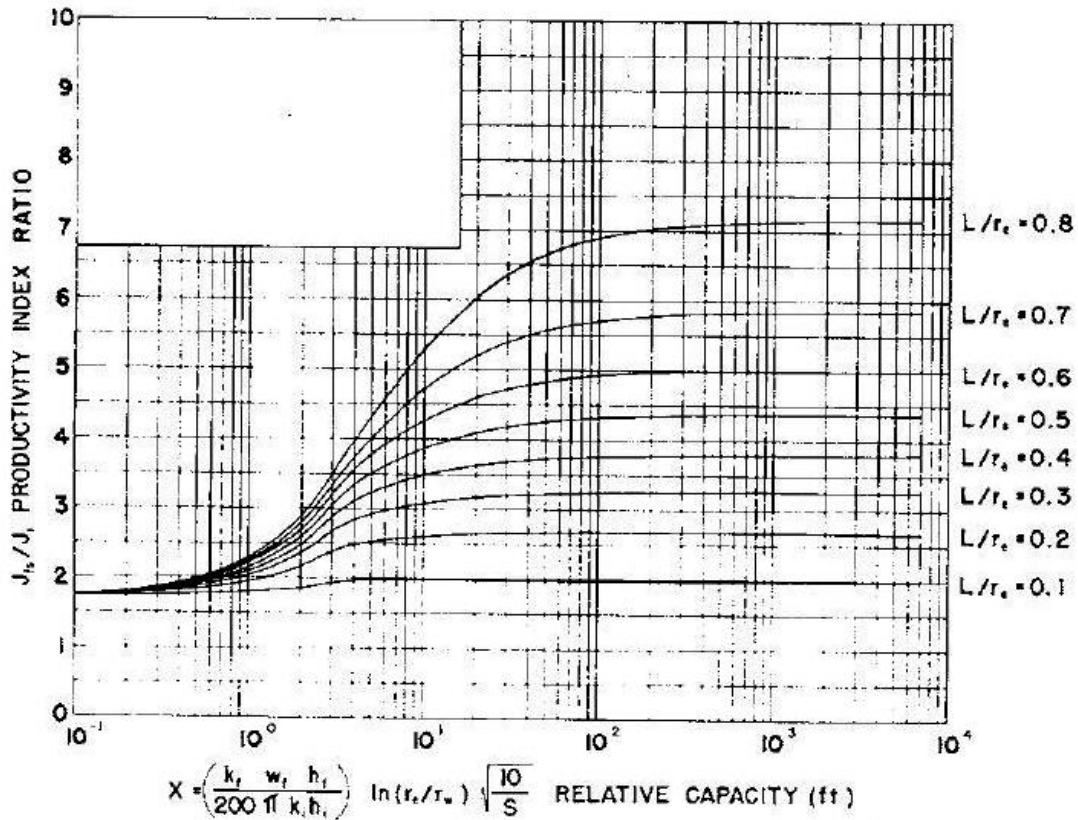
Figure 2. Productivity-index-ratio increase from fracturing, steady-state flow, vertical propped fractures (Tinsley et al., 1969)

The above two plots show steady state productivity which do not apply to low permeability reservoirs strictly because for low permeability reservoirs, flow remains in transient state throughout the major portion of a well's life. Agarwal et al. (1979) and Cinco et al. (1978) developed methods for evaluation of increase in productivity through fracturing treatments for low permeability reservoirs. Figure 3 indicates the plot developed for the case of constant

wellbore pressure system. Figure 4 indicates the same plot developed for constant flow rate system.
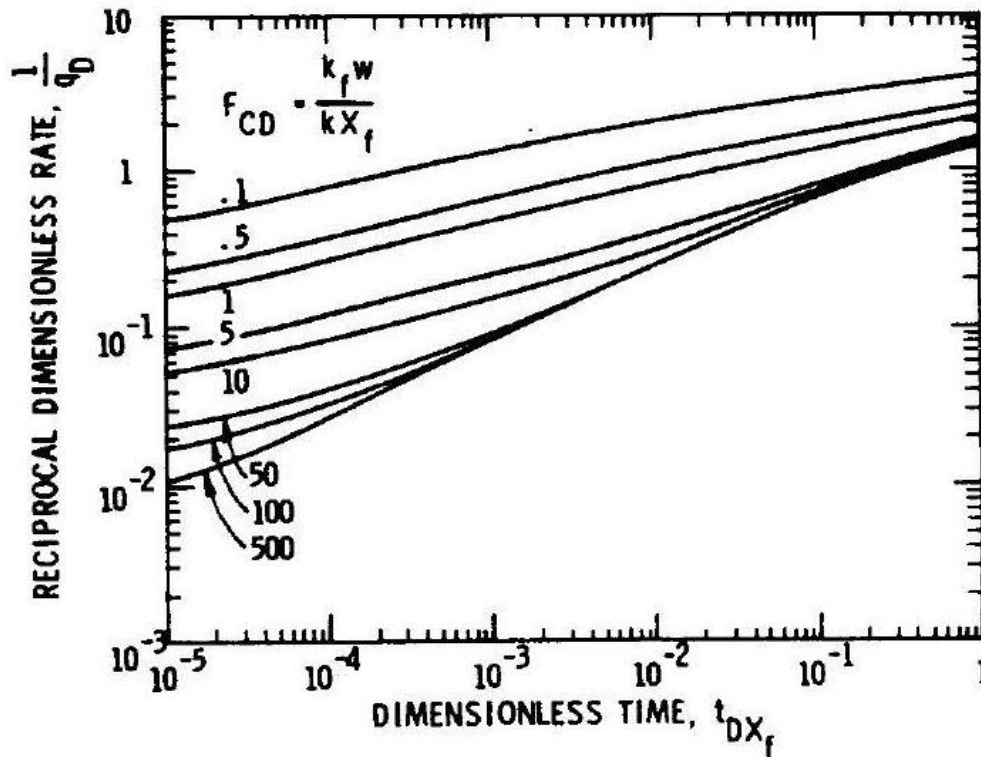
Figure 3. Producing-rate type curves with propped vertical fractures-transient flow, constant wellbore pressure (Agarwal et al., 1979)

The ratio of (fracture conductivity)/(reservoir permeability x fracture half length), i.e., dimensionless fracture conductivity F_{CD}, is a key parameter in these plots. From figures 3 and 4, for any stimulation treatment, higher dimensionless fracture conductivity gives a higher cumulative production over time (or a lower flowing wellbore pressure), but production does not increase much beyond a dimensionless fracture conductivity of 10. It should be noticed, the value for this dimensionless parameter can be >10 for a low permeability reservoir (10^{-4} md) even when the fracture conductivity is small (of the order of 1 mD-ft). Along with fracture

18

penetration, fracture conductivity plays a pivotal role in enhancing production from any fracturing treatment.
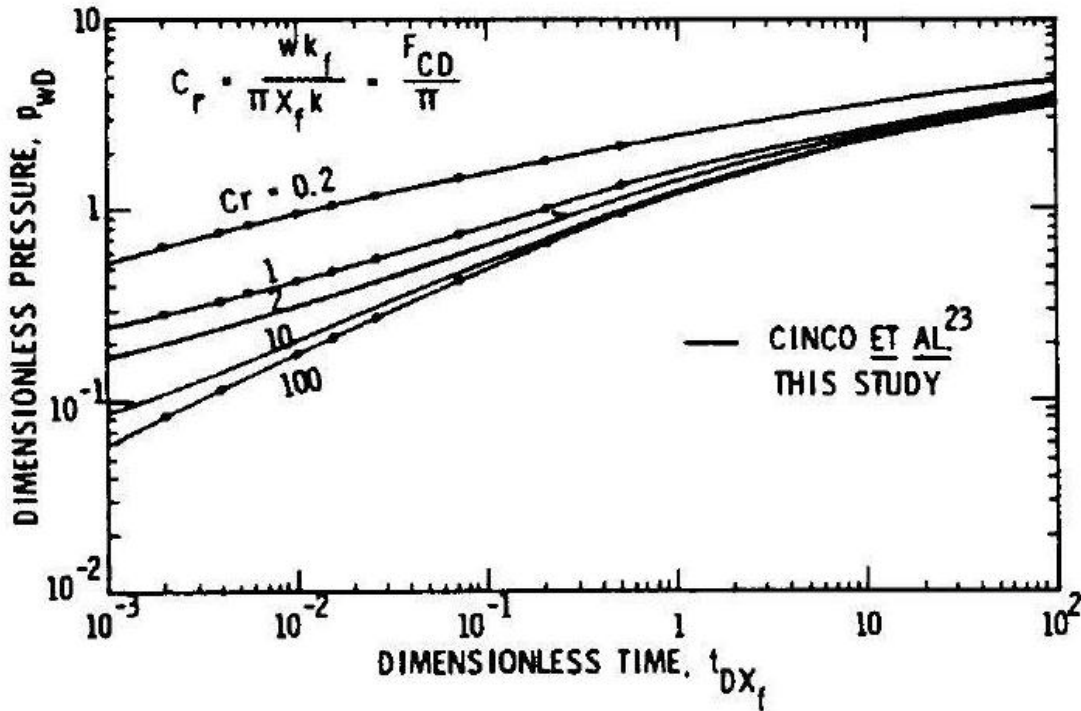
Figure 4. Producing-rate type curves with propped vertical fractures-transient flow, constant flow-rate (Cinco-ley et al., 1978)

It is difficult to place heavier proppants efficiently in between the fracture faces in long fractures because of settling. Rickards et al. (2003) conducted a series of experiments testing the utility of lower density proppants under various stress conditions. The conductivity of light weight proppants relatively low at high stress levels. But with increased usage of slickwater in shale reservoirs, the necessity of using 'easy to transport' proppants in particular stimulation treatments has risen.

Slickwater Fracturing

Palisch and Vincent (2008) in their works have highlighted the importance of slickwater fracturing treatments. More than 30% of stimulation treatments in 2004 have been slickwater fracturing (Schein, 2005). Slickwater fracturing, as defined by Schein, is a fracture treatment that utilizes a large volume of water to create an adequate fracture geometry and conductivity to obtain commercial production from low perm, large net pay reservoirs. These reservoirs come broadly in the area of coal bed methane, tight gas sands and shale gas plays. The most desirable fracture system in these reservoirs is long and narrow. The most important benefits of slickwater fracturing are reduced gel damage, cost containment, higher stimulated reservoir volume, and better fracture containment. But the concerns are poor proppant transport, excessive usage of water, and narrower fracture widths.
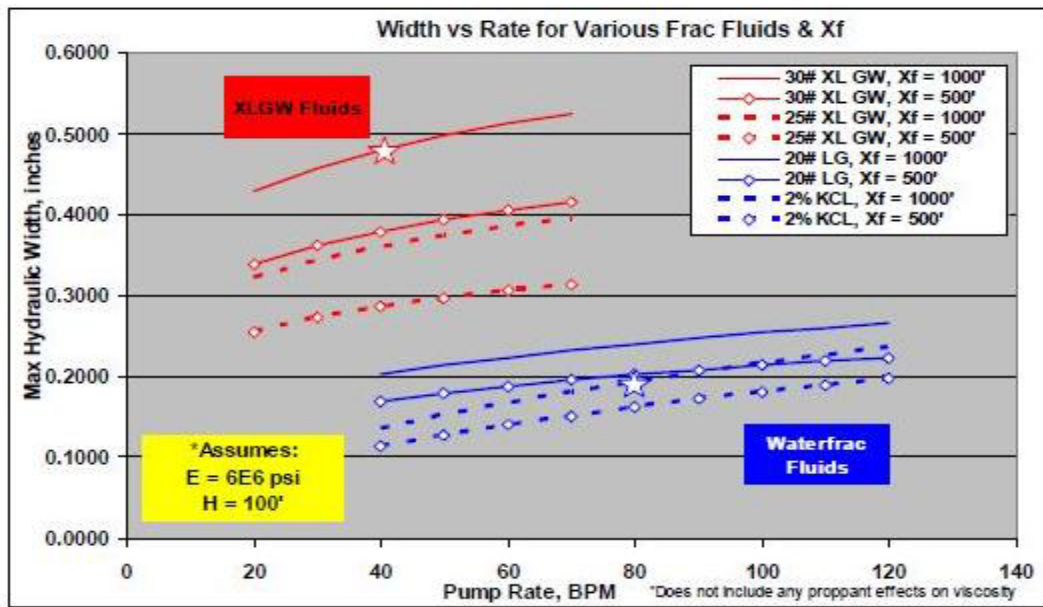
Figure 5. Fracture width comparison for various fracturing treatments (Palisch and Vincent, 2008)

Figure 5 shows the effect of pump rate and fracturing fluids on resulting fracture widths. It indicates a decrease in fracture width, once we switch from cross-linked gels to slickwater. In a nano-darcy permeability reservoir, large fracture width is not needed (F_{CD} does not have to be large); a long-extensive-wide network of fracture system is desired. With longer fractures, SRV (stimulated reservoir volume) would be greater than with short fractures. A larger SRV leads to greater production. To create such a fracture system, a less viscous fracturing fluid like slickwater (unlike crosslinked gels) is needed, which can effectively create thin, long fractures distributed over a larger area. But proppants should be properly placed throughout the fracture network system before the fracturing fluid is withdrawn. Thus there is a need for proppants which are easy to transport throughout the fracture network with slickwater.
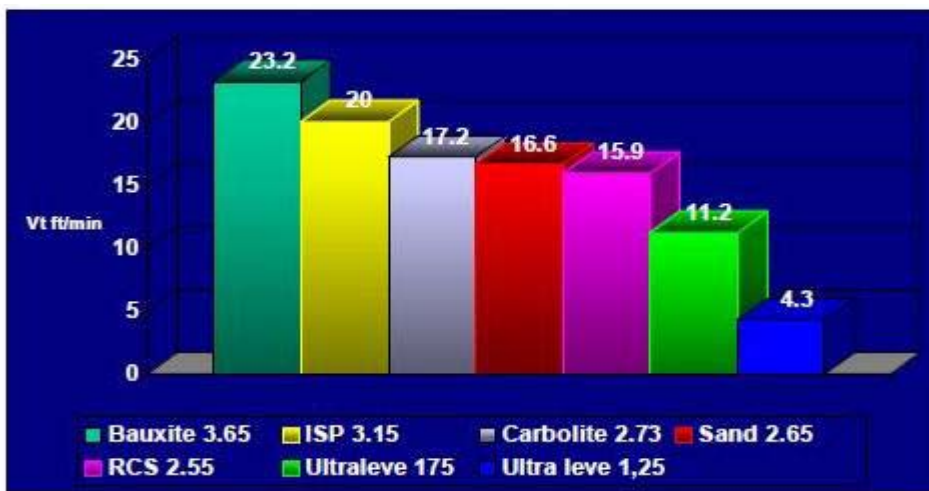
Figure 6. Proppant settling in freshwater for various proppants (Aboud and Melo, 2007)

Aboud and Melo (2007) compared the static settling rates of various proppants in freshwater based on Stoke's law (Figure 6),

$$V_s = [(\rho_p - \rho_f)\, g\, d_p^{\,2}] / (18\mu) \;, \tag{1}$$

where V_s is the Stoke's settling velocity of a single particle, ρ_p and ρ_f are the density of the particle and the suspending fluid, respectively, d_p is the diameter of the particle, g is acceleration due to gravity and μ is the viscosity of the fluid. Stokes law has many simplifying assumptions including laminar flow, spherical particles, and absence of wall effects. In spite of these assumptions, Stoke's law helps us to compare the relative settling rate of various proppants based on their density/size and density/viscosity of the fluid (Palisch and Vincent, 2008). This settling velocity is applicable only for small particles Reynolds numbers (Re_p<2) settling in static fluid when wall effects are not important (Asmolov, 2002). For larger Reynolds numbers, settling velocity is affected by the turbulent wakes generated behind the particle. To account for this, Stokes law has been corrected as,

$$V_{Re} = V_s\, f(Re_p). \tag{2}$$

As indicated in Figure 7 and Figure 8, the creation of wakes due to higher Reynolds number resulted in decrease in settling velocity.
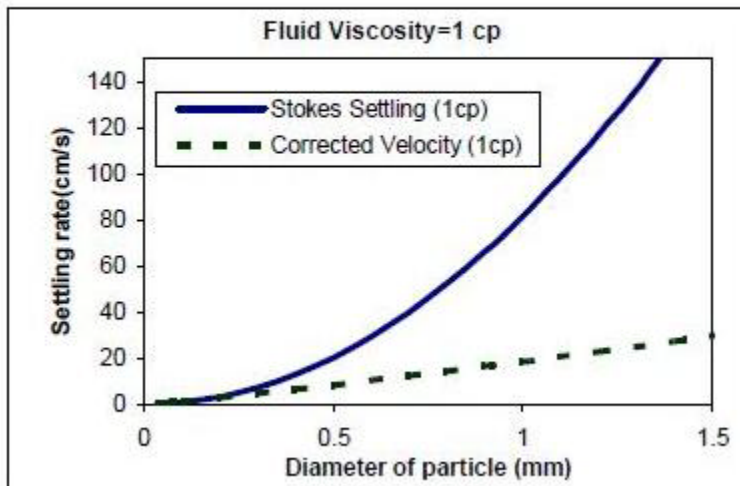
Figure 7. Terminal velocity of different sized particles predicted by Stoke's equation and corrected for inertial effects in 1 cp fluid
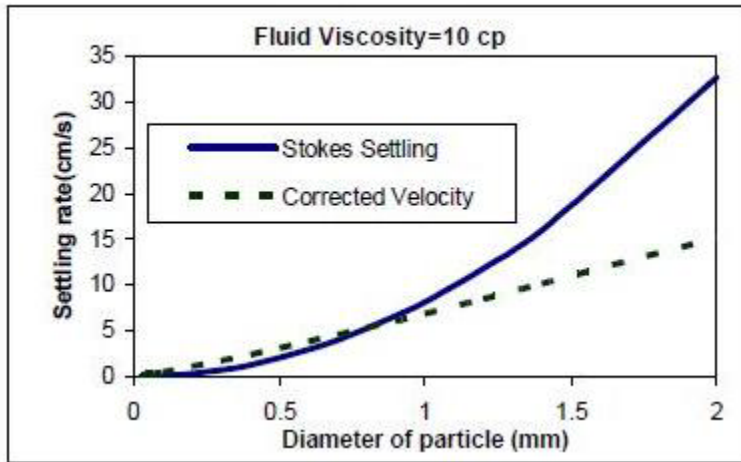
Figure 8. Terminal velocity of different sized particles predicted by Stoke's equation and corrected for inertial effects in 10 cp fluid

These results are applicable to single particles and cannot be applied to proppant slurries which are pumped during any fracturing treatment. Gadde et al. (2004) included the effect of proppant concentration on settling which is shown in Figure 9. The overall effect of higher proppant concentration resulted in reduction of settling.
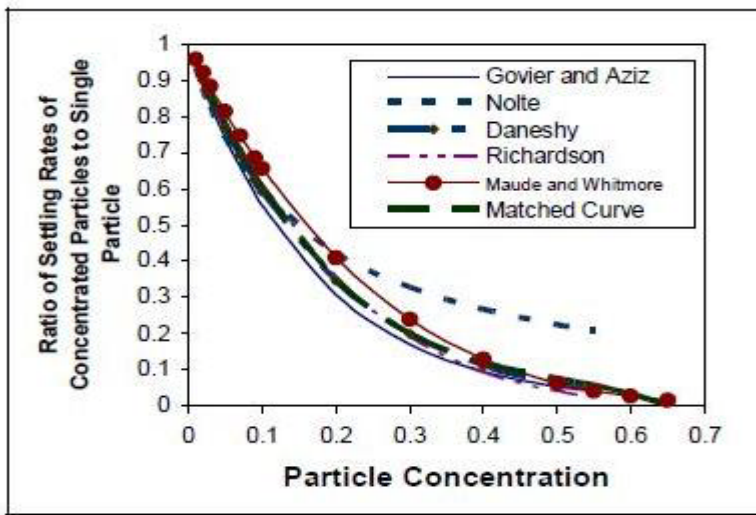
Figure 9. Correlations for effect of solids concentration on settling velocity

Gadde et al. (2004) studied the effect of fracture width on settling velocities and found out the modified stokes settling velocity also depends on ratio of the radius of the particle to the width of the slot, guided by equation 3,

$$V_w = V_s[0.563(a/l)^2 - 1.563(a/l) + 1] \tag{3}$$

where a is the radius of the sphere, l is the distance of the centre of sphere to either wall, V_s is the stokes settling velocity and V_w is the modified settling velocity which includes the wall effects. Figure 10 shows that the wall effects tend to reduce settling of proppant particles.
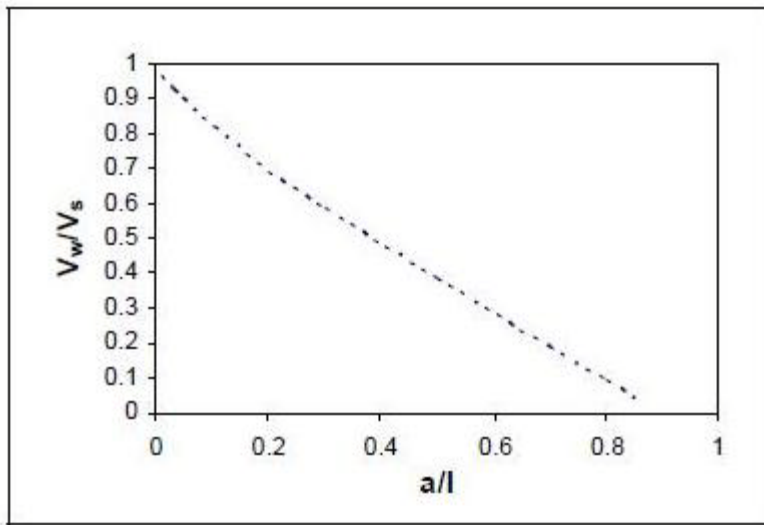
Figure 10. Wall effect on proppant settling velocity (Gadde et al., 2004)

Partial Monolayers

Darin and Huitt (1959) introduced the concept of partial monolayers which is shown in the Figure 11. The porosity of such a pack is small and may give rise to higher fracture conductivity (Figure 12). But doubts on uniform distribution of these proppants, their crush strength and embedment into the fracture faces are some of the concerns. Howard and Fast (1970) tried to determine the percent of proppants crushed when used as a full-monolayer. They tested various concentrations of three different 20/40 proppants (resin coated sand, light weight ceramic and white sand) and tried to determine the amount of fines formed for each of them at 6000 psi stress, the results of which are shown in the Figure 13.
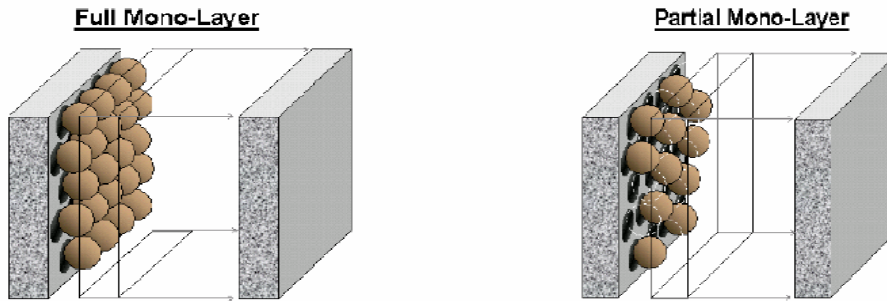
Figure 11. Proppant particles in contact with each other in a full mono-Layer and sparsely distributed particles in a partial mono-layer (Brannon et al., 2004)
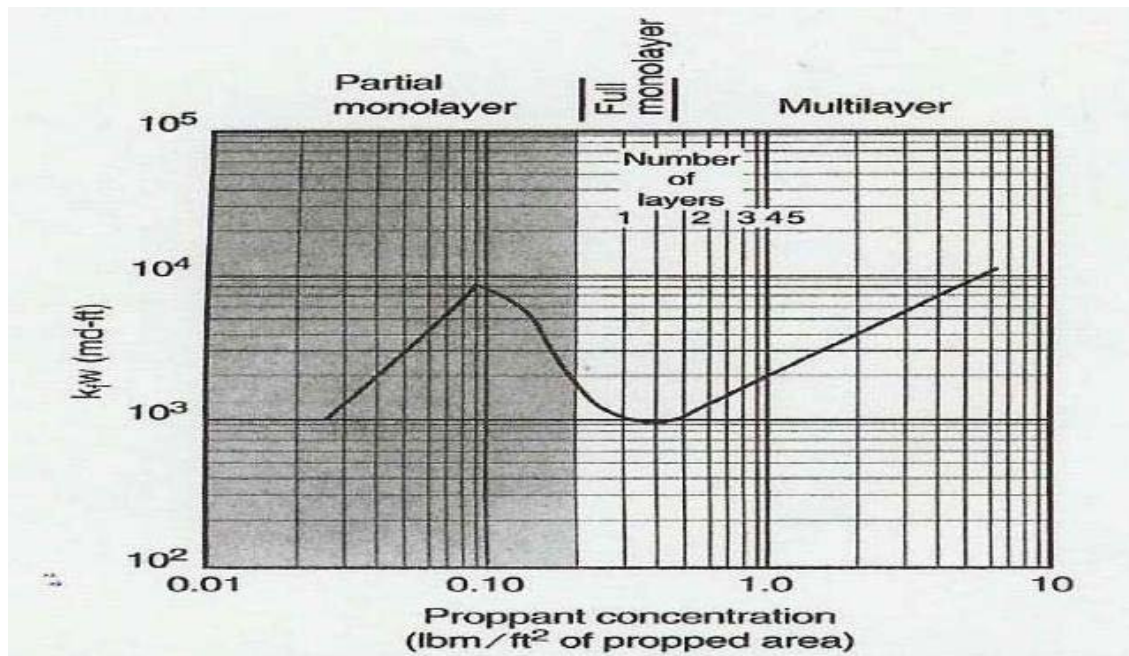
Figure 12. Fracture conductivity of monolayers and thick packs of 20/40 sand (Darin & Huitt, 1959)

If the success of proppant pack is attributed to less crushing of the pack, then, it is clear that at around a concentration of 0.2 lbm/ft^2 (a monolayer) this proppant is a complete failure at 6000 psi stress. Light weight proppants are needed that do not form much fines at a high confining stress.
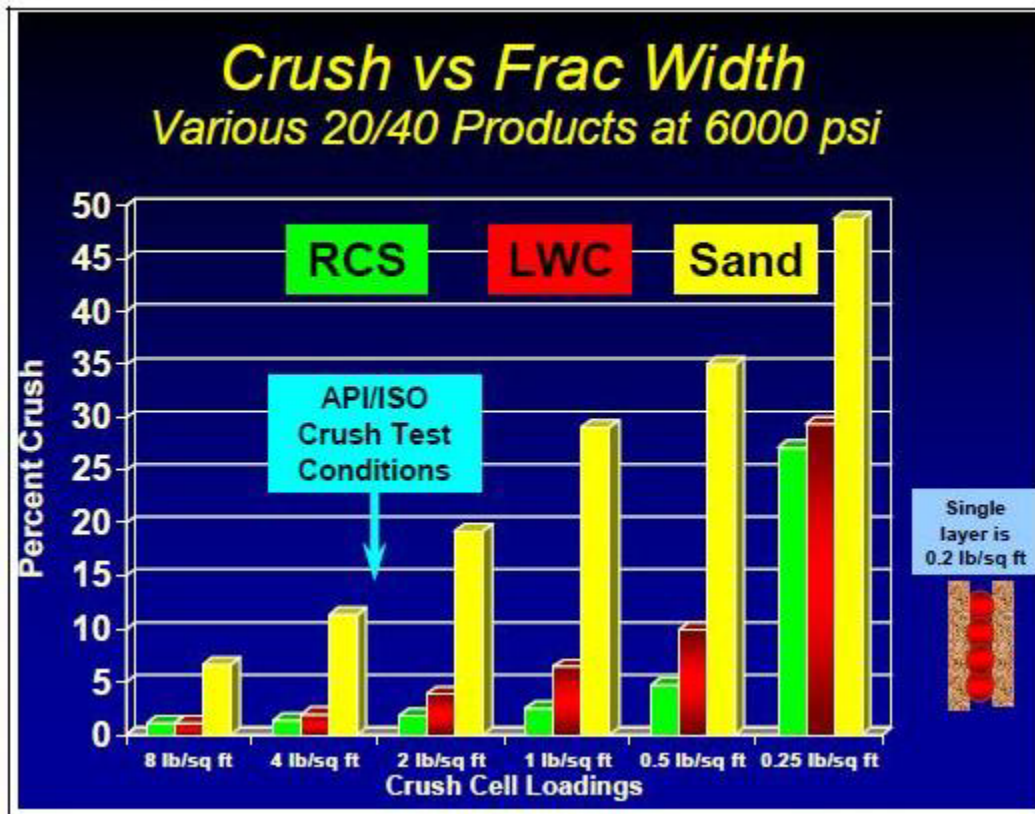
Figure 13. Weight percent crushed for various concentrations at 6000 psi stress (Howard and Fast, 1970)
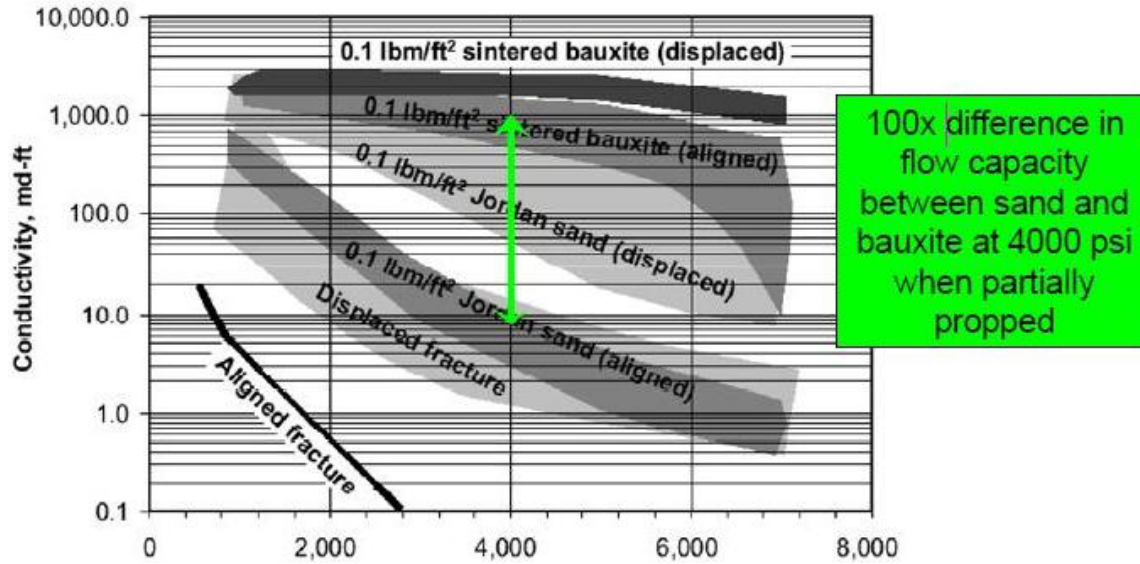
Figure 14. Full monolayers of various proppant being tested for conductivity at 1000 psi stress (Wang, 2008)

Wang (2008) showed (Figure 14) how there can be a two-order magnitude difference in conductivity when using different materials for full monolayers. High strength material like sintered bauxite full monolayer gives 100 times more conductivity than monolayer of white sand at a stress level of 4000 psi. Sintered bauxite is heavier than even conventional proppant (sand), which means, its monolayer placement with slickwater is doubtful.
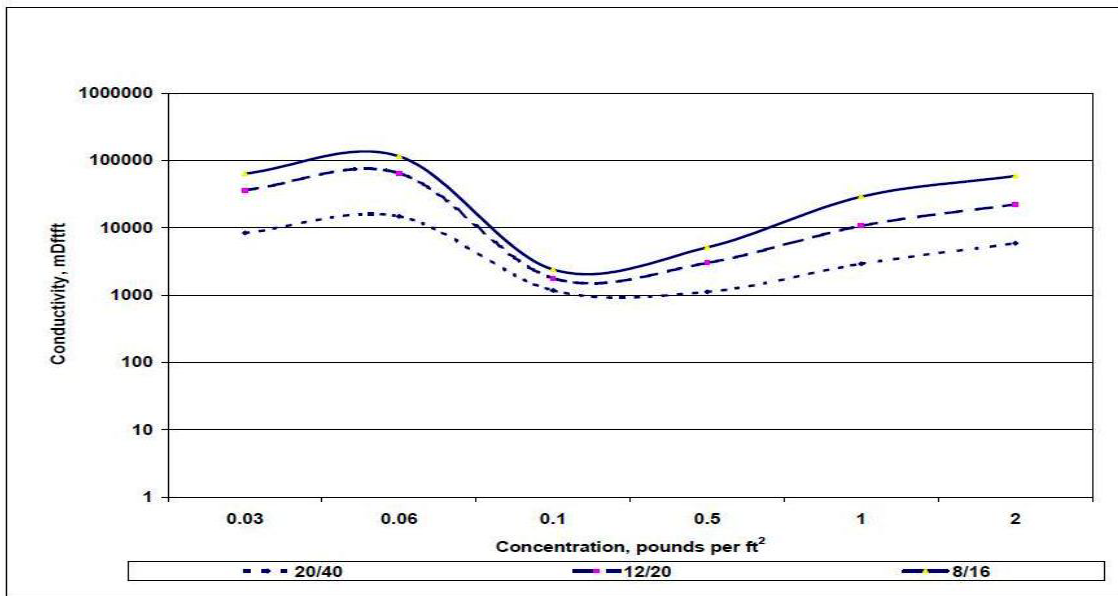
Figure 15. Conductivity vs. proppant concentration for various sizes of Brady sand at 1,000 psi closure stress and 100°F (Brannon et al., 2004)

Brannon et al. (2004) measured the conductivity of differently sized sand proppant particles at different temperatures. They used sandstone cores enclosing proppant pack. In Figure 15 and 16, conductivity results are plotted. The conductivity is a nonmonotonic function of proppant concentration. The conductivities are between 100 and 100,000 mD-ft.
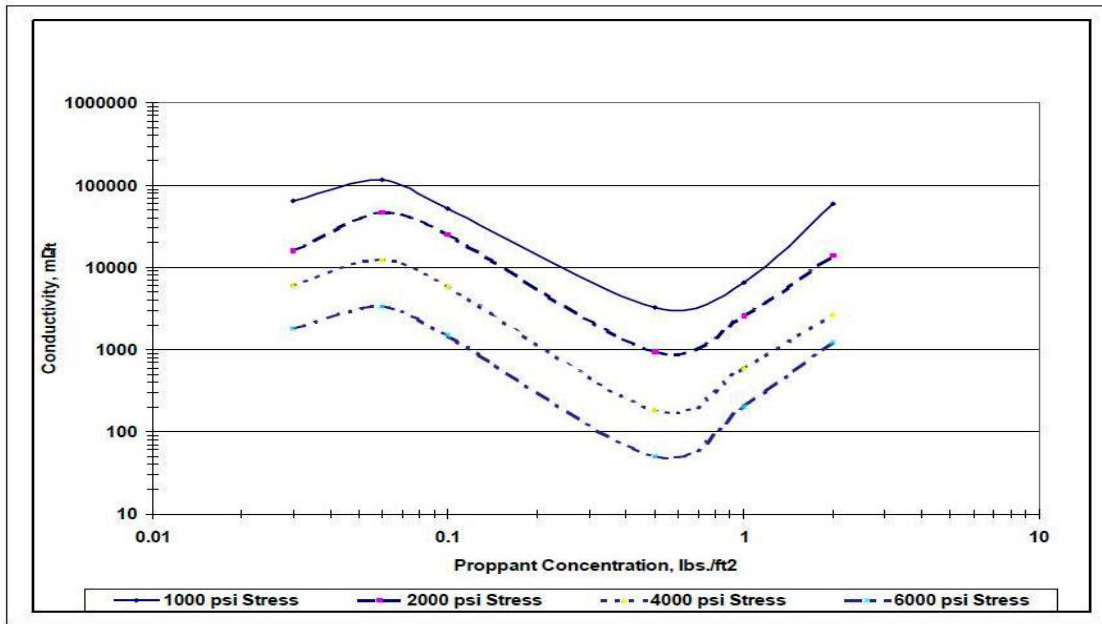
Figure 16. Conductivity vs. proppant concentration for 8/12 Brady sand at various closure stress (Brannon et al., 2004)

Ultra Light Weight Proppants

As Palisch and Vincent (2008) rightly pointed out, the ideal properties of a proppant for its application in slick water fracturing treatments for low permeability reservoirs would be light as water, high strength, and cheap. But, it is impossible to get all these ideal properties in one product. Unless, the concept of monolayer can be rightly applied in the field and these individual proppant particles can sustain high stresses for longer periods of time at reservoir conditions. Rickards et al. (2003) used resin coated/impregnated walnut hull proppants and resin coated porous ceramic proppants in their work, where physical and mechanical properties of these proppants were tested at room temperature. Using Mfrac simulator, they simulated placement properties of light weight proppants with slickwater as compared to sand with slickwater (Figure 17 and Figure 18).
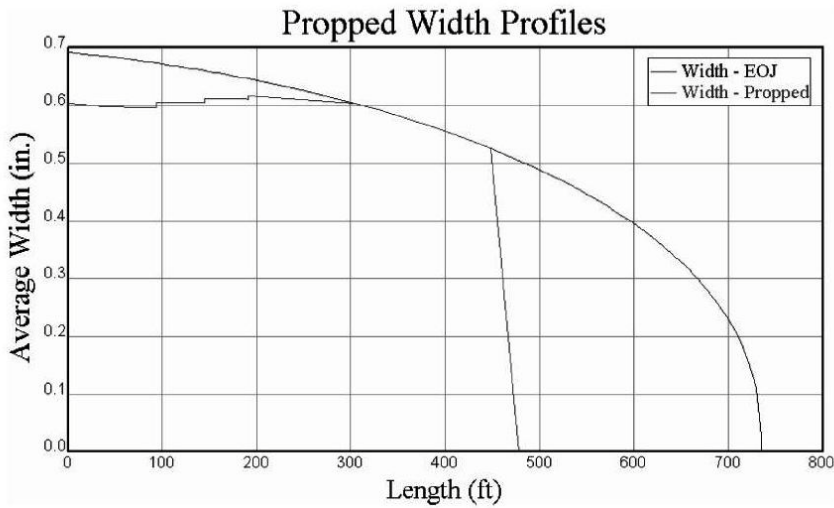
Figure 17. Simulation of Ottawa sand proppant placement at pumping rate of 80 bpm using Mfrac simulator
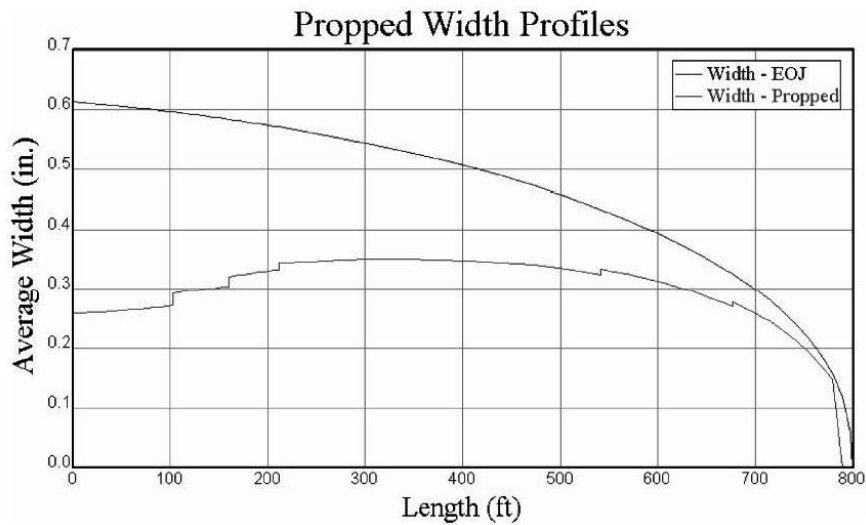
Figure 18. Simulation of light weight proppant placement at pumping rate of 80 bpm using Mfrac simulator

Terracina et al. (2010) in their recent publication stressed on the problem of proppant embedment which is usually overlooked before evaluating proppant performance. While using

proppants in soft rocks (soft shales), significant embedment might decrease the conductivity of a monolayer significantly. Though, monolayer of the same proppant might perform very well when used in harder formations (hard shales).

Methodology

Measurement of Physical Properties of Proppants

Sphericity: Two-dimensional close up images were taken of several proppant particles of each kind and the definition of Riley's sphericity was applied to calculate sphericity. The average of ten readings for all the three proppants was taken as a representative of their kinds. The Riley sphericity (Ψ_R) is defined by,

$$\Psi_R = (D_i/D_c)^{0.5} . \tag{4}$$
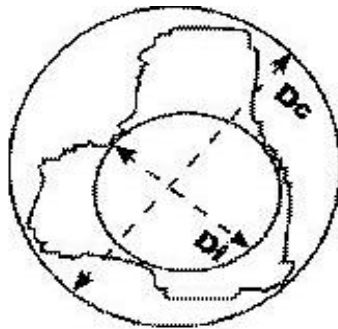
Figure 19. Riley's sphericity definition

A value of $\Psi_R = 1$ indicates completely spherical and a value of $\Psi_R < 0.6$ indicates extreme angularity.

Size Distribution: This data was provided to us by the supplier, namely BJ services.

Density: The specific gravities of the individual proppants were made available to us by BJ services. We obtained the bulk density of these proppant packs under no confining stress which also gave us the porosity of the pack under no confining stress. Proppants of each kind were simply poured into test tubes. These test tubes were weighed and the bulk volume of the proppants was measured. These values were used for calculation of bulk density.

Assessment of Mechanical Behavior

To assess the mechanical behavior, we performed a strength test in a Humboldt material testing machine. The test tool has three components. A base, a cap and a cylinder surrounding the extended portions of the base and cap. The proppant particle/pack is placed between the extended portions of the base and the cap, where it is tested for its strength.
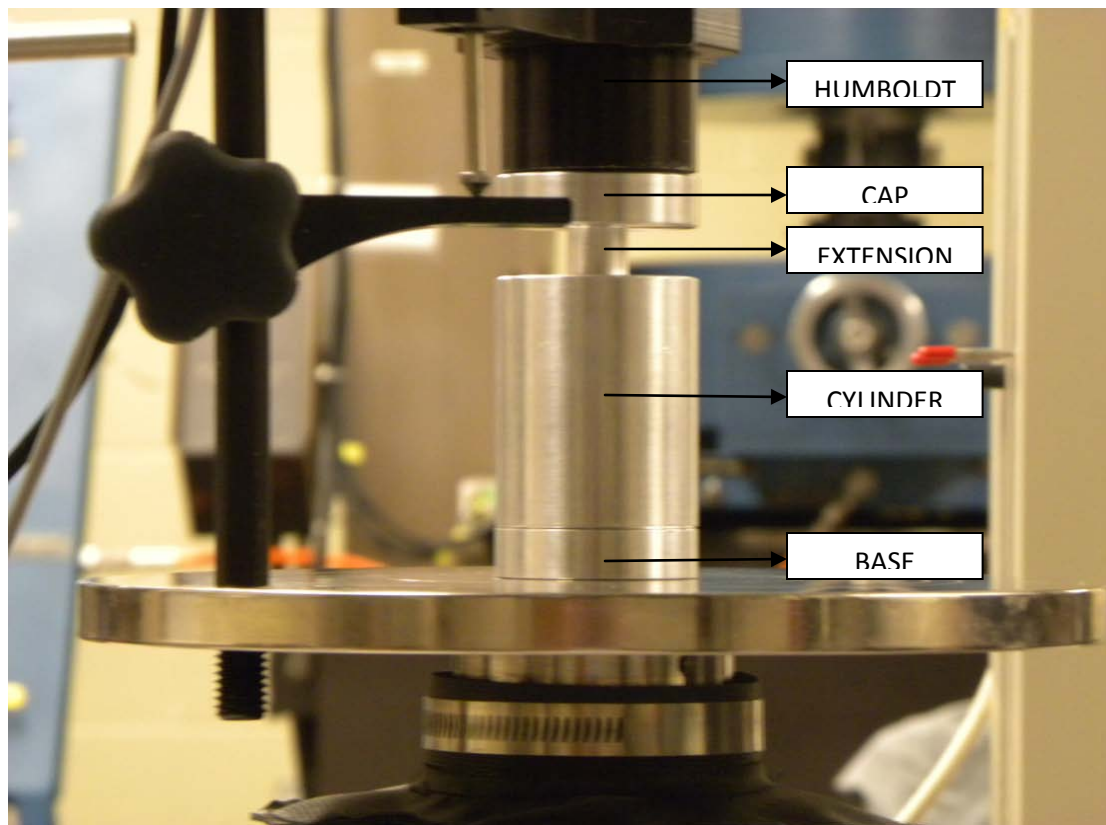
Figure 20. Image of the strength test tool placed on the HUMBOLDT MASTER LOADER-3000

The tests were performed on several proppants of each kind at room temperature and also at an elevated temperature encountered in Barnett shale. Some of the typical properties of the Barnett shale are listed in the following:

Depth: 5000-8000 ft

Thickness: 100-500 ft

Gas content: 100-300 scf/ton

Reservoir Pressure Gradient: 0.52 psi/ft

Minimum Horizontal Stress: 1365-2184 psi

Maximum possible values for Horizontal Stress: 2357-3771 psi

Average Temperature: 90° C

Proppant Pack Strength Test and Fines Formation: A 5 mm high pack of each proppant was tested for its strength. The aim of this test was to test the compressive strength of proppant packs to increasing stress and also the amount of proppants lost due to the formation of finer particles.

Crush Strength: Crush strength is defined as the load at the failure point in the load versus deformation test. This strength is one of the factors considered in the choice of proppants for a particular shale. This test was done at room temperature and at 90° C which allowed us to compare the behavior of proppants at different temperatures.

Deformability: The measurement of the average value of Young's modulus before failure in effective stress versus effective strain test gave us a tool to assess the deformability of individual proppants. Also, the shape of the particles after the test was carefully examined which qualitatively showed the deformable/brittle nature of particles. The variation in temperature in our tests indicated the change in the deformability of the proppants with increasing temperature, which was visible in the load versus deformation test.

Compatibility of Proppants: The proppants were soaked in water and surfactant-water solutions. Their appearance was checked.

Fracture Conductivity

Figure 21 shows the stress range which proppants have to endure while providing a reasonable conductivity for flow of gas for a few gas plays. This study currently focuses on application of proppants in Barnett, so the overburden stress is varied in the range of 2000-6000 psi.
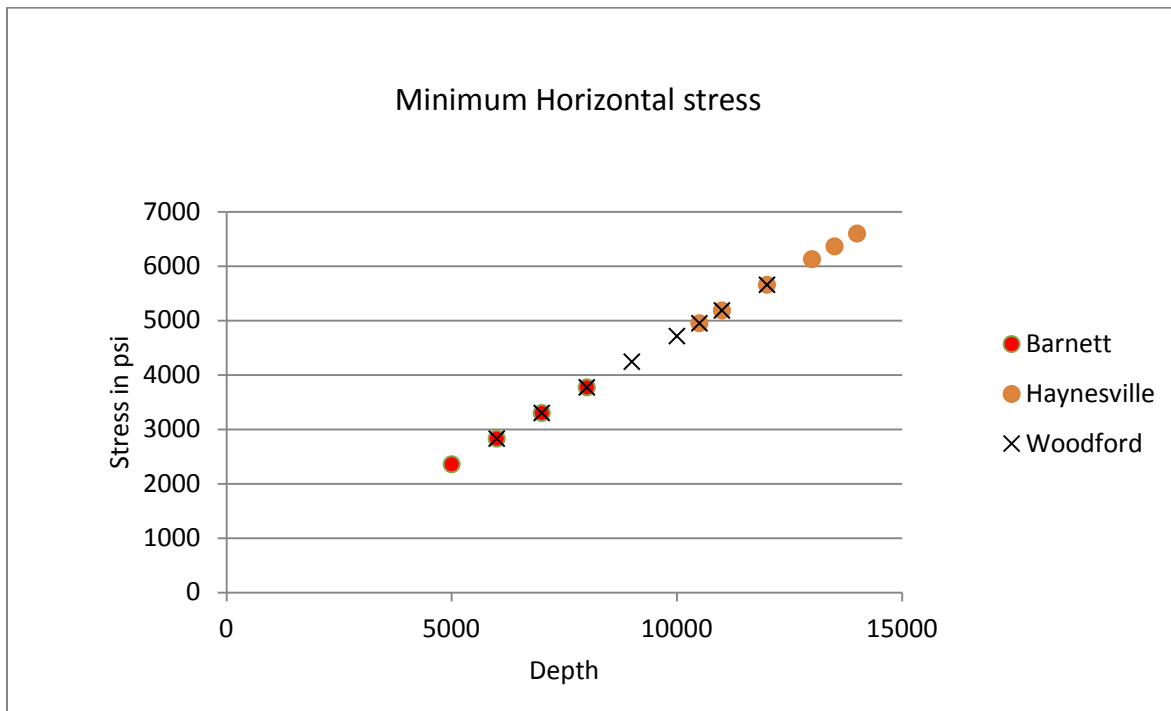
Figure 21. Typical values for horizontal stresses in various shale plays

A standard API conductivity cell is used to measure the fracture conductivity with different proppants. Following the procedures listed in ISO 13503-5, we performed conductivity tests using the API cell, on the three different proppants available to us. For ultra light weight (ULW) proppants, the conductivity of partial monolayers is as important as those of thick proppant packs.

Our study focuses on application of ULWs in Barnett shale, so conductivity tests are conducted at Barnett shale temperature of around 95°C. The Barnett shale rock is very hard and embedment of proppants in fracturing faces during Barnett shale fracturing has not been an issue. This is the reason why we used steel shims to enclose the proppant pack in our conductivity tests. For softer shales, these tests would be conducted with reservoir cores. Thus the results of conductivity experiments are shale specific.
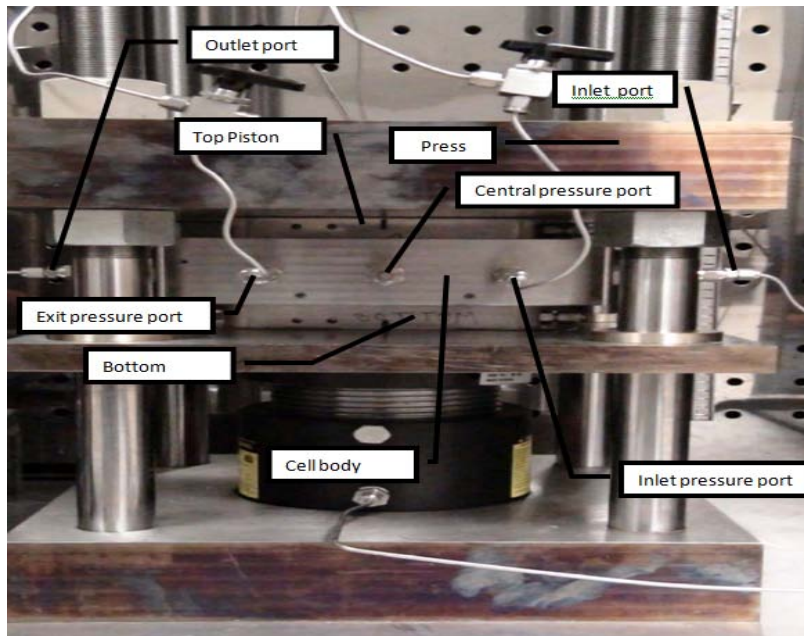
Figure 22. API conductivity cell inside an oven maintained at 95°C

Figure 22 shows the arrangement for our conductivity set-up. The whole equipment is kept within an oven maintained at 95°C. All the experimental fluids are also maintained at 95°C. The detailed procedure of testing conductivity is listed in ISO 13503-5, in a very descriptive manner. A major problem we encountered in our tests was that of leakage. To overcome this problem, we used high temperature resistant thin rubber gaskets, above and below the metal

shims. On application of stress, the rubber sheets provided good seal, and the entire fluid flow was through the proppant pack in between the metal shims.

Static Foam Stability Test
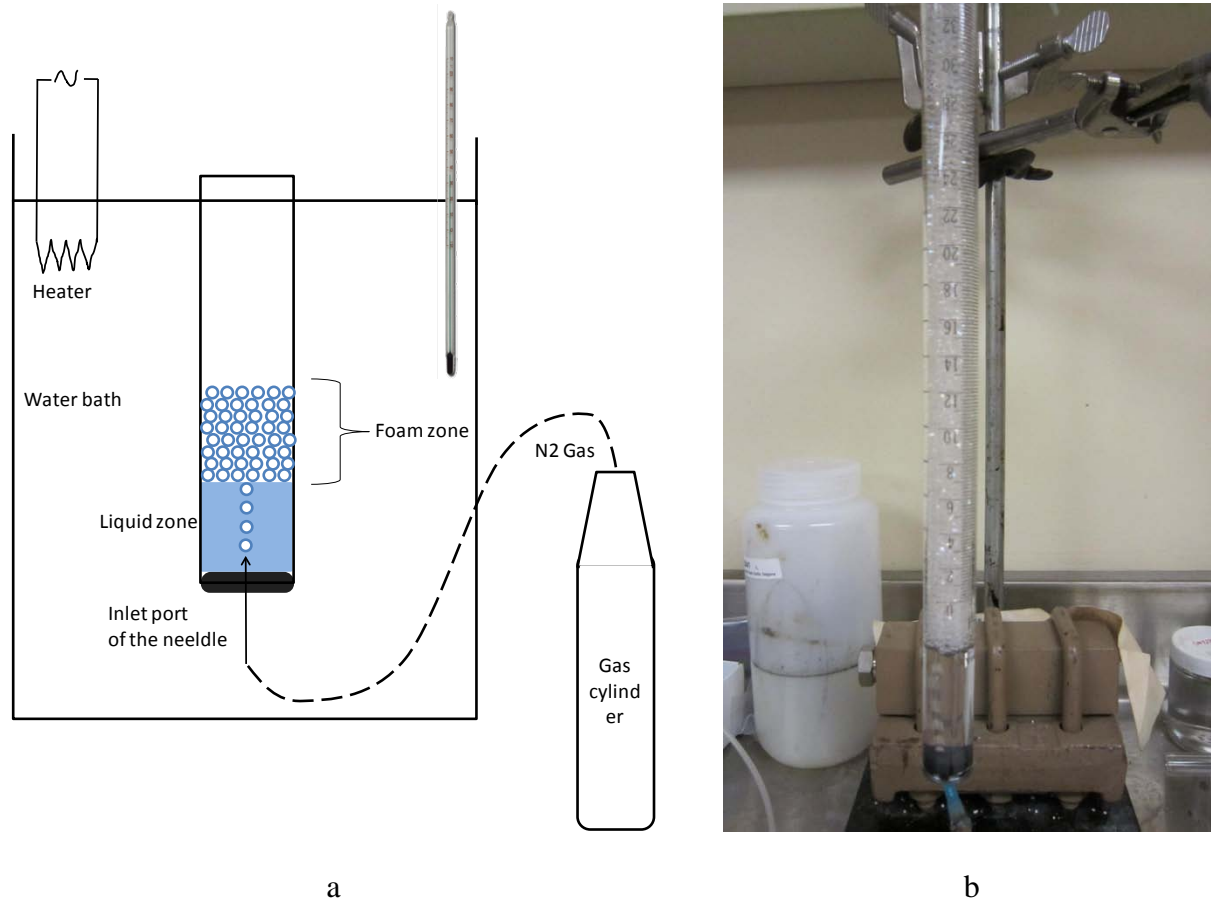
Figure 23. Setup for stability test (a: schematic ; b: foam column)

The experimental setup is shown in Figure 23. A calibrated glass tube, 63 cm in height and 1.52 cm in inner diameter, is sealed at one end by a rubber plug. A needle connected to a N_2 gas cylinder is inserted through the rubber plug. A steady-state column of foam is generated by blowing N_2 gas into a surfactant solution inside the tube. By changing the gas injection rate and the needle size, uniform bubbles with different diameters can be produced. After a certain height is achieved, gas injection is stopped and the height of the foam column is measured as the time passing. The time when the foam column height reduces to its half is defined as half life time of

the foams, which is commonly used to evaluate the stability of the foams by quantity. The whole setup can be put in a water bath, which can be heated from room temperature to no higher than 100 ^{o}C.

In our test, one anionic surfactants (Anionic 1), one series of nonionic surfactants (Nonionic 1(NP10/30/50/70)), eight cationic surfactants (Cationic 1-8.), and one amphoteric surfactant (Amphoteric 1) are used as foaming agents. The stabilizer is glycerol. Temperature is varied between 20 and 80 ^{o}C. To evaluate the effects of parameters (liquid composition, concentration, quality, and temperature) on stability, we hold all of them constant except one and measure its effect. Thus the static stability test is divided into four groups. The first group of tests is about the effect of the liquid composition, including surfactants and one stabilizer. The stability of the foams produced from different surfactant solutions with the same concentration are measured and compared. Then, the stabilizer glycerol is added at different concentrations and the stability of foams is measured again. Following that, we combine an amphoteric surfactant or an anionic surfactant with one of the cationic surfactant and study the effect of the combination. Finally, the effect of the length of the group [CH$_2$CH$_2$O] of the nonionic surfactant Tergitol is also investigated. The other three groups study the effects of concentration, temperature and quality, respectively. In the second group of tests, surfactants with different concentrations are used to produce foams and the stability results are collected and compared. In the third group of tests, the Bio-terge surfactant solution with activity concentration of 0.1% is used to produce foams. And the foam half life time is measured under the temperature of 20 ^{o}C to 80 ^{o}C. In the final group of study, the cationic surfactant BTC 1010 is used as the foaming agent. The foam columns with different bubble sizes and qualities are made by changing the gas flow rate and the diameter of the gas injection port.

Foam Rheology Test

A circulating loop is built to generate different quality foams at different temperatures and pressures. As soon as foams are generated, they are circulated in the loop at different flow rates and pressure differences are measured. The whole loop is covered with thermal insulators, except one part with the heating jacket. The heating jacket can heat the circulating fluid to a temperature around 70 ^{o}C. The back pressure within the loop is set at 1000 psi. A transparent view cell is adopted to observe the foam texture. Figure 2 shows the schematic diagram and the photograph of the circulating loop.

a

Pressure Transducer · PC · Mass Flow Meter · Visual Cell · Gear Pump · Air Injection · Fluid Injection · Outlet · Foam Loop · Heating Pipe and Temperature Controller
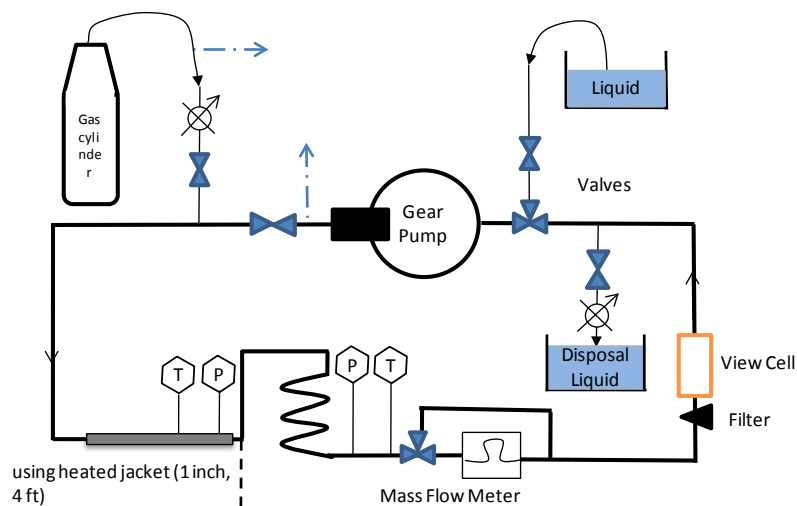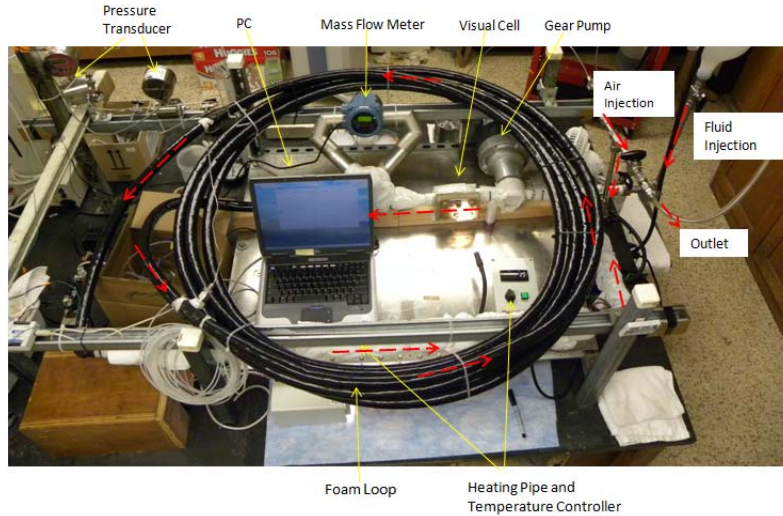
b

Figure 24. The recirculating loop for foam rheology test

(a: schematic figure; b: photograph)

The foam rheology measurement consists of the following steps:

Step1: The pipe is cleaned by pre-flushing with a base solvent.

Step2: The loop is filled with the base solvent by the gear pump. Then, the system is heated to the desired temperature.

Step3: The pump and the drain valve are shut off. A back pressure such as 1000 psi is applied by the gas cylinder.

Step4: The base liquid is recirculated in the loop. The reference pressure differences and flow rates are recorded.

Step5: N_2 gas is introduced into the loop and the liquid phase is drained out through the drainage valve to the disposal tank.

Step6: As the desired quality is achieved, the two phase fluid is circulated at a flow rate of 1000 s^{-1} until the homogeneous foam is generated.

41

Step7: The data of the pressure differences and the flow rates are processed in the computer to obtain the wall shear stress, τ_w (=$d\Delta P/4L$) and the apparent shear rate, γ_w (=$8v/d$). The shear rate at the wall, γ_{w_R} is calculated as $-(3n'+1)\gamma_w/4n'$, where $n' = \ln(\tau_w)/\ln(\gamma_w)$. Then wall shear stress and the real shear rate at the wall can be fit to the power law model to get the flow behavior index n', the consistency index K', and further, the apparent viscosity, $\mu_a = -\tau_w/\gamma_{w\_R}$.

Step8: The step5 to step7 are repeated to investigate foam rheology at different qualities.

Dynamic Settling Test

During the test, the foams are circulated out of the loop and into the slot. At the same time, proppants are added to the flowing foams through the other hose. The proppant transport process is recorded by a video camera. The slot is made of transparent Lucite plate, with a dimension of 45''x 6'' x 0.16''. Figure 25 shows the schematic diagram and the photograph of the fracturing slot.
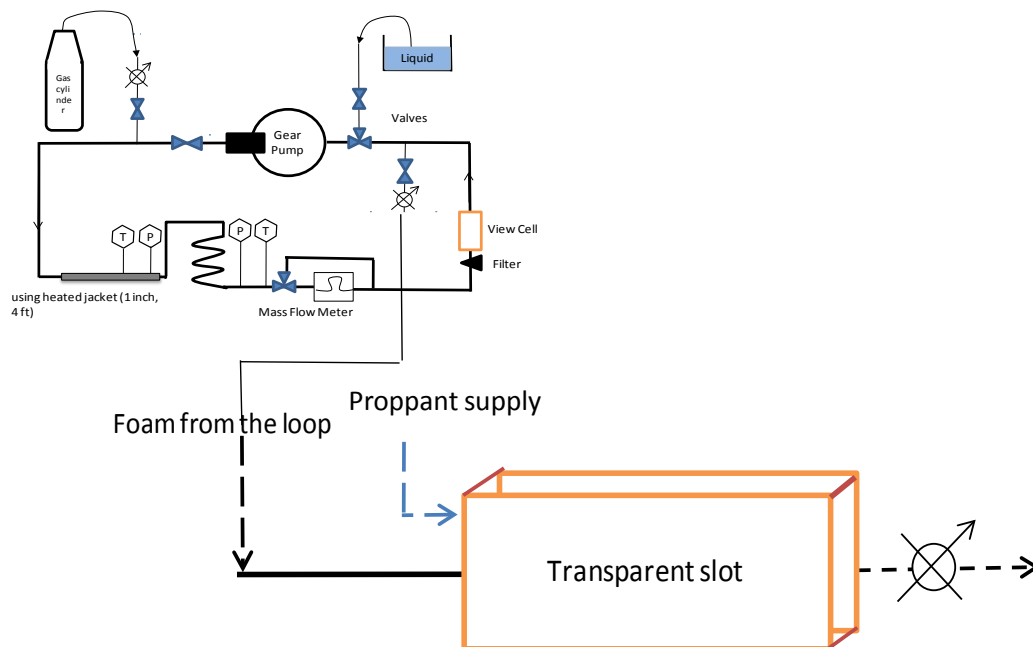
a

b

Figure 25. The one-pass strategy for dynamic settling test(a: schematic figure; b:

photograph)

Fluid Preparation: In the preliminary tests, one anionic surfactant, one nonionic surfactant, one cationic surfactant, and one amphoteric surfactant were used. Glycerol (99%) was used used as a stabilizer in some of the tests. The rheology of three different surfactant fluids (Fluid A: 0.5 vol% anionic surfactant fluid, Fluid B: Fluid A + 2 vol% glycerol, Fluid C: 0.5 vol% viscoelastic surfactant fluid) as well as their foams were evaluated in a flow loop under high pressure and temperature.

Proppants Preparation: Three types of ULW proppants provided by BJ Service Company and sands are used for the settling test. The physical properties of the proppants are listed in the table below,

Table 1. Proppants properties

Type	Specific gravity	Average Major Diameter	Characteristics
ULW1 Polymer (polymeric)	1.08	1.2 mm	Most deformable with a least young's modulus
ULW2 Resin-Walnut (resin coated ground walnut hull)	1.25	1.3 mm	Moderate deformable with a intermediate young's modulus
ULW3 Resin-Ceramic (resin coated ceramic)	1.75	1.0 mm	Most brittle with a highest young's modulus
Sand	2~2.5	1.1 mm	Similar to ULW3 Resin-Ceramic

Mathematic Model of Fracture Propagation

In this work, the PKN model is adopted to simulate fracture propagation. Below are the key assumptions:

1. The fracture height is constant and independent of fracture length.

2. The fracture fluid pressure is constant in the vertical cross sections perpendicular to the propagation orientation.

3. 2D plane-strain deformation is assumed in the vertical plane.

4. The cross section takes an elliptic shape with maximum width in the center.

$$w(x,z) = \frac{(1-v)}{G}(h^2 - 4z^2)^{1/2}(P[x] - \sigma_{h\min})$$

$$w_{\max}(x) = \frac{(1-v)h}{G}(P[x] - \sigma_{h\min})$$

$$w_{average}(x) = \frac{\pi}{4}w_{\max}(x)$$

$$(5)$$

5. The pressure through a narrow, elliptical flow channel can be given as,

$$\frac{\partial(P - \sigma_h)}{\partial x} = -\frac{64}{\pi h w_{\max}^3}\mu q$$

$$(6)$$

6. $P(x) = \sigma_{h\min}$ at the fracture tip.

7. The continuity equation for an incompressible fluid in one-dimensional flow is:

$$\frac{dq}{dx} + q_l + \frac{\pi}{4}h\frac{dw_{\max}}{dt} = 0$$

$$(7)$$

where leakoff term q_l takes the form,

$$q_l = \frac{2Ch}{\sqrt{t-\tau}}$$

$$(8)$$

where C is the leak-off coefficient given by experiment correlation, t is pumping time, and τ is the time when the fracture is first opened at a given position.

Combining the equations above, we derive the following non-linear differential equation:

$$-\frac{G}{64(1-v)h}\frac{d}{dx}\left[\frac{\partial(w_{\max}^4)}{\mu\partial x}\right] + \frac{8C}{\pi\sqrt{t-\tau}} + \frac{dw_{\max}}{dt} = 0$$

$$(9)$$

which is subjected to the following initial and boundary conditions,

45

$$w_{\max}(x, 0) = 0$$
$$w_{\max}(x \geq l_f, t) = 0$$

$$\left.\frac{\partial(w_{\max}{}^4)}{\partial x}\right|_{x=0} = -\frac{256(1-v)\mu}{\pi G}q_{inj} \tag{10}$$

For the non-linear problems, there are already analytical solutions for the simplest case (constant viscosity, constant injection rate) [Gidley et al., 1989]:

$L_D = 1.32\, t_D{}^{4/5}$; $w_D = t_D{}^{1/5}$ for low leak-off

$L_D = (2/\text{Pi})\, t_D{}^{1/2}$; $w_D = 0.798\, t_D{}^{1/8}$ for high leak-off \qquad (11)

where

$$t_D = \frac{1}{\pi^2}\left[\frac{(1-v)\mu h q_{inj}{}^2}{32 C^5 G}\right]^{-2/3} t \qquad L_D = \frac{1}{\pi}\left[\frac{(1-v)\mu h q_{inj}{}^5}{256 C^8 G}\right]^{-1/3} L \qquad w_D = \left[\frac{16(1-v)\mu h q_{inj}{}^2}{C^2 G}\right]^{-1/3} w \,.$$

Mathematic Model of Proppant Transport: The proppant is tracked with a separate transport equation as below,

$$\frac{d[wc]}{dt} + \frac{d[v_x k_{retx} wc]}{dx} + \frac{d\left[(v_z - v_{set})k_{retz} wc\right]}{dz} = 0 \tag{12}$$

where c is the concentration of the proppant, k_{ret} is the retardation factor calculated by experiment correlations, v_{set} is the proppant settling velocity calculated by Stokes Law, v_x and v_y are horizontal and vertical linear velocities of the slurry.

Assuming there is no vertical velocity of the fluid and k_{retx}, k_{retz} are dependent on inertial effect, concentrations and wall widths, the finite difference form of the above equation is given by,

$$\frac{w^{n+1}(i,j)c^{n+1}(i,j) - w^n(i,j)c^n(i,j)}{\Delta t}$$

$$= \frac{k_{retx}v_x{}^{n+1}(i-1,j)w^{n+1}(i-1,j)c^n(i-1,j) - k_{retx}v_x{}^{n+1}(i+1,j)w^{n+1}(i+1,j)c^n(i+1,j)}{2\Delta x}$$

$$+ \frac{k_{retz}v_{set}{}^{n+1}w^{n+1}(i,j+1)c^n(i,j+1) - k_{retz}v_{set}{}^{n+1}w^{n+1}(i,j-1)c^n(i,j-1)}{2\Delta z} \tag{13}$$

Rearranging the equation above, we can have,

$$\Delta x \Delta z w^{n+1}(i,j)c^{n+1}(i,j)$$

$$= \Delta x \Delta z w^n(i,j)c^n(i,j)$$

$$+ \frac{\Delta z \Delta t k_{retx}v_x{}^{n+1}(i-1,j)w^{n+1}(i-1,j)}{2}c^n(i-1,j) - \frac{\Delta z \Delta t k_{retx}v_x{}^{n+1}(i+1,j)w^{n+1}(i+1,j)}{2}c^n(i+1,j)$$

$$+ \frac{\Delta x \Delta t k_{retz}v_{set}{}^{n+1}w^{n+1}(i,j+1)}{2}c^n(i,j+1) - \frac{\Delta x \Delta t k_{retz}v_{set}{}^{n+1}w^{n+1}(i,j-1)}{2}c^n(i,j-1) \tag{14}$$

The horizontal retardation factor k_{retx} is affected by two effects, which are fracture walls and proppant concentrations. The correlation below is used to calculate the factor [Liu, 2006].

$$\frac{1}{w^2} = \frac{1}{w_{real}{}^2} + a\left(\frac{1}{d_p{}^2} - \frac{1}{w_{real}{}^2}\right)c^b \qquad for \quad c_{max} = 0.65 \qquad b = 0.8, a = 1.411 \tag{15}$$

$$k_{retx} = 1 + \left(\frac{d_p}{w}\right) - 2\left(\frac{d_p}{w}\right)^2 \tag{16}$$

The vertical retardation factor k_{retz} is calculated by multiplying independent correction factors for the inertial, proppant concentration and fracture walls [Liu 2006],

$$f(\text{Re}_p) = \frac{0.3736\mu^{0.57}}{\rho_f^{0.29}(\rho_p - \rho_f)^{0.29}d_p^{0.86}} \qquad f(c) = -5.9c^3 + 8.8c^2 - 4.8c + 1 \qquad f(w) = 0.563\left(\frac{d_p}{w}\right)^2 - 1.563\left(\frac{d_p}{w}\right) + 1 \tag{17}$$

$$k_{retz} = f(\text{Re})f(c)f(w)$$

The settling velocity can be given by Stoke's Law,

$$v_{stokes} = \frac{(\rho_p - \rho_f)gd_p^2}{18\mu} \quad ; \qquad v_{set} = v_{stokes} \tag{18}$$

Proppant Conductivity Correlation: The correlations of conductivity as a function of concentration are developed for three ULW proppants and sand.

Foam Rheology Correlation development: Foam quality is defined as the percentage of gas volume in the total volume of the foam.

$$Q = \frac{100 \times V_{g(T,P)}}{V_{g(T,P)} + V_l} \% \tag{19}$$

The foam rheology can be described by the power law equation below

$$Power\, Law : \tau = K\gamma^n \tag{20}$$

The apparent viscosity of the foam fluid at any shear rate is given as

$$\mu_a = -\frac{\tau_w}{\gamma_{wi}} = K\gamma_{wi}^{\,n-1} \tag{21}$$

By curve fitting the rheograms, the power-law model parameters (*n* and *k*) are obtained for different quality foams under different measured conditions. Based on these parameters, correlations are developed to predict the flow behavior and consistency indices for aqueous foams.

Leakoff Correlation Development: The fracturing fluid leakoff coefficient is described by the following equation [Gidley et al., 1989],

$$C = 0.171 \left[\frac{K\Delta P\phi}{\mu} \right]^{1/2} \qquad . \tag{22}$$

For water, the measured apparent viscosity is 2.44 cp at typical shear rate of 200 s^{-1} under 1000 psi and 155 F. For our nitrogen foams with a quality over 60% at the same measured condition,

the apparent viscosity is measured as 24-114 cp. According to the leakoff correlation Eq. 22, the foam coefficient should be 1/3-1/7 of that for water. Assuming that the matrix permeability is 100 nD, the porosity is 4%, and the pressure difference is 1000 psi, the water leakoff coefficient is calculated to be 5.67E-07 $m/s^{1/2}$. Since the leak-off coefficient for foam is expected to be 1/3-1/7 of that for water; it is assumed that the foam leakoff coefficient is 1E-7 $m/s^{1/2}$.

Results and Discussion

Physical Properties

	ULW-1	ULW-2	ULW-3
Average	1	0.67	0.82
Maximum	1	0.76	0.94
Minimum	1	0.53	0.67

Table 2. Comparison of Riley's sphericity for the three proppants tested

Sphericity: ULW-1, a polymeric proppant, was uniformly spherical to the naked eye and this sphericity was reflected in the ten particles tested. The average value for Ψ_R came out to be one with zero standard deviation. The average spericity is listed in Table 2 for the three proppants. Given below is a two-dimensional image for a ULW-1 particle which was used for sphericity evaluation.
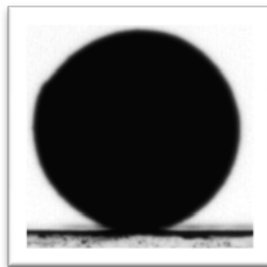
Figure 26. Image of an ULW-1 proppant

ULW-2, which is a ground walnut hull coated/impregnated by a resin, was angular. For the ten particles tested, the average value for Ψ_R came out to be 0.62 with a maximum value of 0.69 and a minimum value of 0.49.
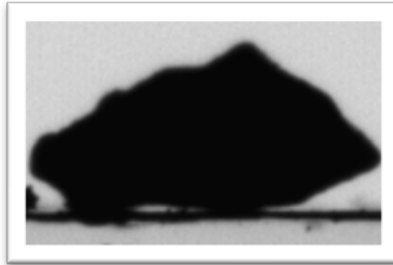
Figure 27. Image of an ULW-2 proppant

ULW-3, a ceramic proppant, gave an intermediate value for sphericity, i.e., $\Psi_R = 0.78 \pm 0.11$. The distribution of sphericity is shown in Figure 29.
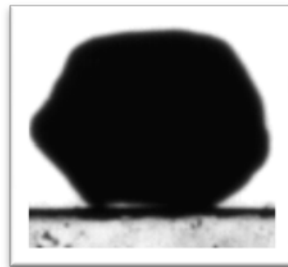
Figure 28. Image of an ULW-3 proppant
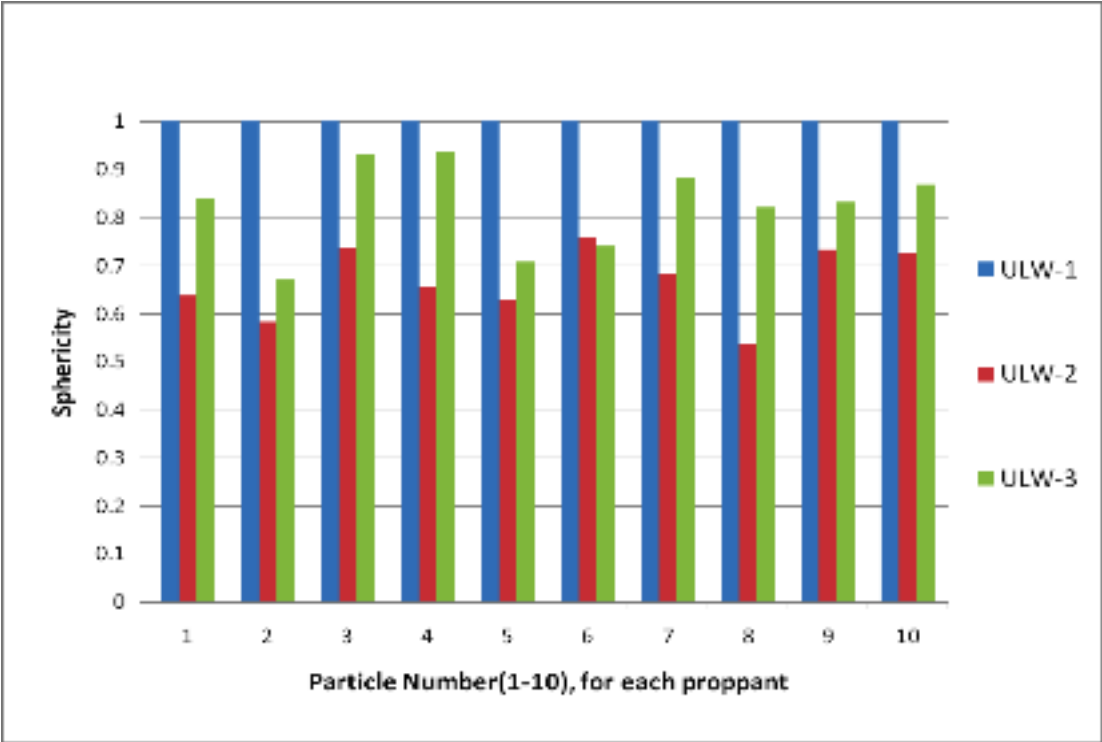
Figure 29. Comparison of Riley's sphericity for ten particles of each proppant

Size Distribution: The size distribution of each proppant tested was determined by sieve analysis and was made available to us by the supplier. The size distributions are shown in Figure 30. ULW-1 has a sieve size of 14-40 and the distribution is the broadest of the three proppants tested. ULW-2 has a sieve size of 14-30. ULW-3 has a sieve size of 20-35, the narrowest.
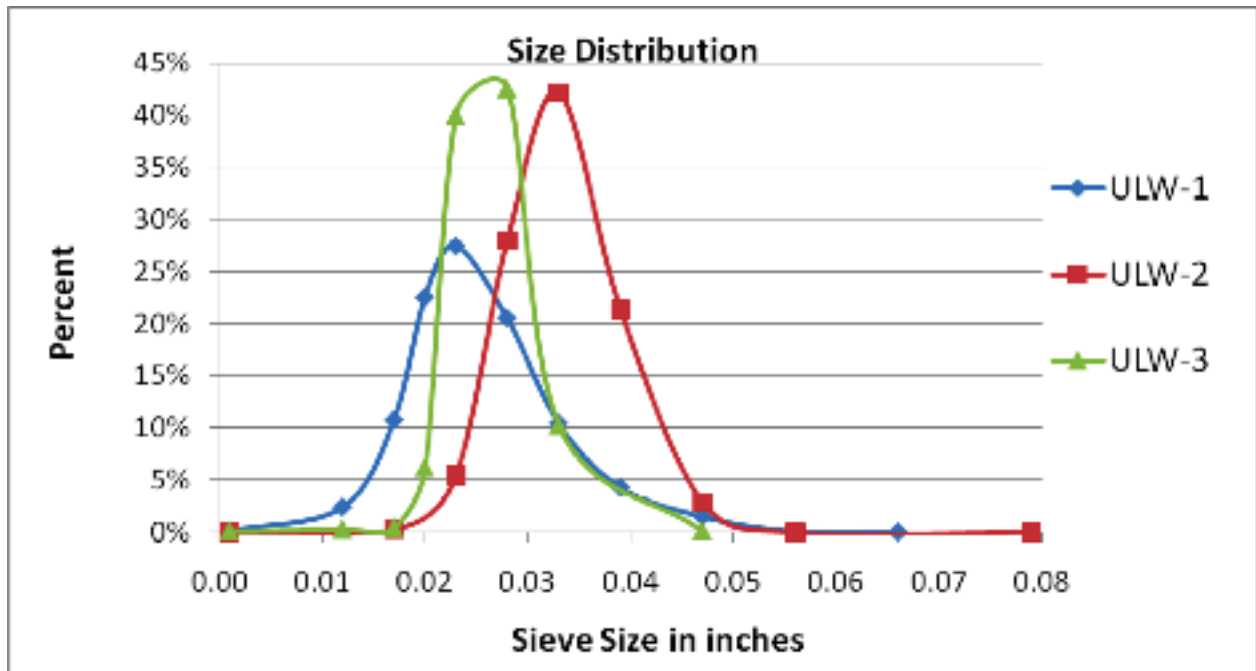
Figure 30. Sieve size distribution

Bulk Density: The specific gravities of the individual proppant particles were provided to us by the supplier. In this study, we were interested in finding out the bulk density and the respective porosity of the proppant pack of the individual ULW's under no confining stress. This porosity would be compared to the porosity of the proppant pack under closure stress, when we conduct flow capacity tests in the future. The bulk density and porosities are listed in Table 3. Note that with increasing specific gravity, the bulk density increases and the corresponding porosity decreases.

	ULW-1	ULW-2	ULW-3
Specific Gravity	1.08	1.25	1.75

53

Bulk Density (g/cc) (without any closure stress)	0.6	0.8	1.2
Porosity of Pack (without any closure stress)	44 %	36 %	31%

Table 3. Bulk Density and Porosity Measurements

Compatibility of Proppants: The proppants were soaked in water (for about a month) and surfactant-water solutions (for about a week). Their appearance did not change. It appears that the proppants are compatible with the fracturing fluids.

Mechanical Behavior

Minimum Horizontal Stress: The stresses which the proppants endure in the fractures are the effective minimum stress, which usually is in the horizontal direction. The absolute vertical stress, σ_v is given by

$$\sigma_v = (1.1 \text{ psi/ft}) \text{ h, where 'h' is the depth in feet.} \tag{23}$$

The effective vertical stress, σ_v' is given by

$$\sigma_v' = \sigma_v - \alpha \, p, \tag{24}$$

where α is Biot's poroelastic constant and has a value of 0.7 for hydrocarbon bearing formations[1] and p is the pore pressure. The effective minimum horizontal stress, σ_H' is given by

$$\sigma_H' = (\nu/ (1-\nu))\, \sigma_v', \qquad\qquad\qquad (25)$$

where ν is the Poisson's ratio, and has been assigned an average value of 0.3 for this study. This value might be different for different formations. We will focus our attention on maximum possible value for minimum horizontal stress, which the proppants are expected to endure when the reservoir is completely depleted. These values range from around 2400 psi to 6600 psi, and have been plotted in Figure 31 for the gas plays in discussion. The figure also supports the idea, that, "No two shale gas plays are alike". In this study, we focus on application of ultra light weight proppants in Barnett shale at about 90 $^{\circ}$C.
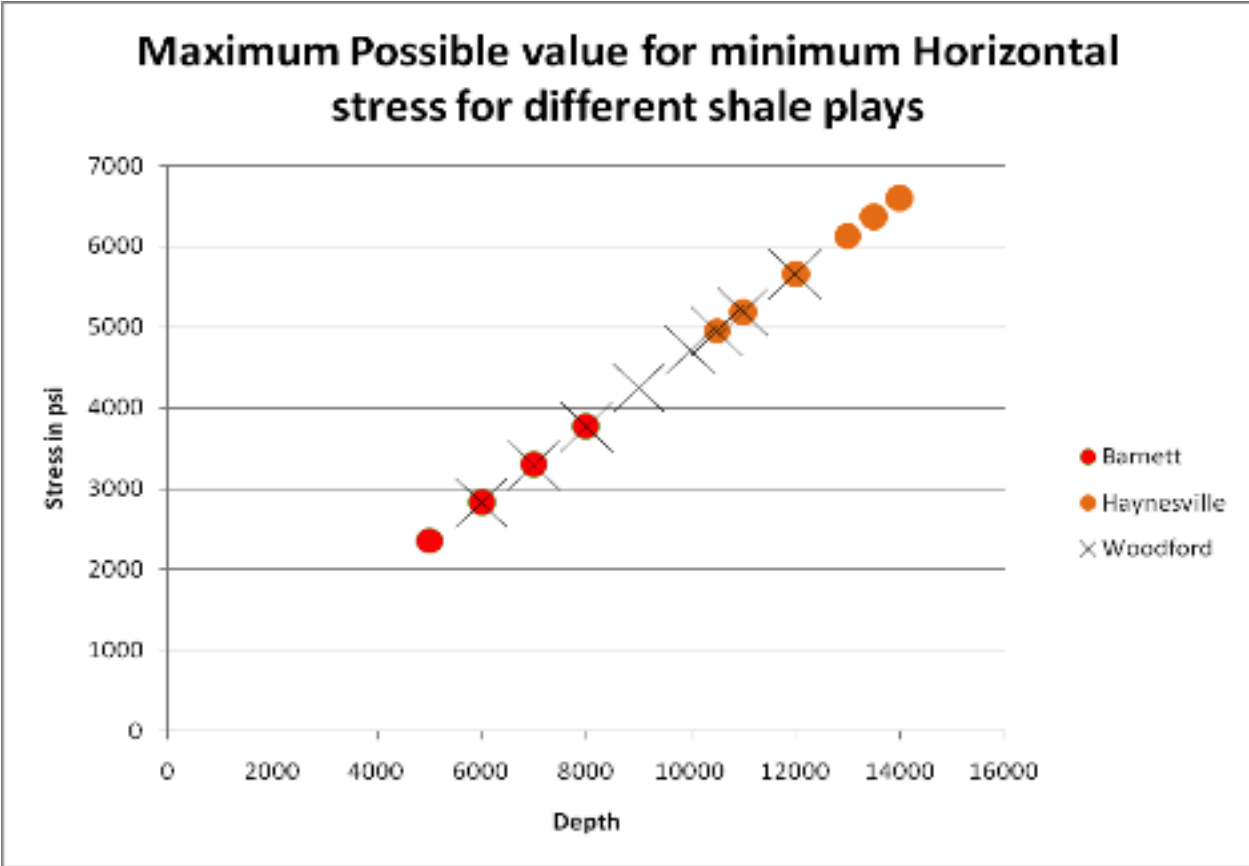
Figure 31. Maximum Possible values for minimum horizontal stresses for different shale gas

plays

Proppant Pack Stress Test and Fines Formation: Stress test was conducted on 1ml (bulk

volume) pack of each proppant, simulating a proppant pack between fracture faces. The aim of

this test was to study the strength of a pack as well as the formation of finer particles as a result

of crushing. Figures 32-34 show the stress-strain for the three proppant packs. It is to be noted

that a high failure stress of a proppant pack alone does not necessarily mean its applicability to a

formation with lower stress. This is because, even if the proppant pack does not really get

crushed on application of typical reservoir stresses, the proppants in the pack might deform

making the whole pack almost impermeable. Again, the conductivity of proppants would be

56

evaluated in future. The failure stress for ULW1 Polymer proppant pack is about 40,000 psi (Figure 32). The amount of fines created at the end of the experiment is also reported in the figure captions and they are small (<5 %). ULW2 Resin-Walnut pack shows (Figure 33) a behavior similar to that of ULW1 Polymer. ULW3 Resin-Ceramic shows a similar failure stress (Figure 34), but much higher fines formation. The blue band shown in each figure is the expected total stress in Barnett shale formation. The failure stress of proppant packs for each proppant was significantly higher than the stresses encountered in any shale formation.
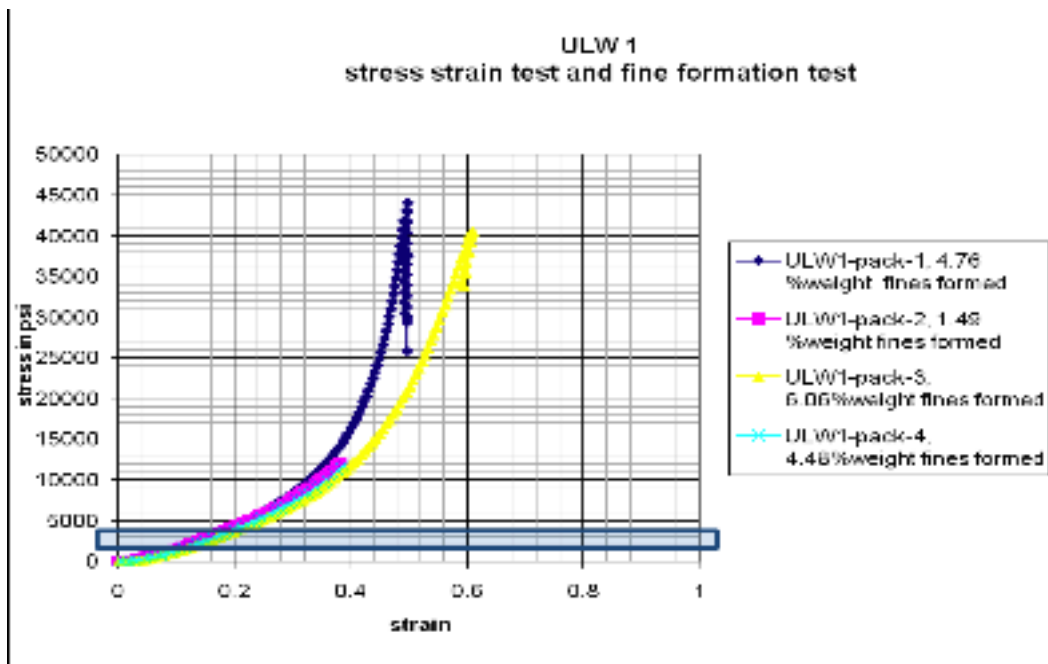
Figure 32. Deformation of ULW-1 proppant pack at room temperature
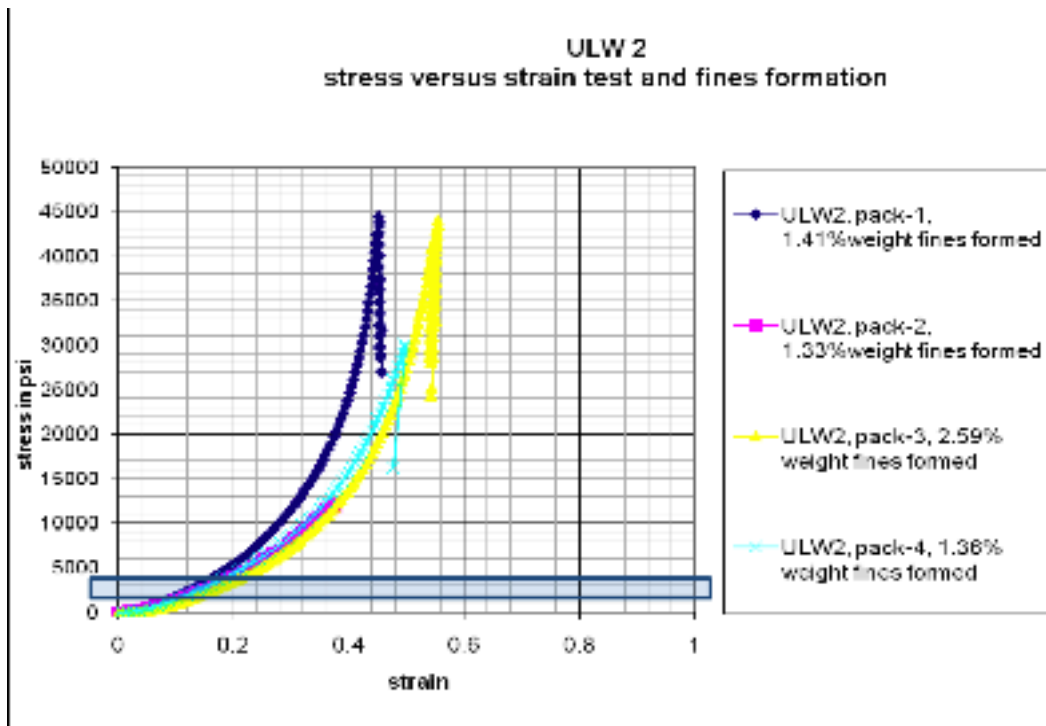
Figure 33. Deformation of ULW-2 proppant pack at room temperature
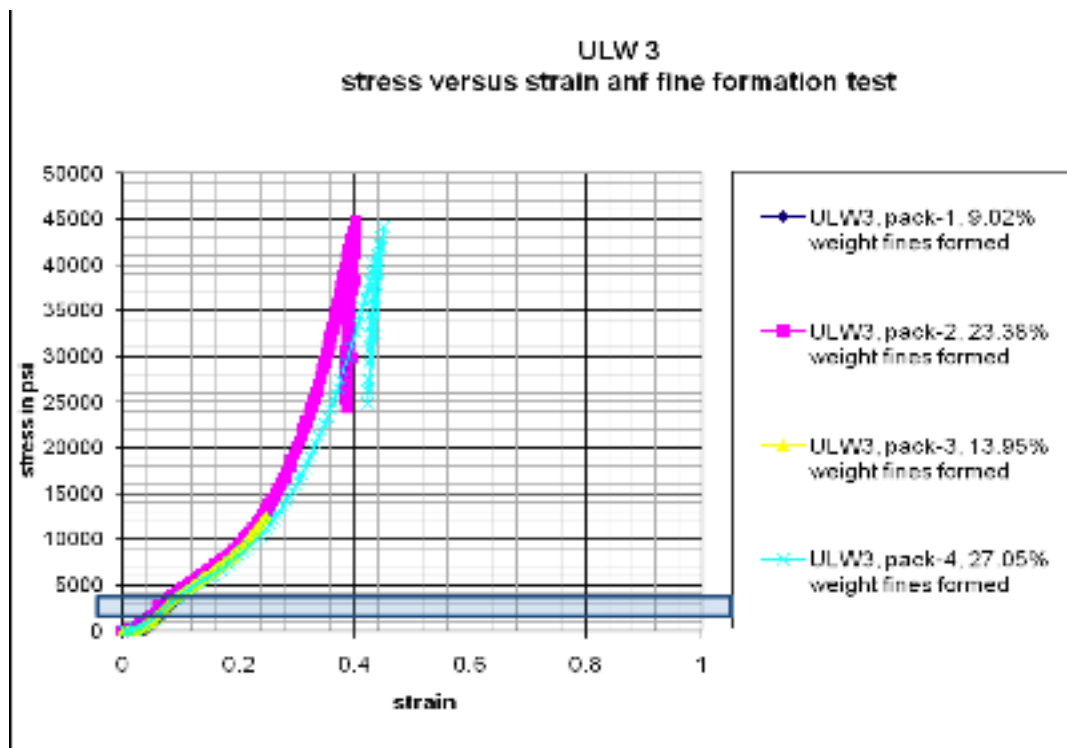
Figure 34. Deformation of ULW-3 proppant pack at room temperature

The amount of proppant lost because of formation of finer particles for each of the tests is presented in Table 4. The fines generation in ULW1 Polymer and ULW2 Resin-Walnut are small.

	Maximum stress reached <= 45000 psi	Maximum stress reached <= 45000 psi	Maximum stress reached <= 30000 psi	Maximum stress reached <= 30000 psi
ULW 1	4.76 %	6.06 %	1.49 %	4.48 %
ULW 2	1.41 %	2.59 %	1.33 %	1.36 %
ULW 3	23.38 %	27.05 %	9.02 %	13.95 %

Table 4. Percent loss in weight of proppant pack due to formation of finer particles

Particle Stress Tests: After the strength test of the pack, we evaluated the strength behavior of individual proppant particles to examine the variation among the proppants. The mechanical behavior was tested at both room temperature and Barnett shale temperature (90° C) to assess the change in behavior of proppants with the increase in temperature and also to determine the applicability of the proppants in Barnett shale.

ULW-1
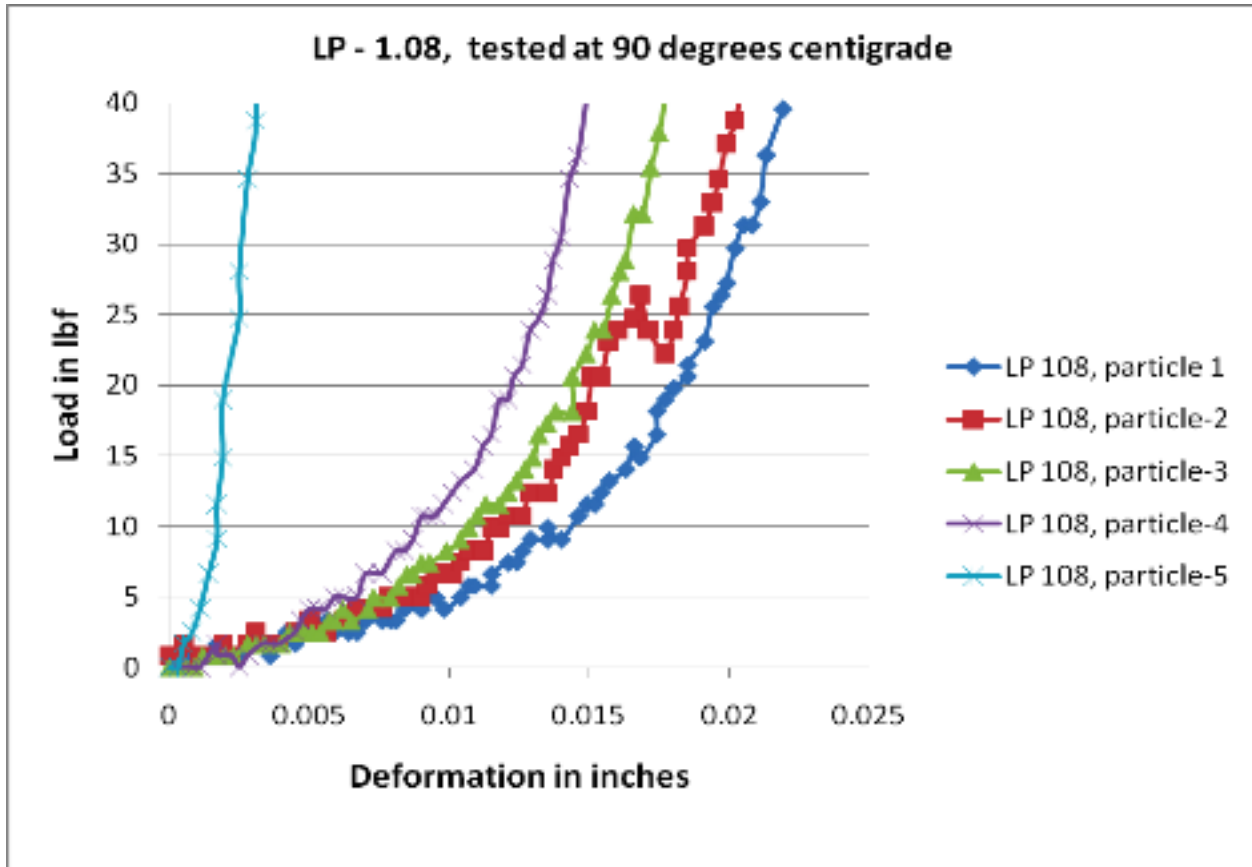
Figure 35. Strength test of ULW-1 done at 90 $^{\circ}$C

Figure 35 shows the applied load and the resulting deformation for 5 single ULW-1 particles tested at 90 $^{\circ}$C. Particles 1, 3-5 do not show definite failure points. Particle 2 fails at 27 lbf. Figure 36 shows the applied load and the resulting deformation for 10 single particles tested at the room temperature. The load at failure is lower at the room temperature compared to that at 90 $^{\circ}$C. These proppants can withstand the stress without getting crushed. This is due to the deformable nature of this polymeric proppant. Of course, these proppants deform under stress and reduce the fracture conductivity. Fracture conductivity would be studied in the next task when the applicability of the proppant can be determined.
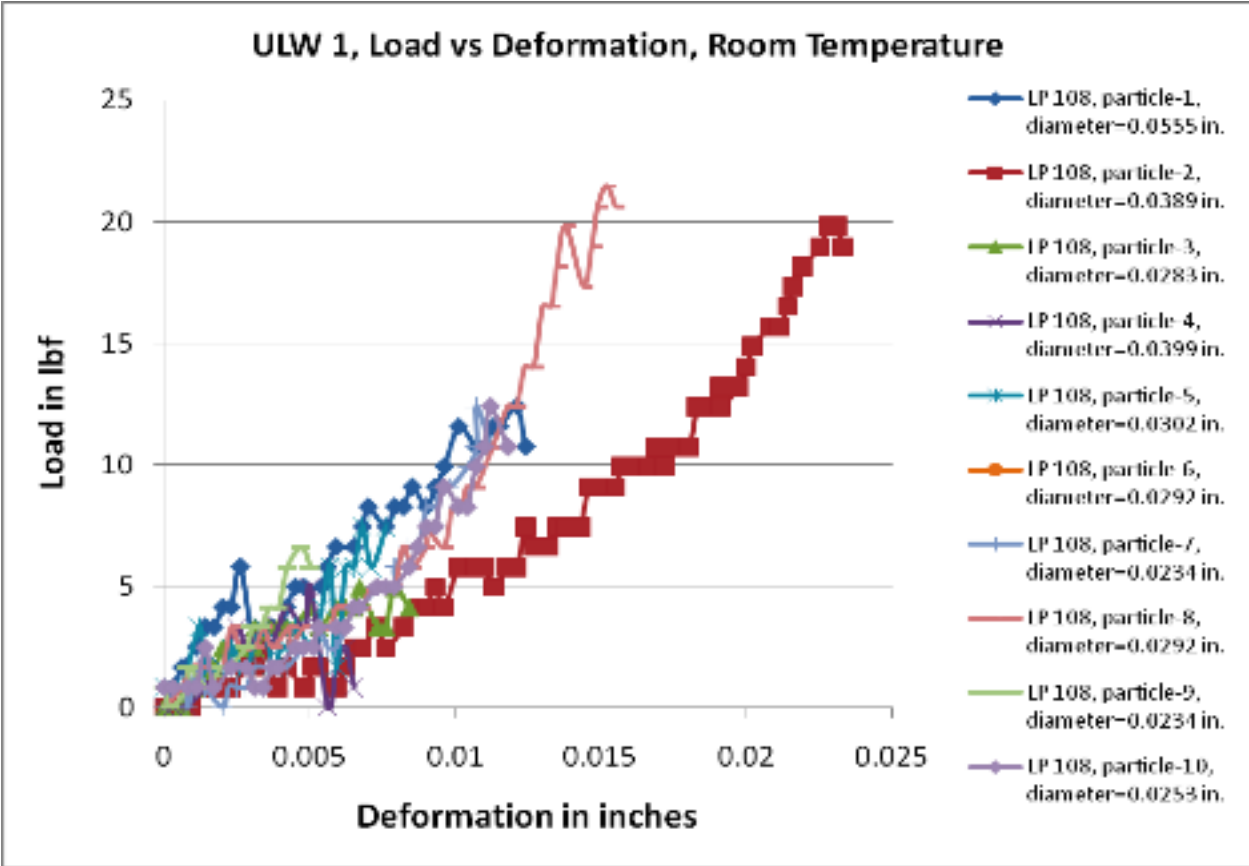
Figure 36. Strength test of ULW-1 done at room temperature
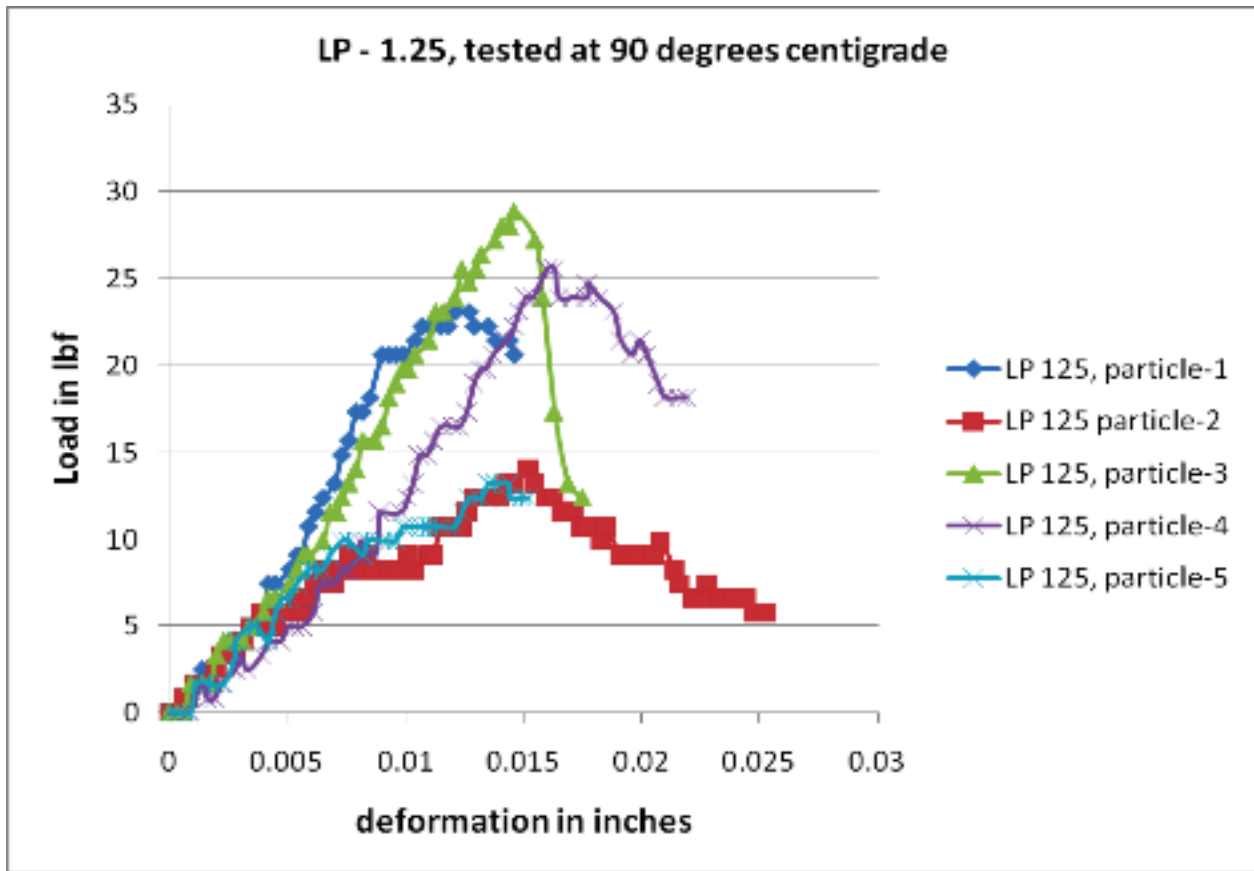
ULW-2

Figure 37. Strength test of ULW-2 done at 90 ^{o}C
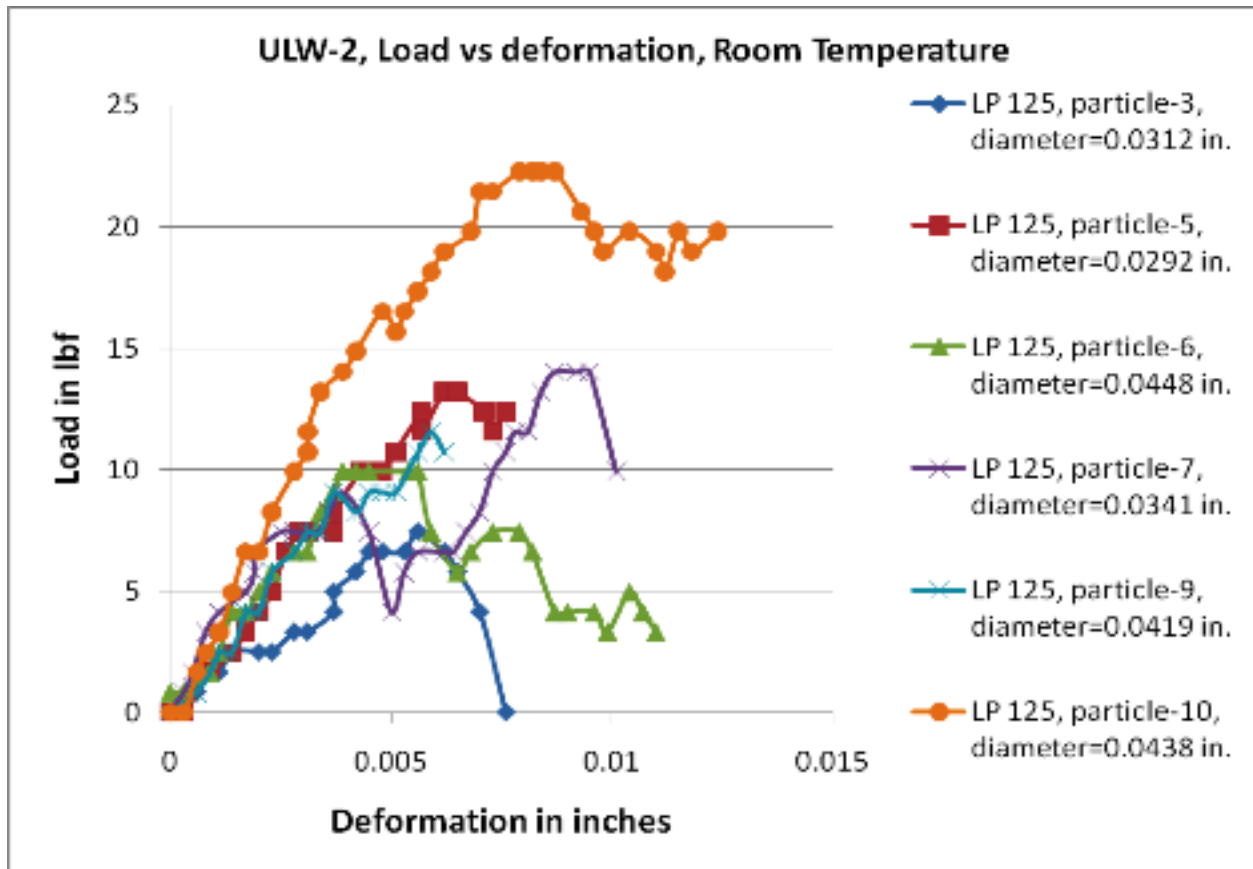
Figure 38. Strength test of ULW-2 done at the room temperature

Figures 37-38 show the applied load and the resulting deformation for 5 single ULW-2 particles tested at 90 ^{o}C and room temperature, respectively. At the higher temperature, the curves seemed to have stretched, i.e., deformations are larger for the same load applied, indicating increase in elasticity of the proppants with increasing temperature.

ULW-3

Figures 39-40 show the applied stress and the resulting strain for 5 single ULW-3 particles tested at 90 ^{o}C and room temperature, respectively. The deformations at which individual particles fail

are very low compared to those of the previous two proppants, indicating the brittle nature of

ULW-3, a ceramic proppant.

ULW 3, tested at 90 degrees centigrade
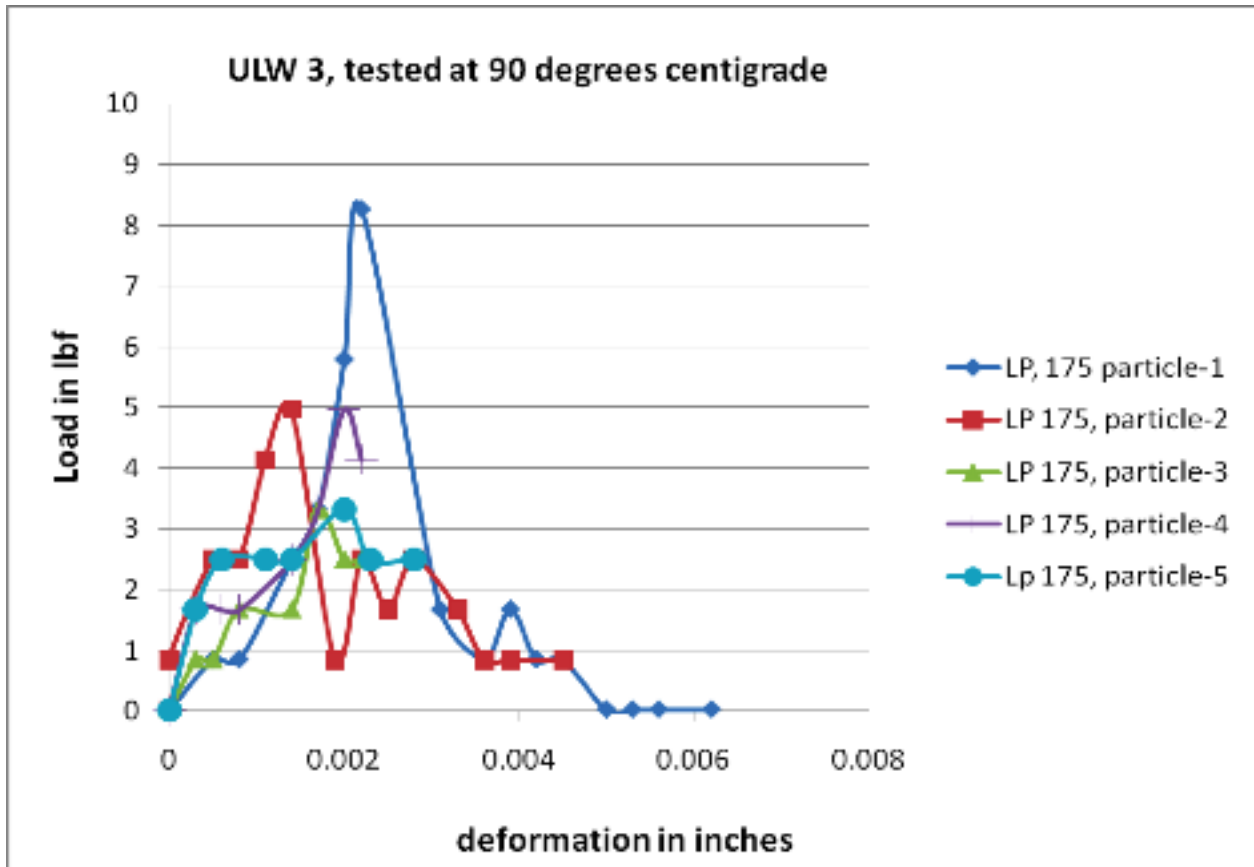
Figure 39. Strength test of ULW-3 done at Barnett shale temperature of 90° C
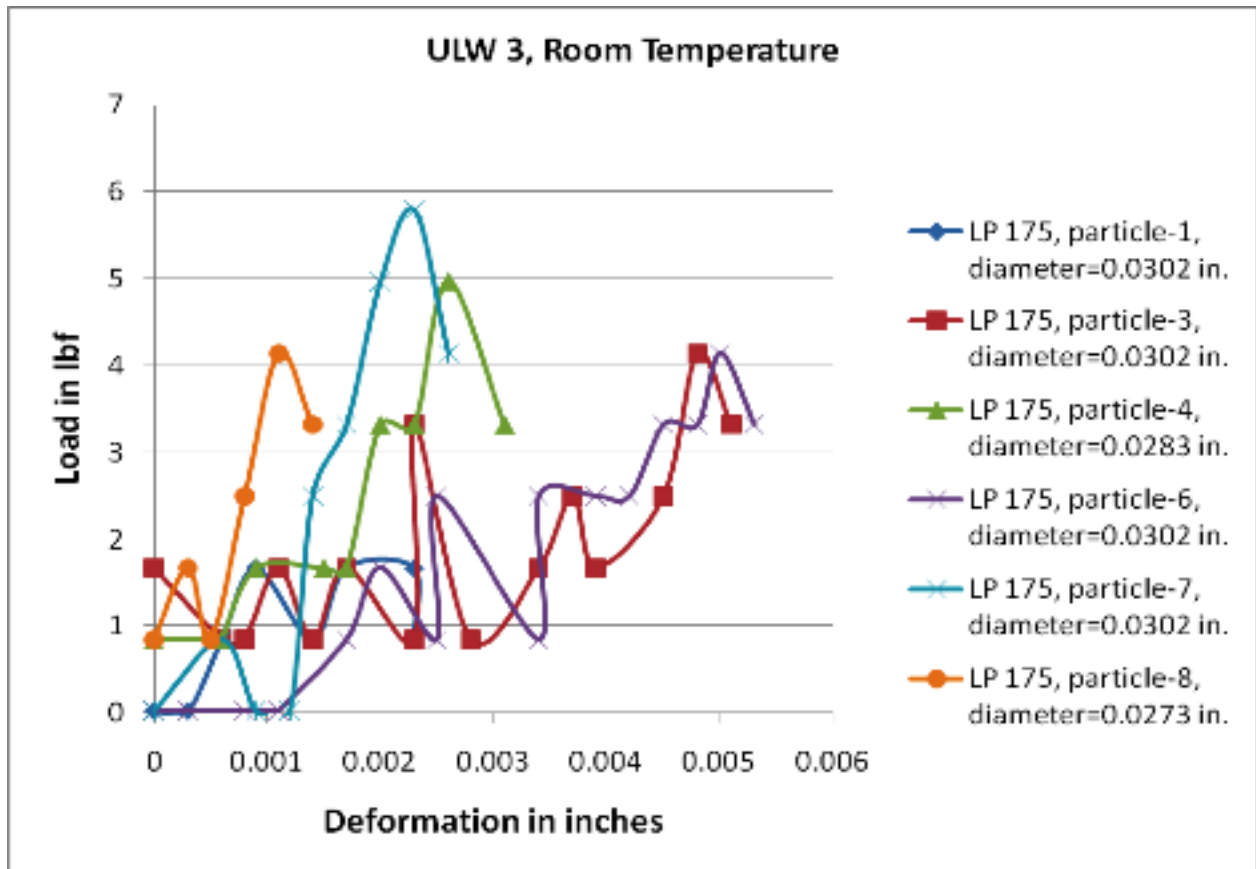
Figure 40. Strength test of ULW-3 done at room temperature

Deformability: The load-deformation data for individual proppants have been converted to "effective stress" versus "effective strain" plots (Figures 41-42). The values of stress and strain have been calculated on the basis of the initial dimensions of the particle. It is an effective value because the particles deform and the distribution of stress is not uniform on round particles. It is to be noted that the strain scale in all the three plots is kept constant to show the elasticity of proppants with respect to each other. A higher slope (or higher value of Young's modulus) indicates less elasticity.

Figure 41 shows that ULW-1 is the most deformable. Many particles deform beyond an effective strain of 0.5 without failing. The Young's modulus varies significantly between

particles. The largest particle had the highest Young's modulus in this sample. ULW-2 is not as deformable as ULW-1. Many of the particles fail at about 0.2 effective strain. Young's modulus for these particle are higher than those for ULW-1. ULW-3 particles are brittle; many particles fail below 0.2 effective strain. The Young's modulus is the highest for ULW-3 particles.
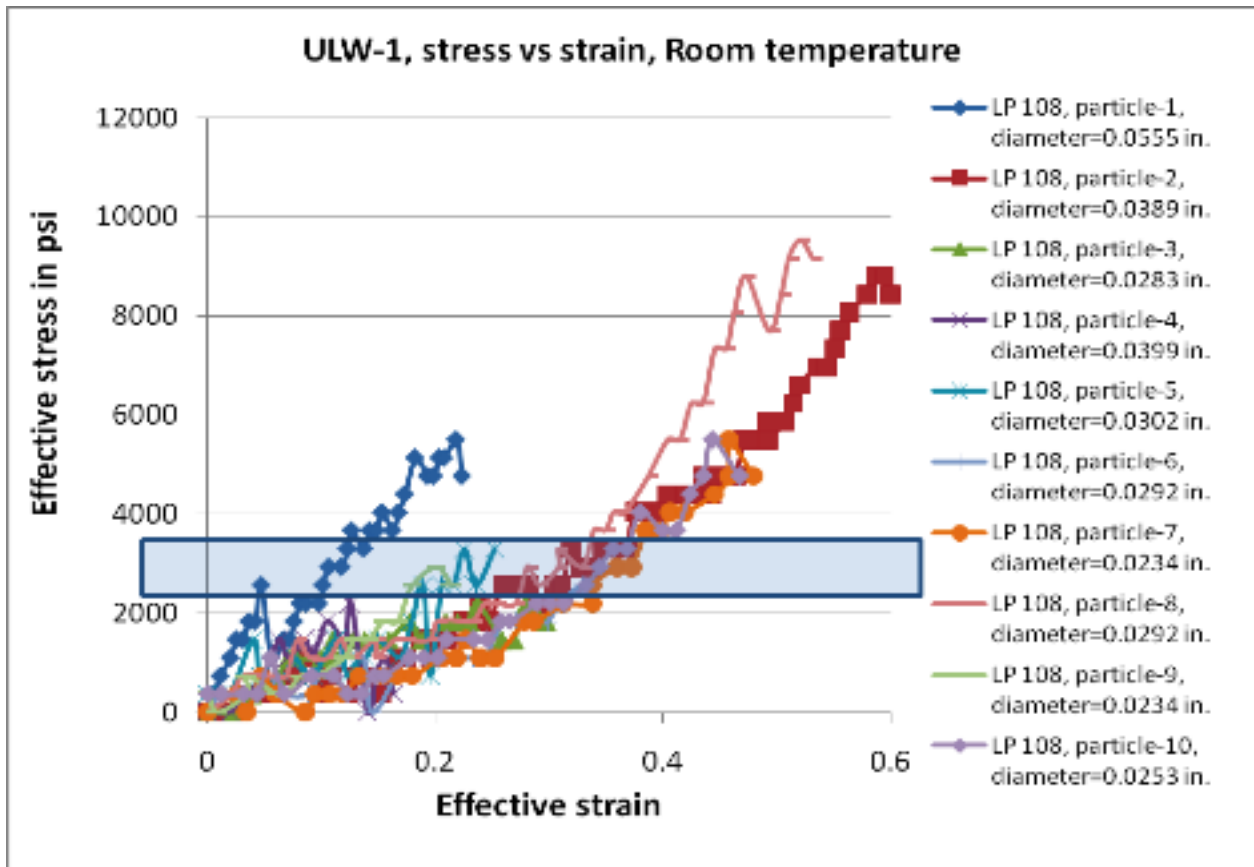
Figure 41. Elastic modulus of ULW-1 at room temperature
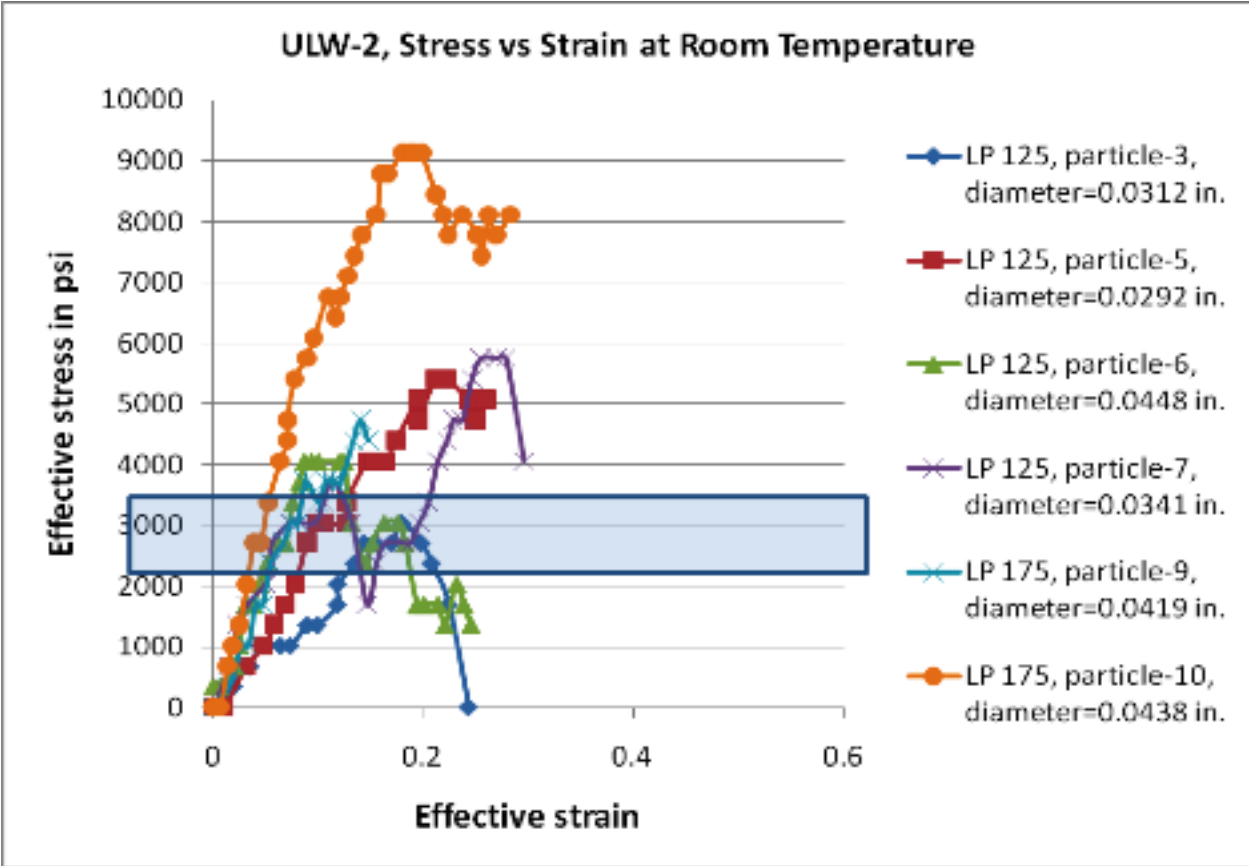
Figure 42. Elastic modulus of ULW-2 at room temperature
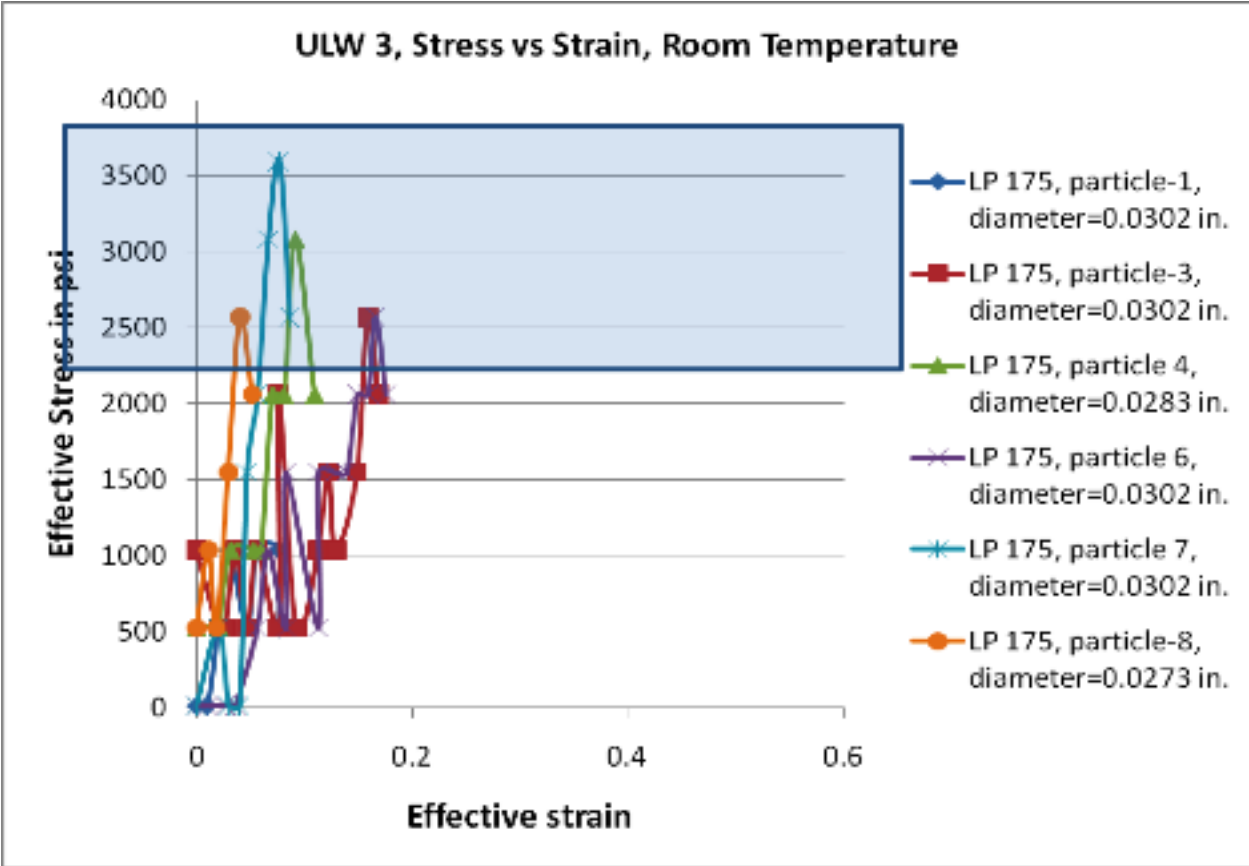
Figure 43. Elastic modulus of ULW-3 at room temperature

Young's moduli are calculated from the above figures. At the room temperature, the Young's modulus of ULW-1 is around 15,400 psi. For ULW-2, at the same temperature, this value is higher around 38,900 psi. ULW-3 shows the highest value of Young's modulus of around 41,100 psi. At the end of each test, the particles were closely inspected with naked eye. It was found out, ULW-3 shattered into pieces confirming its brittle nature. ULW-1 particles stayed intact. They got flattened with increasing stress, but never got broken into several pieces. ULW-2 showed moderate deformability.

Fracture Conductivity

Conductivity vs Proppant Cencentration @ various stress levels, ULW-1
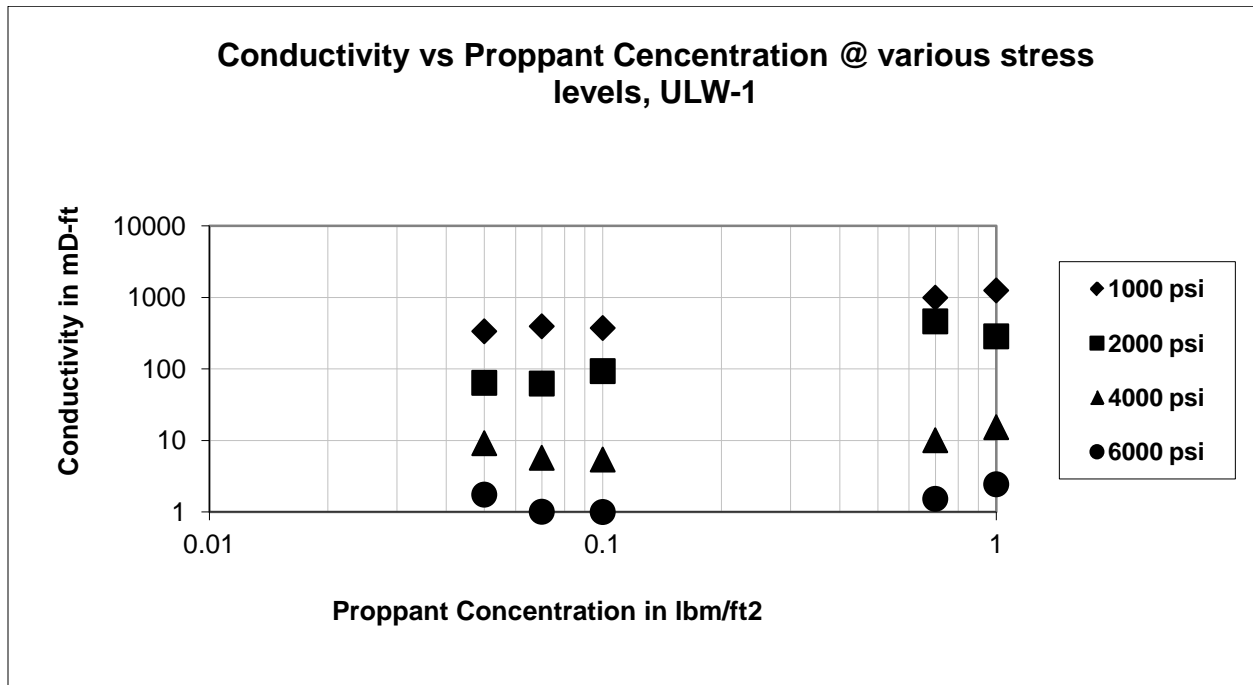
Figure 44. A plot of conductivity vs. proppant concentration at various stress levels for ULW 1

Figure 44 shows the conductivity for ULW 1, a polymeric proppant. As the proppant concentration increases, the conductivity first decreases and then increases. The decrease in conductivity with the increase in proppant concentration is due to the decrease in porosity in partial monolayers. The increase in conductivity with the increase in proppant concentration is due to the increase in width of the fracture due to multilayer thick proppant packs. At a stress of 1000 psi, a thick proppant pack (0.7 lbm/ft^2 to 1 lbm/ft^2) provides conductivity double that of either a full monolayer or a partial monolayer (0.07 lbm/ft^2 to 0.1 lbm/ft^2). For a stress level of 2000 psi, a thick pack of 0.7 lbm/ft^2 shows the best conductivity at this stress. But at higher stress levels, the partial monolayers turn out to be as effective as thick proppant packs. Multilayer packs get squeezed more at a higher stress and lose their porosity and conductivity to a greater extent.

Thus partial monolayers of these proppants should be preferred over multilayer packs in these fracturing treatments. The conductivities measured for these proppants (1-10 mD-ft) are a lot lower than those for Ottawa sand, but high enough for fractures in shales and tight gas reservoirs where permeability is of the order of 10^{-4} mD. If the conductivity ($k_f w$) is 1 md-ft, the fracture half length (X_f) is 1000 ft and the permeability of the shale is 10^{-4} md, then the dimensionless fracture conductivity, F_{CD} equals 10. As shown in Figure 3, this dimensionless fracture conductivity enhances gas production significantly.
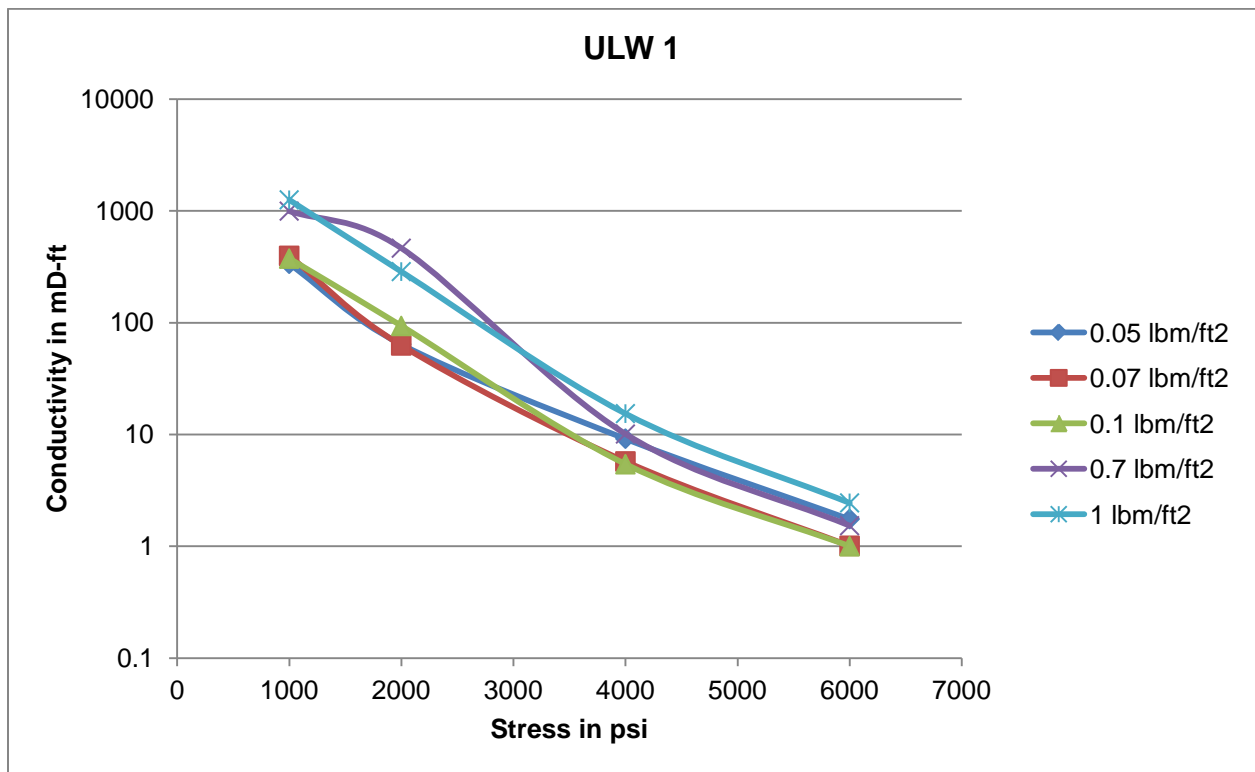
Figure 45. A plot of conductivity vs. stress for various proppant concentrations for ULW 1

Figure 45 shows the same data, plotted a little differently, mainly to highlight the deteriorating performance of proppants with increasing stress. As the proppant is polymeric, it gets squeezed as the stress increases leading to lower porosity and conductivity. These proppants can be used in reservoirs like Barnett, but not for much deeper reservoirs.

ULW 2

The conductivity of ULW 2 proppants are shown in Figure 46; they behave similar to the ULW 1. A partial monolayer of proppant (0.07 lbm/ft^2) provides as much conductivity as thick packs, at all stress levels. A full monolayer (0.1 lbm/ft^2 to 0.4 lbm/ft^2) on the other hand shows least conductivity when compared to other concentrations of proppant at various stress levels. Again, the conductivity values are high enough to allow stimulation of shale formation at various stresses. Figure 47 shows the decrease in conductivity with the increasing stress. These proppants get squeezed and the conductivity decreases with stress because the Young's modulus is small for these walnut hull proppants.
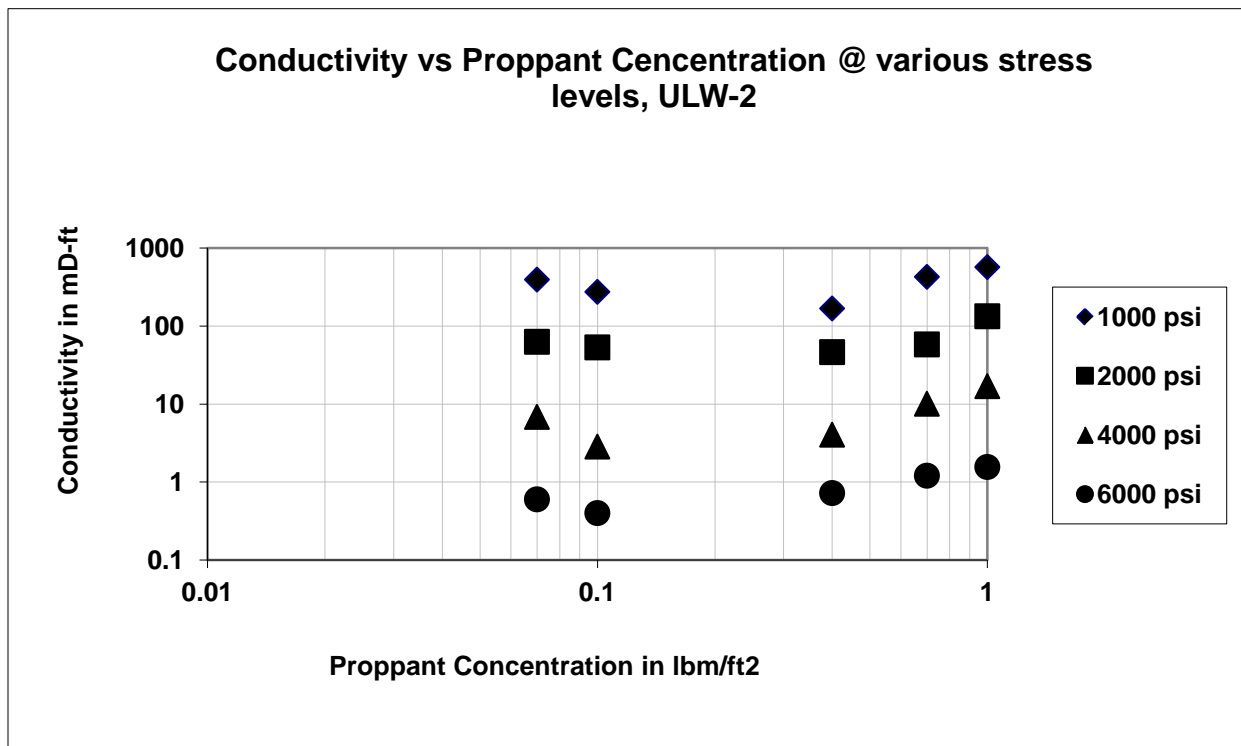
Figure 46. A plot of conductivity vs. proppant concentration at various stress levels for ULW 2
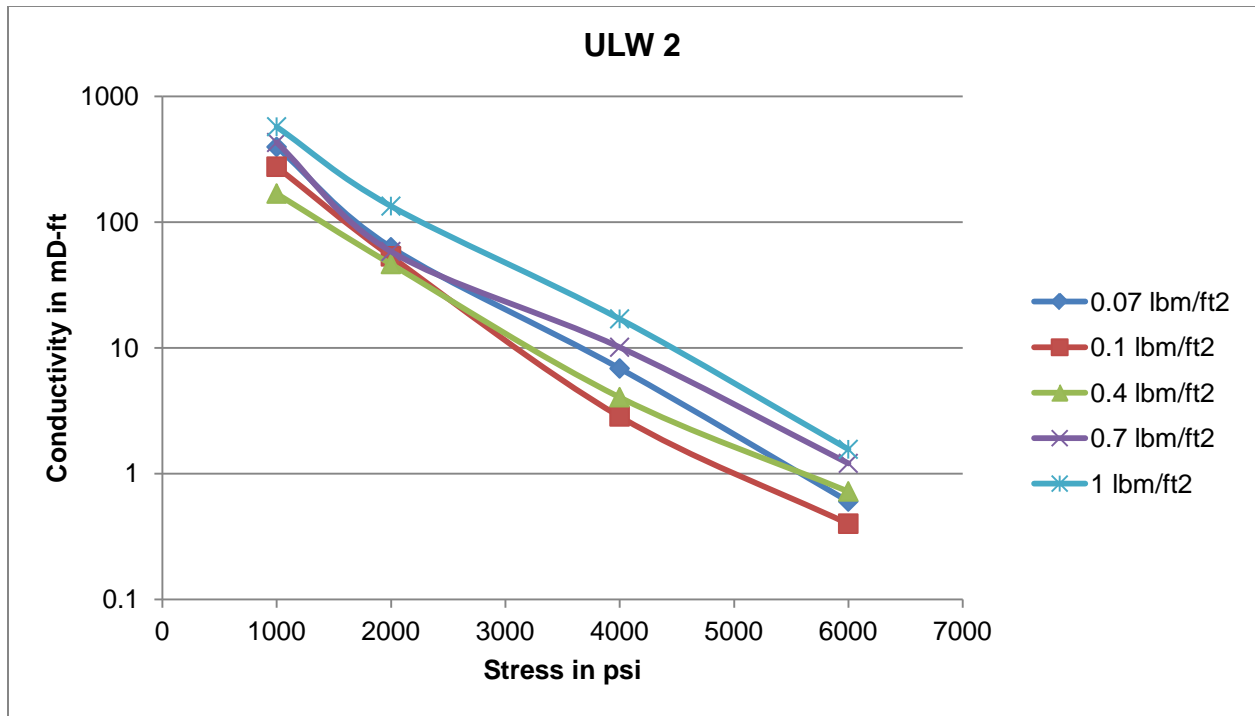
Figure 47. A plot of conductivity vs. stress for various proppant concentrations for ULW 2

ULW 3

For ULW 3, as shown in Figure 48, the conductivity values for thick proppant packs are ten times higher than those of ULW 1 and ULW 2. However, for partial monolayers, the conductivity is almost equal to those of the other two proppants. One striking feature of these ceramic proppants is that their partial monolayers are not as effective as their thick packs. The conductivity is a monotonic function of the proppant concentration. This is due to the fact that these proppants are more rigid (higher Young's modulus) than the other two proppants. These proppants can be used as thick packs for higher conductivity. The conductivity values of both partial monolayers and thick packs are again high enough for stimulating shale gas reservoirs. Figure 49 shows the decreases in conductivity with an increase in stress for ULW 3. The decrease in conductivity for a thick proppant pack is not as much as it is for the other two

proppants. The smaller decrease is due to the higher rigidity of the resin-coated ceramic proppants.
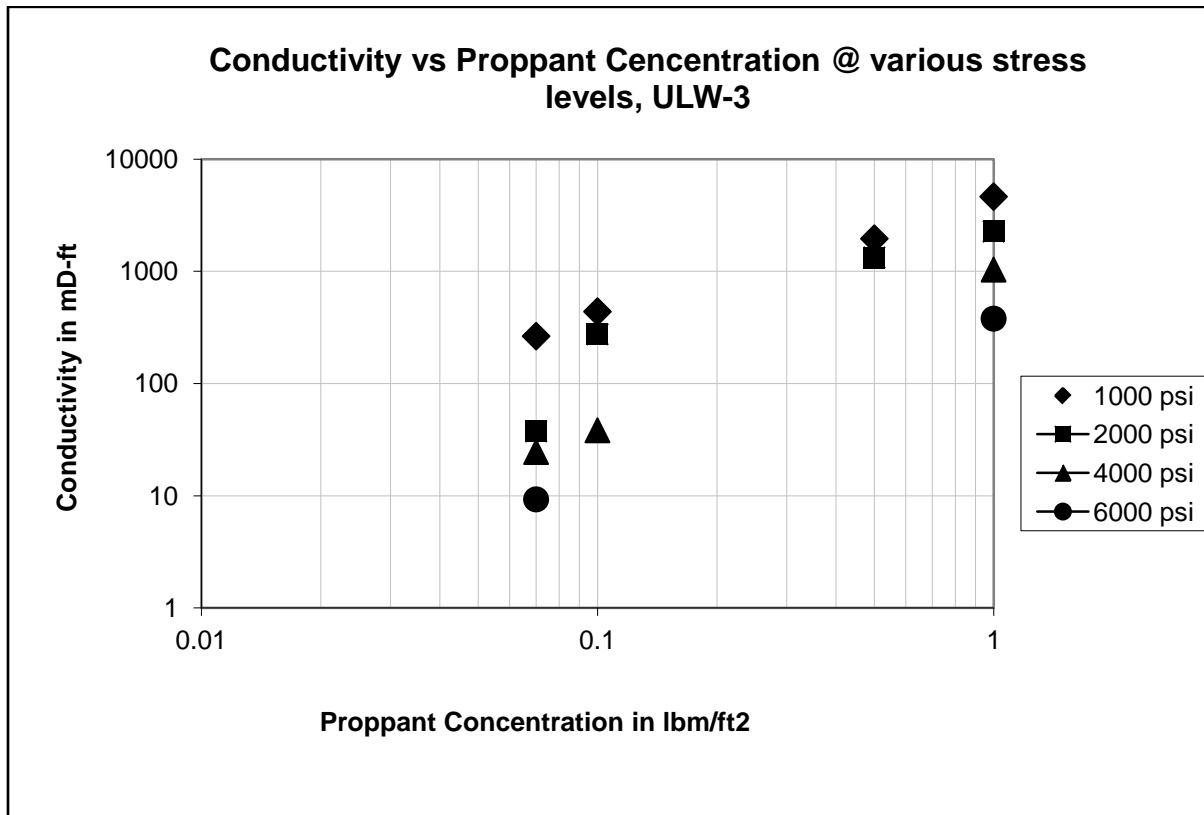
Figure 48. A plot of conductivity vs. proppant concentration at various stress levels for ULW 3
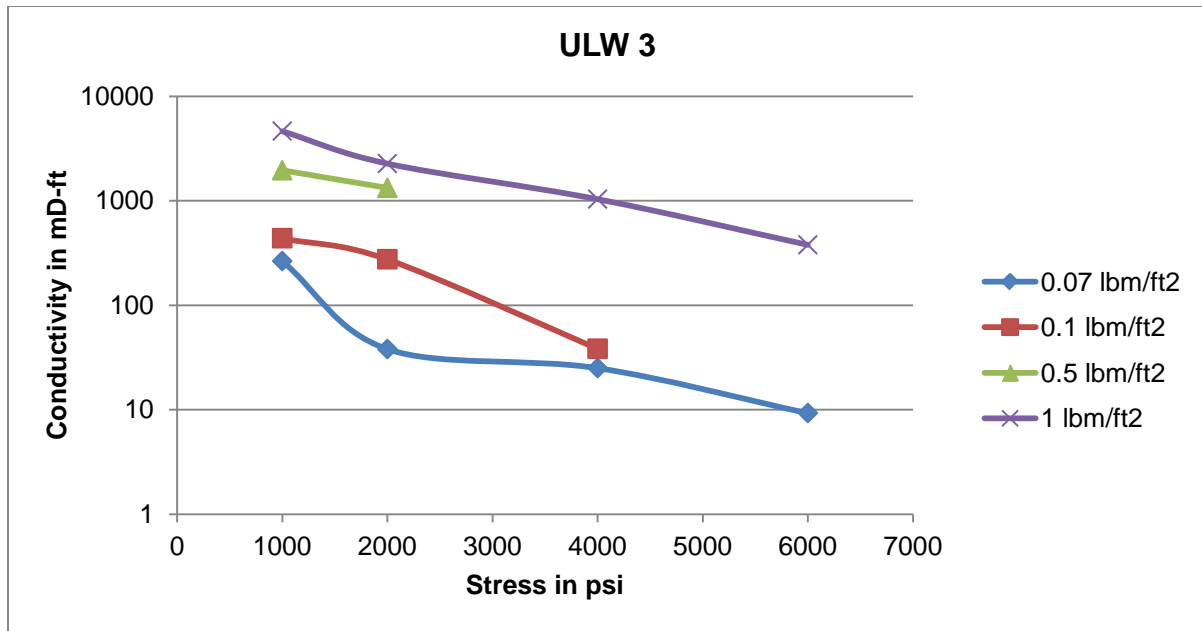
Figure 49. A plot of conductivity vs. stress for various proppant concentrations for ULW 3

Foam Static Stability Test

Effect of Composition

Figure 50 shows the foam stability with three surfactants Anionic 1, Cationic 1, and Nonionic NP30. All samples have a surfactant concentration of 1 wt%. The foams have the same bubble size of around 2mm in diameter. The foam volume is monitored as a function of time. The half-life time (defined by time taken to reach half the initial foam volume) is measured. The foam made with the surfactant Anionic 1 maintains its volume and its half-life is much larger than 40 min. The volume of the foam made with surfactant Cationic 1 decreases considerably in the first 40 min; the half-life is about 19 min. The foam made with the surfactant Nonionic 1 (NP30) collapses very fast with a half-life of about 3 min. Thus the foam stability depends on the type of surfactant. The decline of foam volume is often discontinuous and contains several steps. This is because breakage of one foam bubble often leads to the breakage of many other bubbles.

74

This may be due to the thinness of the lamella and the breakage of one bubble creates perturbations to which other lamellae are not stable.

Because the foam made with the nonionic surfactant was not very stable, glycerol was added to increase its stability. As shown in Figure 50, foam collapse rate decreased with the increase in glycerol concentration. Glycerol concentration of 1.25% and 2.24% can increase the half life time of NP30 foams to 6 minutes and 22 minutes, respectively.
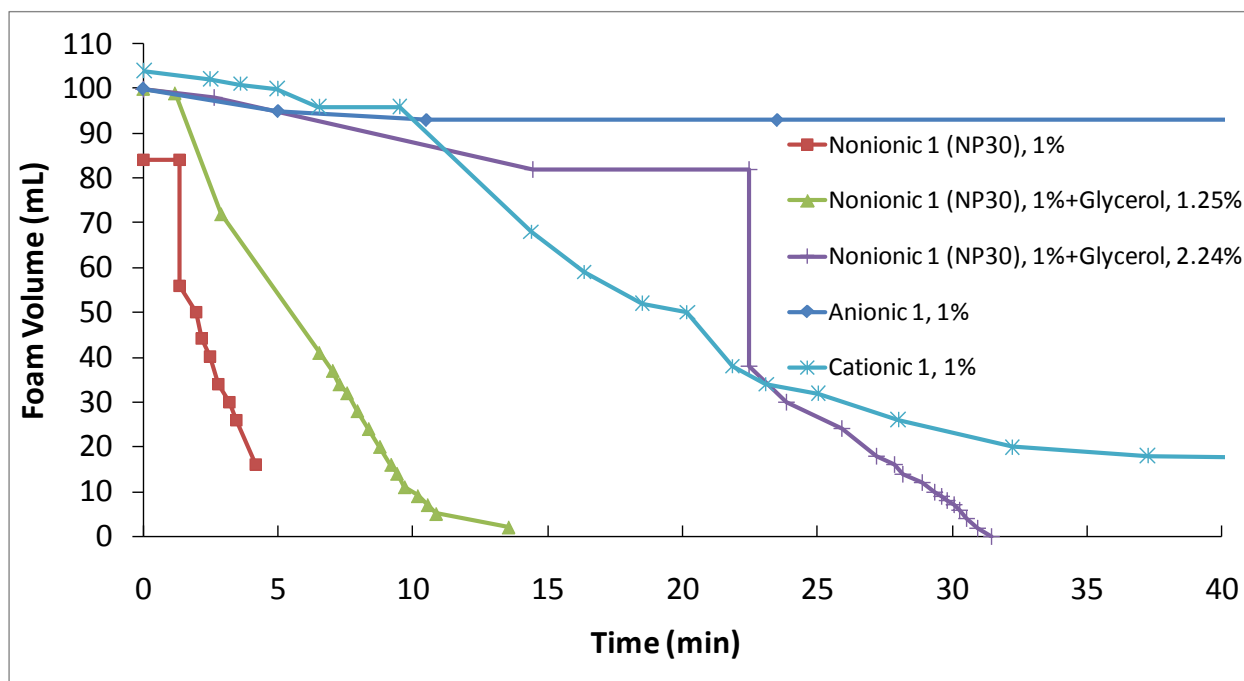
Figure 50. Effect of different types of surfactant and the addition of stabilizer (Glycerol)

Table 5. Activity of the cationic surfactants tested

Cationic Surfactant	Activity
Cationic 1	50%
Cationic 2	80%
Cationic 3	80%
Cationic 4	95%
Cationic 5	78.5%
Cationic 6	90%
Cationic 7	98%
Cationic 8	98%

Next, we tested eight cationic surfactants, which are listed in Table 5. The eight surfactant solution samples with 1% active concentration were made and placed in small test tubes shown in Figure 51. The foam is generated by shaking all the tubes together. Figure 51 shows the initial state of the foams. It is noted that the different cationic surfactants have different foam generation capabilities. The cationic surfactants 1, 2 and 3 can produce foams easily. Cationic 5 formed no foam at all.
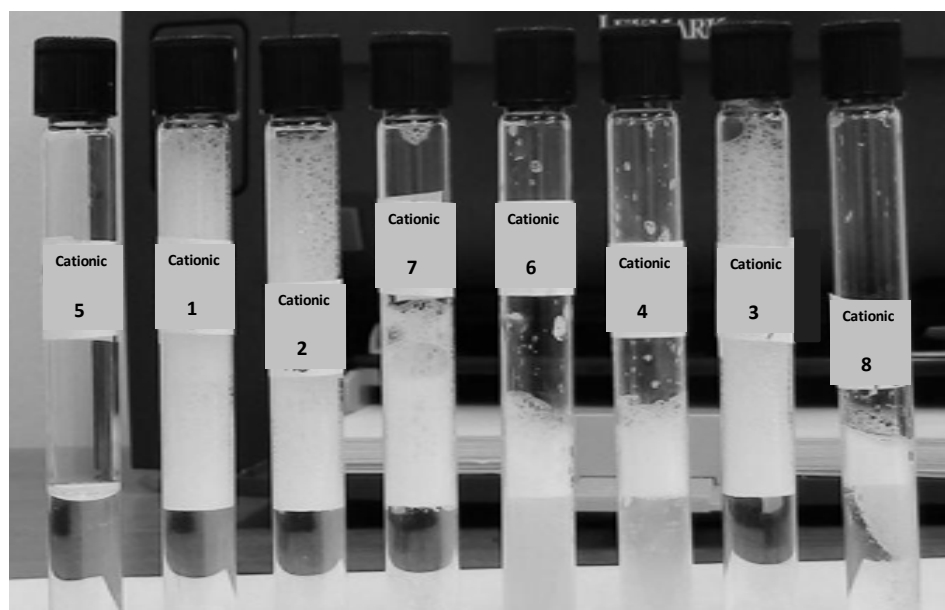
Figure 51. Foams produced by the 1% cationic surfactant solution with no other additives

The state of the foam was monitored by a handy-cam and Figure 52 shows the state after 4 min. The foam stability follows the following relationship: Cationic 1> Cationic 4= Cationic 6> Cationic 7> Cationic 3= Cationic 2> Cationic 8.
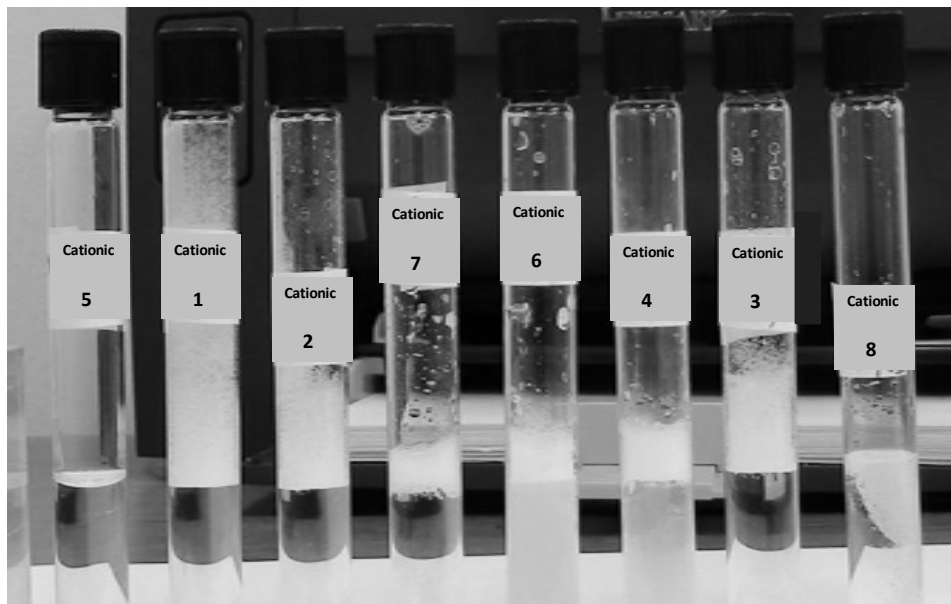
Figure 52. Foam height after 4 minutes (1% cationic surfactant solution with no other additives)

The effect of adding successively an amphoteric surfactant and an anionic surfactant to the cationic surfactant was tested next. First, Amphoteric 1 was added to the 8 cationic solutions at an active concentration of 1% and the stabilities of the foams were measured. Following that, the Anionic 1 was added at a concentration about 0.2~0.4%. The foam stability change was evaluated. Table 6 shows the composition of the all samples.

Table 6. Compositions of foam samples

	Cationic Surfactant	Amphoteric 1 Weight (g)	Amphoteric 1 Concentration	Anionic 1 Weight (g)	Anionic 1 Concentration
Sample	Cationic 1	0.0539	1.08	0.0454	0.35412
Sample	Cationic 2	0.0543	1.09	0.0363	0.28314
Sample	Cationic 3	0.0520	1.04	0.0372	0.29016
Sample	Cationic 4	0.0546	1.09	0.0301	0.23478
Sample	Cationic 5	0.0550	1.10	0.0378	0.29484
Sample	Cationic 6	0.0550	1.10	0.0391	0.30498
Sample	Cationic 7	0.0520	1.04	0.0508	0.39624
Sample	Cationic 8	0.0524	1.05	0.0518	0.40404
Sample	water	0	0	0.0396	0.30888

0% Amphoteric 1, 0%

Anionic 1
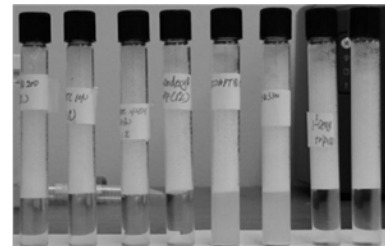
0 min

1% Amphoteric 1, 0%

Anionic 1

0 min

1% Amphoteric 1, 0.3%

Anionic 1

0 min
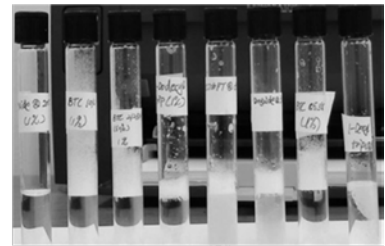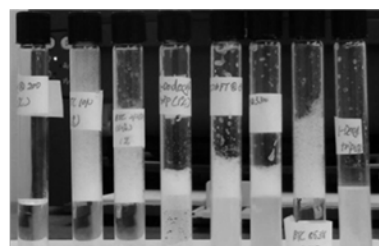
0% Amphoteric 1, 0%
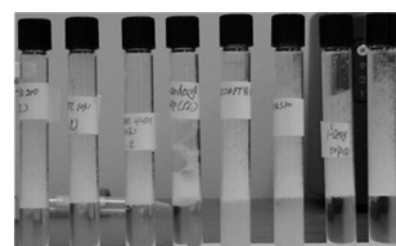
Anionic 1

4 min

1% Amphoteric 1, 0%

Anionic 1

4 min

1% Amphoteric 1, 0.3%

Anionic 1

4 min
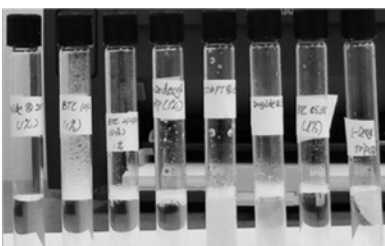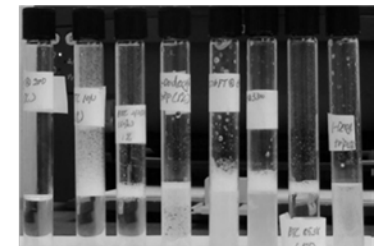
0% Amphoteric 1, 0%
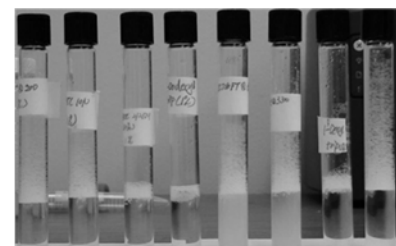
1% Amphoteric 1, 0%

1% Amphoteric 1, 0.3%

Anionic 1	Anionic 1	Anionic 1
27 min	27 min	27 min
Figure 53. Bubble height varies with the time		

Figure 53 shows the foam collapsing process; Sample 9 is shown only in the third column because that was the only sample 9 with surfactants. The addition of Amphoteric 1 does not change the foam generation capability of the cationic surfactants. For example, the Cationic 5 surfactant solution fails to generate foams either with or without the Amphoteric 1. However, Amphoteric 1 can somehow slow down the foam collapsing process slightly for some kinds of cationic surfactants, such as Cationic 1, 2, 3, 4, and 6. Addition of anionic surfactant Anionic 1 can significantly increase the foam generation capability of all cationic surfactant solutions, but does not help in slowing down the collapsing of the bubbles. The earlier experiments showed that the pure anionic surfactant solution with a very low concentration can already have a very good foam generation ability and stability. The addition of the cationic surfactant and the amphoteric surfactant did not enhance these properties significantly.

0 min	34 min	140 min
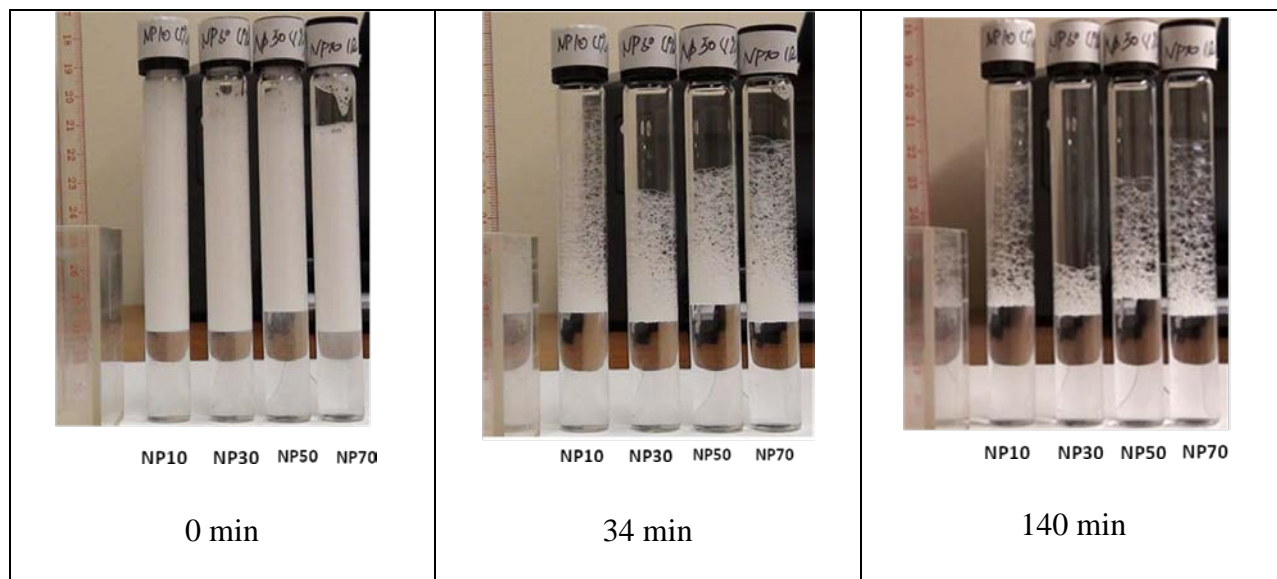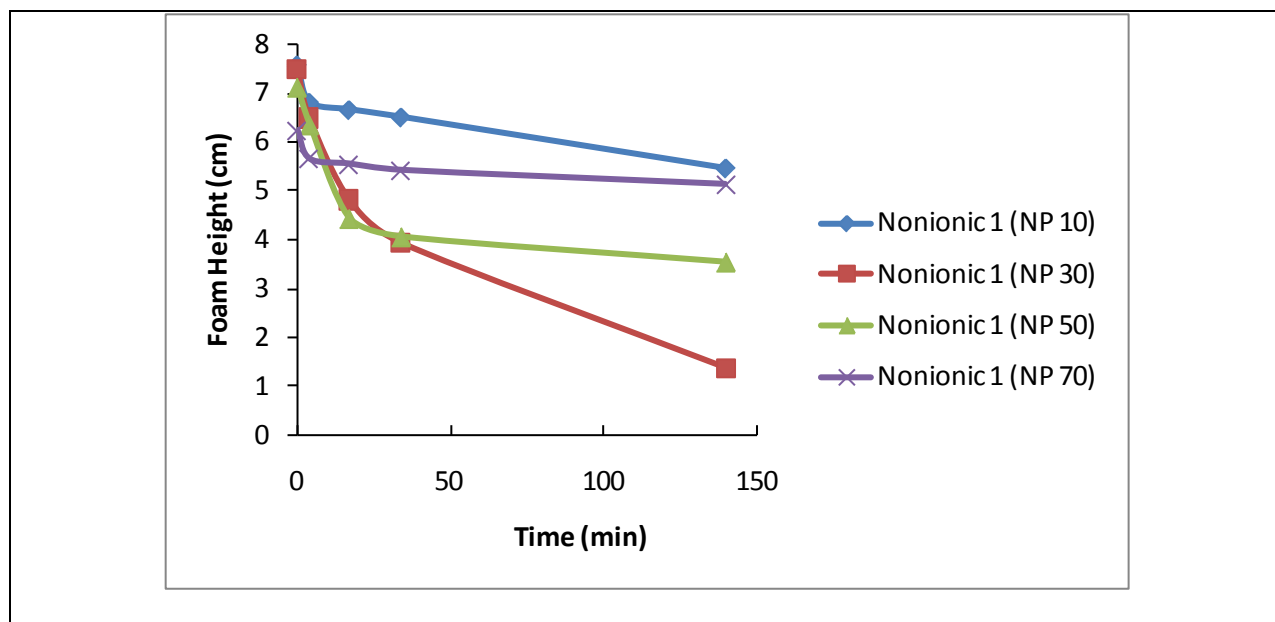
Figure 54. Foam stability for different NP numbers

The last experiment in this section is the investigation of the effect of hydrophilic length on foam stability. In our test, Nonionic 1 (NP10/30/50/70) surfactants were used to make surfactant solutions with the active concentration of 1%. The n in NPn represents the number of units of ethoxy groups [CH_2CH_2O]. Figure 54 shows the foam columns made by shaking the tubes together. The results show that the number of ethoxy groups does affect the stability of the foams. NP10 had the highest stability; NP30 has the least stability. With the exception of NP10, the foam stability is improved as the NP number increases.

Effect of Surfactant Concentration

In this test, three surfactants, Anionic 1, Nonionic (NP30) and Cationic 1, are used at different surfactant concentrations. The foam column is produced by injecting N_2 gas through the bottom of the static solution. The foam volume evolution with the time is measured and plotted in Figure 55.
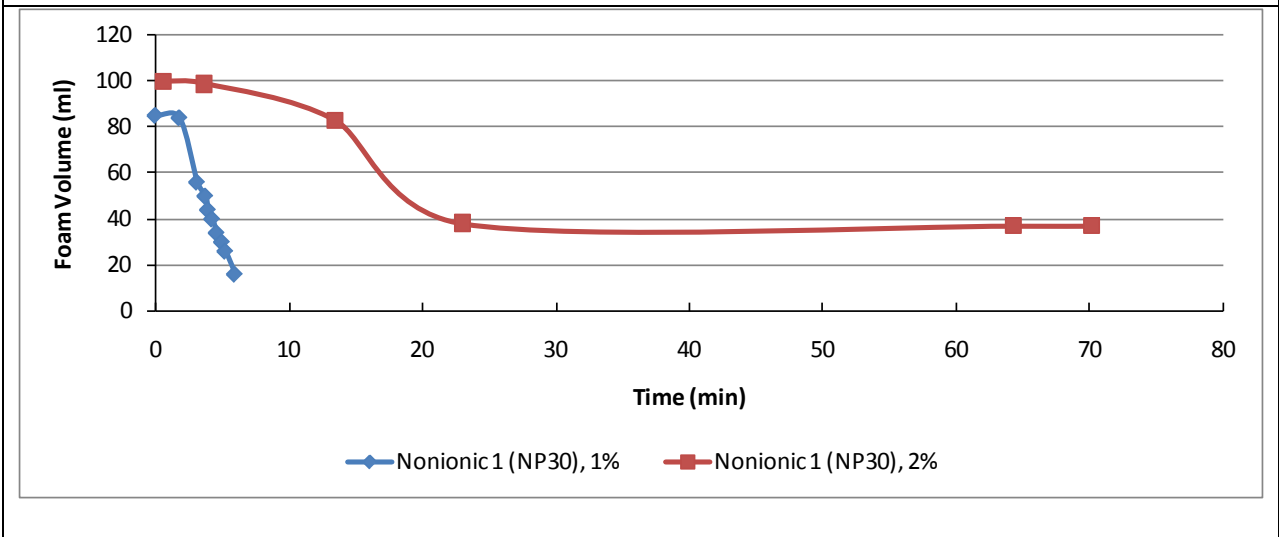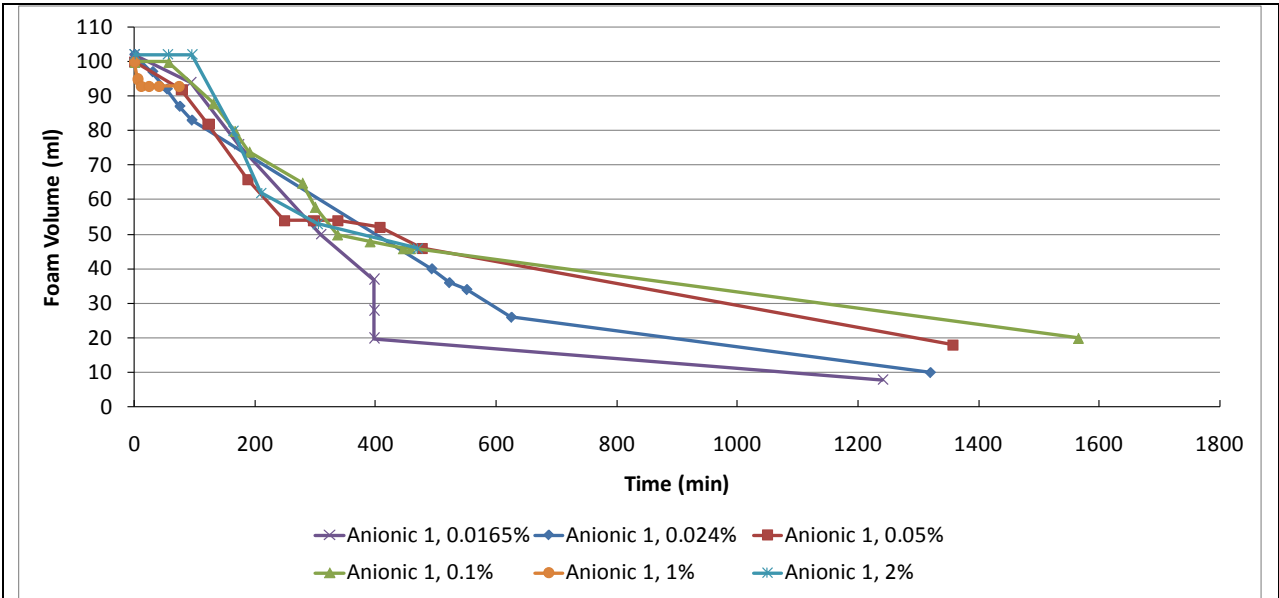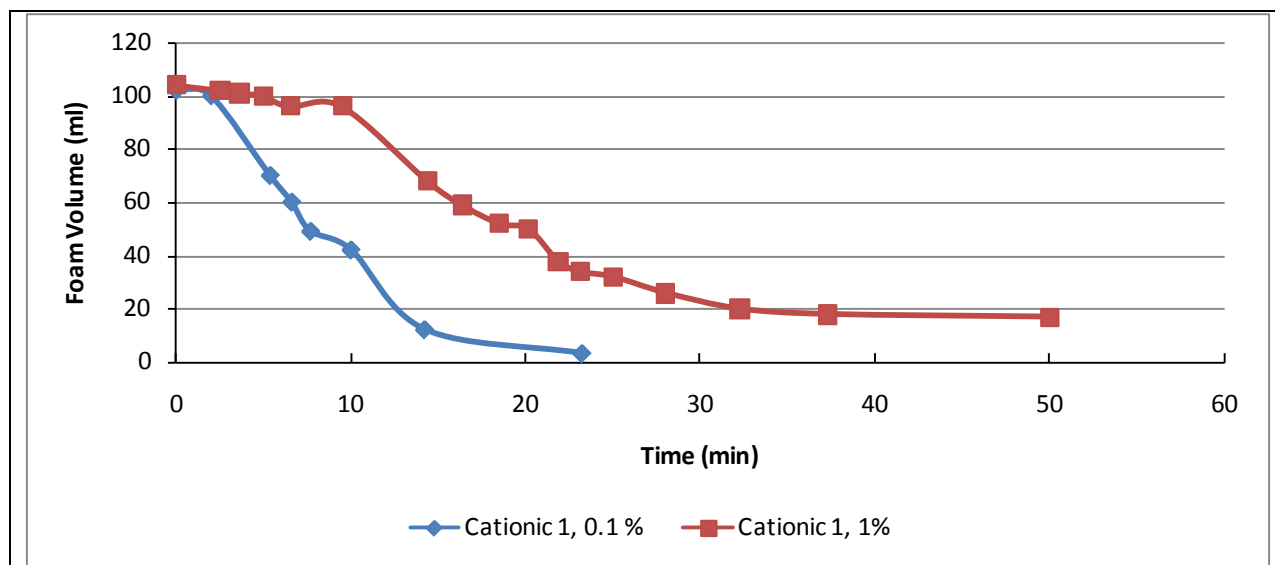
Figure 55. Foam stability for different surfactant concentrations

It is shown that the stability of the foam is increased with the increase of the surfactant concentration, because the high density of the surfactant molecules can guarantee a good strength of the lamella film and retard the diffusion of the bubble gas through the liquid film. These plots show that the anionic surfactant is much more stable (half-life ~ 400 min) than the cationic and nonionic surfactants tested.

It should also be noted that at the beginning of the foam collapsing process, there is a short period during which the height of the foam column changes very little. This period is defined as a drainage time zone. In this time zone, the liquid phase drains down from the top to the bottom of the foam column according to the gravity and capillarity and thins the lamellae. Increasing the surfactant concentration or adding glycerol can increase this time period.

Effect of Temperature

In these experiments, a water bath is used to keep the foam columns at a stable high temperature. It should be noted that the gas expands as the temperature increases. So we need to

put the whole system including the gas pipe line in the water bath. The anionic surfactant (Anionic 1) solution with a concentration of 0.1% is used. The results are plotted in Figure 56.
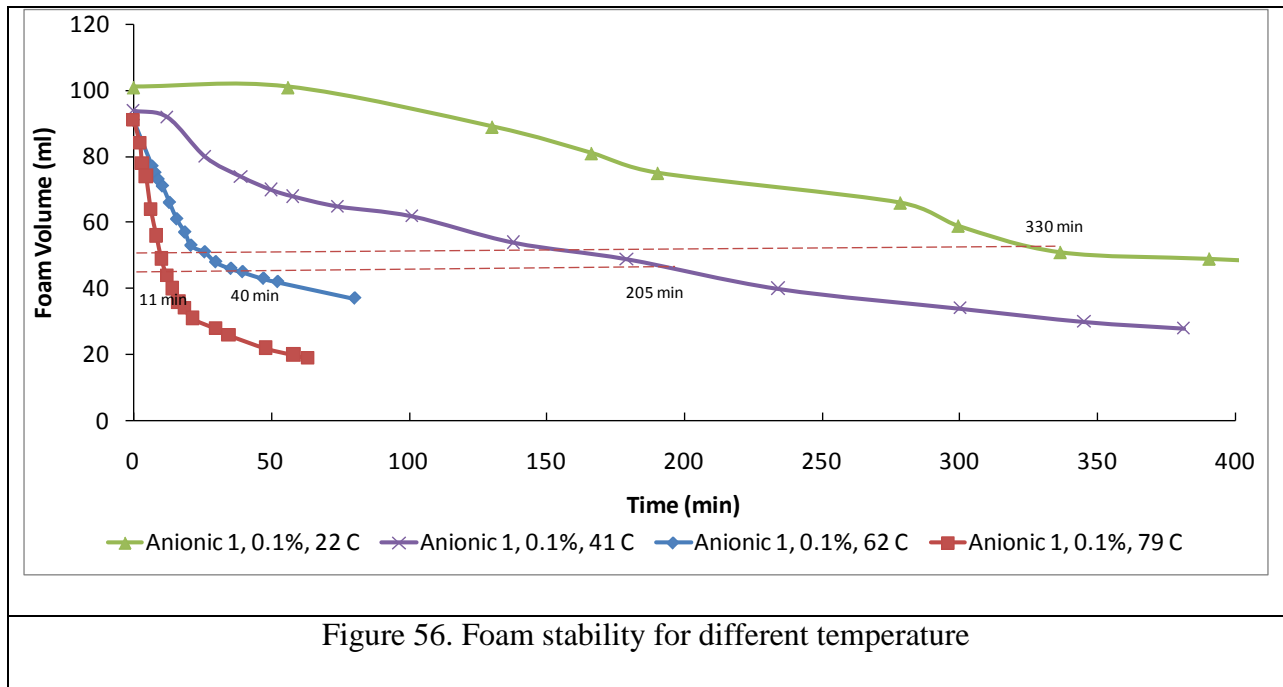
Figure 56. Foam stability for different temperature

The foam collapse rate increases as the temperature increases. The half-life of the foam column drops down significantly as the temperature increases. The high temperature decreases the liquid viscosity and increases liquid drainage. It also speeds up the evaporation of the liquid phase. The decrease of half-life with temperature is shown in Figure 57.
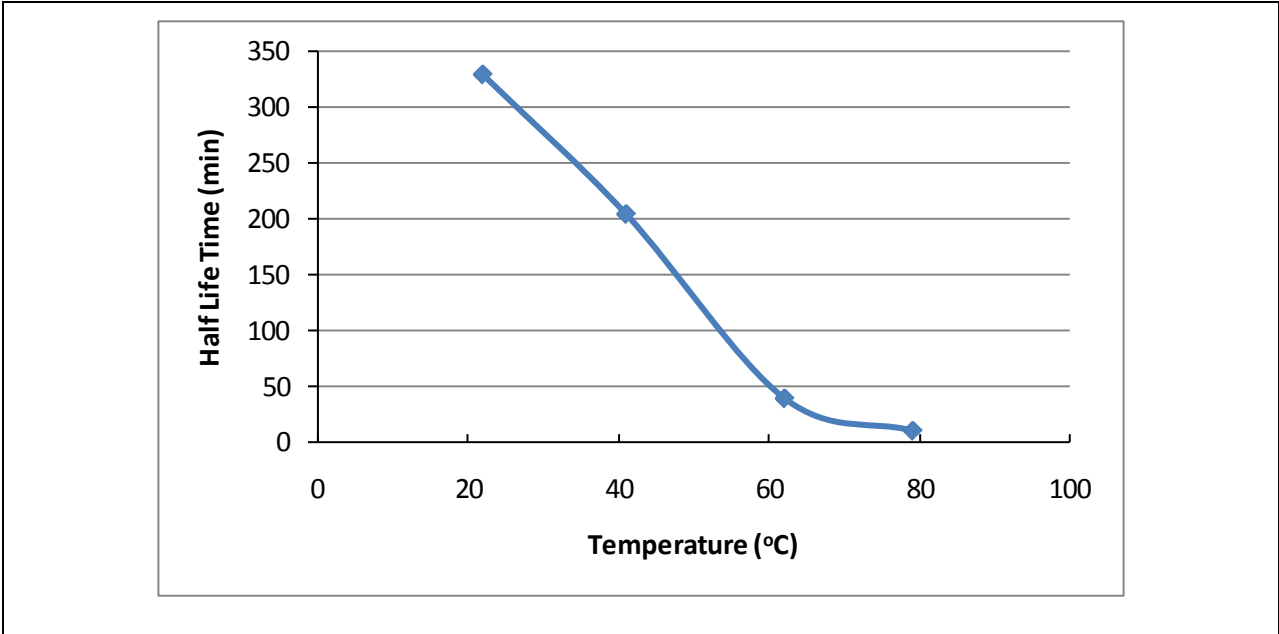
Figure 57: Effect of temperature on half-life of foams

Effect of Quality and Bubble Size

Experiments were conducted to study the effect of foam quality and bubble size. The quality was changed by controlling the produced bubble size. We used gas injection needles of different sizes as well as different gas injection rates to get different bubble sizes. Figure 58 shows bubble sizes obtained for the Cationic 1 solution at the concentration of 0.1%.

| D: 0.5 mm | D: 1mm | D: 2mm | D: 3 mm |
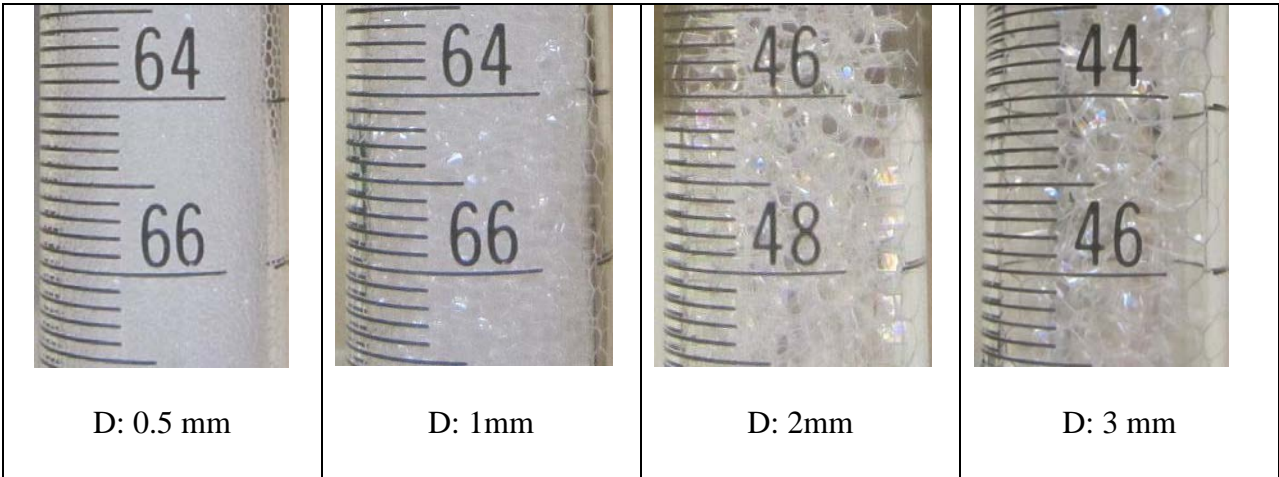
Figure 58. Different bubble size ('D' means typical diameter of the bubbles)

Table 7. Foam size and quality for Cationic 1

Typical Bubble Diameter (mm)	Quality (%)
0.5	95.74
1	99.21
2	99.72
3	99.76

Table 7 shows the quality of these foams. According to the table, when the bubble diameter is larger than 1mm, the quality is above 99% and changes a little. The time dependent volume of the four foam columns with different qualities and bubble sizes were measured and plotted in Figure 59. A smaller bubble size with a lower quality produces a more stable foam column.

Figure 59. Foam volume against time at different bubble size
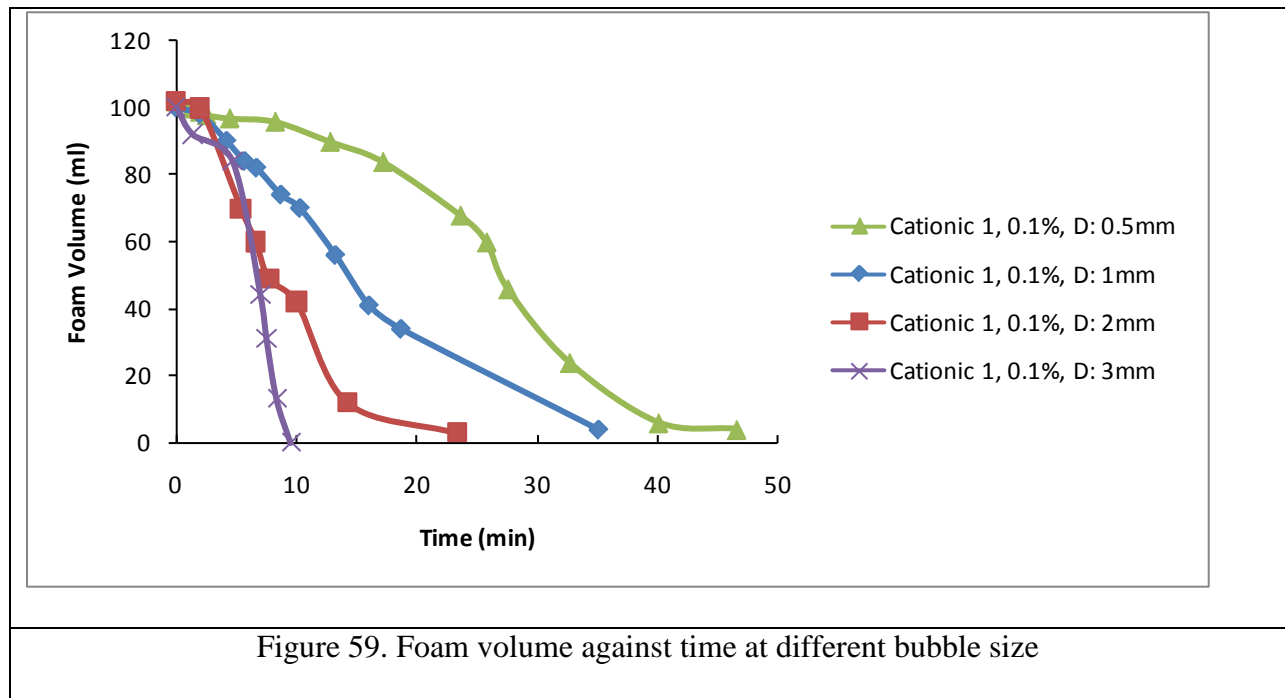
Static Settling Test

The proppants were placed at the top of a column of fluid and a handy-cam was used to monitor the downward movement. The fluids used in our test were water and foams. The proppants were white sand, and three kinds of ultra light weighted proppants (ULW1 Polymer-3). Figure 60 shows the size and shape of different proppant samples. It should be noted that the proppant ULW2 Resin-Walnut is not as spherical like other three.

Ave D_ULW1 Polymer: 1.2 mm	Ave D_ULW2 Resin-Walnut: 1.3mm	Ave D_ULW3 Resin-Ceramic: 1 mm	Ave D_sand: 1.1 mm

Figure 60. Proppant size

Table 8: Density of proppants from Happel correlation

Proppants	ρ_s (g/cm^3)	$\rho_{s\text{-ref}}$ (g/cm^3)
ULW1 Polymer	1.05	1.08
	1.07	
	1.05	
	1.04	
ULW2 Resin-Walnut	1.23	1.25
	1.18	
	1.10	
	1.26	
ULW3 Resin-Ceramic	1.60	1.75
	1.77	
	1.36	
	1.71	
White Sand	2.11	2
	1.96	
	2.08	
	2.10	

The first set of tests was conducted with water. As a proppant settled down in the water, its positions were measured at different times. Its velocity can be obtained by linear regression of

the data. In this test, the Reynolds number (Re) varied from 10 to 300, which is larger than 2 and smaller than 500. So, the Happel correlation is adopted to understand the data, i.e.,

$$V_{Re} = \frac{20.34(\rho_p - \rho_f)^{0.71} d_p^{1.14}}{\rho_f^{0.29} \mu^{0.43}}$$

The density of each proppant derived from the Happel correlation is listed in Table 8. Comparing the measurement densities with the reference ones, it is noted that our test results agree well with the Happel correlation.

Proppant settling experiments were then conducted in the foams made from 0.1% Anionic 1 solution at room temperature. The proppants were mixed with the foam at the initial condition. As shown in Figure 61, the ULW1 Polymer proppants do not fall through the foam. The foam has enough viscosity to hold ULW1 Polymer without settling. As the foam collapsed, the proppants would either drop down or stick to the wall of the bottle. Similar observations were made with all four proppants. None of the proppants fell through this foam.

Figure 61. Proppants ULW1 Polymer stay in the foam

Foam Rheology Test

Three fluids are investigated in the foam rheology test. The test matrix of the foam fluids tested is shown in the table below.

Table 9. Test Matrix

	Liquid phase	Temp (F)	Pressure (psi)	Quality (%)	Pipe Size (inch)	Mixing Shear Rate (s^{-1})
Fluid A	Water + 0.5vol% Anionic Surfactant (39%)	95,125,155	1000	0-80	0.5	1000-1100
Fluid B	Water + 0.5vol% Anionic Surfactant (39%)+ 2vol% Stabilizer(99%)	95,125,155	1000	0-80	0.5	1000-1100
Fluid C	Water + 0.5vol% Viscoelastic Surfactant (99%)	95,125,155	1000	0-80	0.5	1000-1100

Figure 62 shows the measured wall shear stress against apparent shear rate for fluid A. As the apparent shear rate increases, so does shear stress. The foam is shear thinning at qualities above 50% and shear thickening at the qualities below 50%. As temperature increases, the shear stress decreases, but the effect is small. In Figure 63, the shear stress (for foams of different qualities) are plotted against the apparent shear stress in a log-log scale. The linear trends are

observed, which indicates that the power law model can be adopted to analyze the flow behavior of foams. The power law model is given as,

$$\tau = K' \gamma_w^{n'} \tag{26}$$

The flow consistency index K' and flow behavior index n' are obtained by linear regression for three fluids.

According to the results above, low quality foams (below 50%) generated from fluid A and B behave more like a dilatant fluid, while high quality foams (above 50%) are more like a pseudo-plastic fluid. The reason is that low quality foams are no longer laminar flow at the shear rate above 300-400 s^{-1}, due to its low viscosity. At high shear rates, the turbulence increases the flow resistance and makes the fluid behave like a shear thickening fluid. Unlike fluid A and B, fluid C always behaves like a pseudo-plastic fluid from 0% quality to high quality, that is because its liquid phase has a much higher viscosity, which is 2 to 13 times larger than the viscosity of the fluid A or B.

Based on the parameters obtained, the apparent viscosity is calculated by the equation below,

$$\mu_a = \tau_w/\gamma_w = K' \gamma_w^{n'-1} \tag{27}$$

The shear rate effect, quality effect, temperature effect, pressure effect and liquid component effect have been investigated based on the apparent viscosity results.
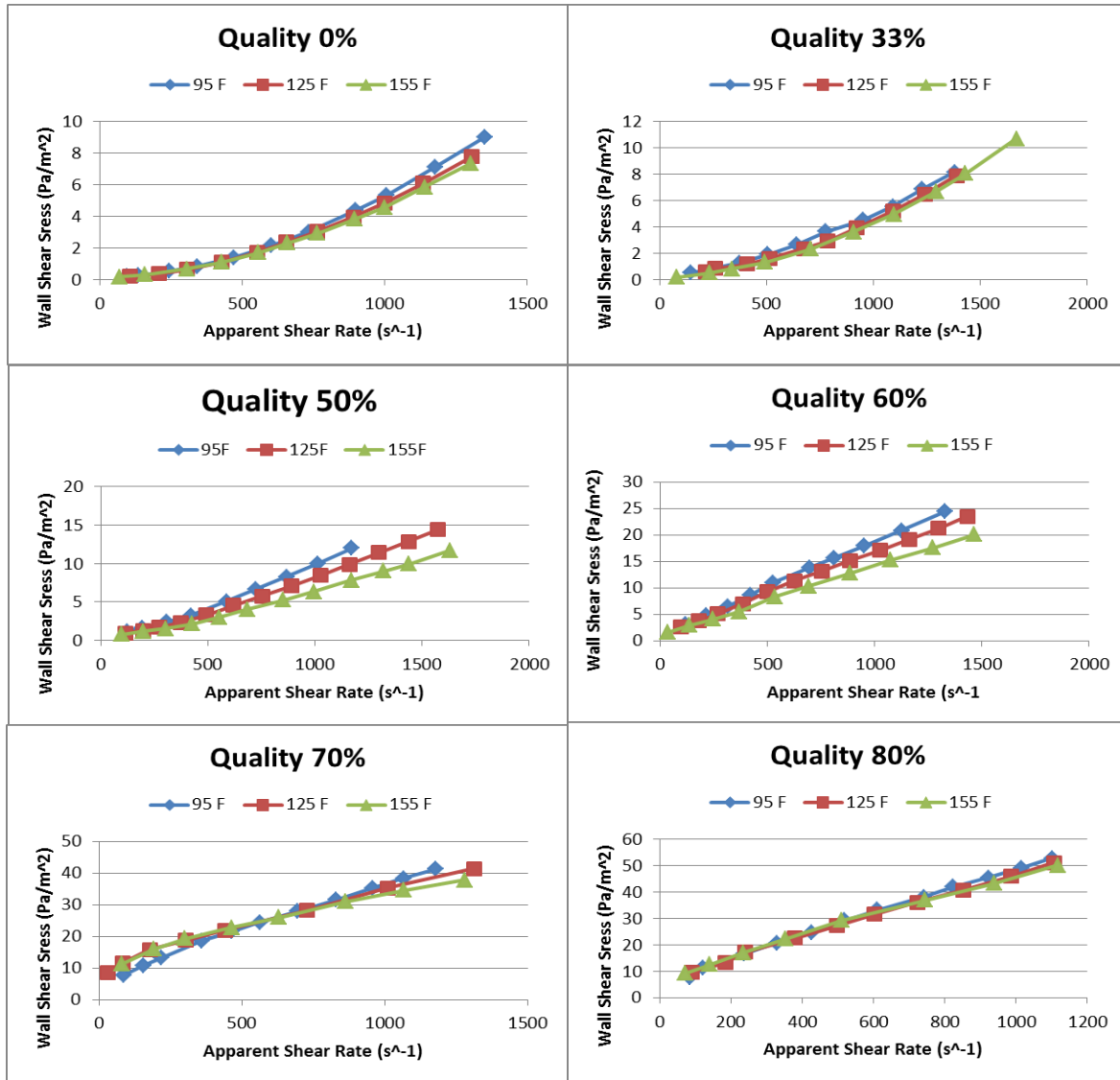
Figure 62. Wall shear stress vs. apparent shear rate for fluid A
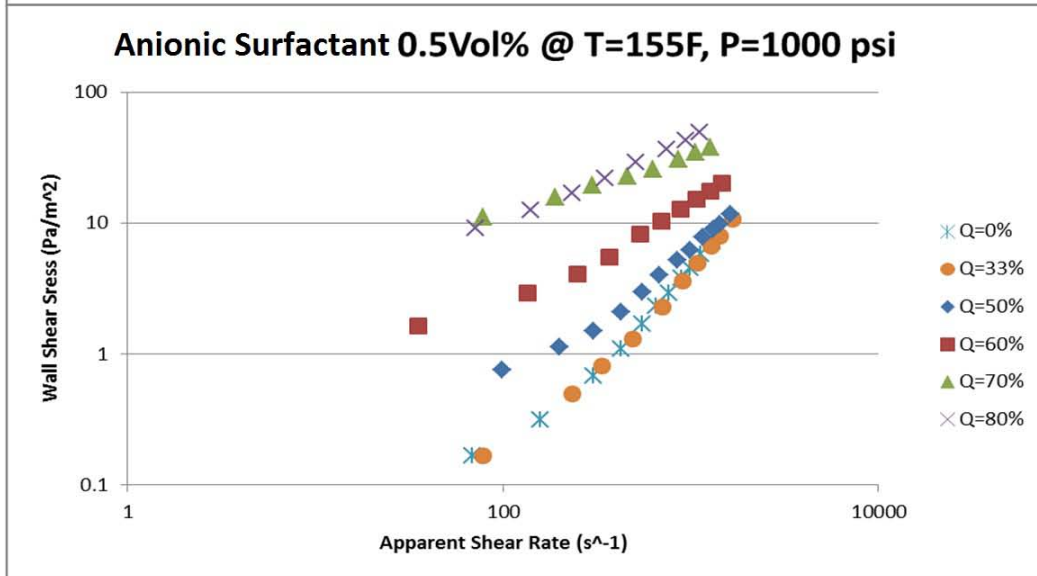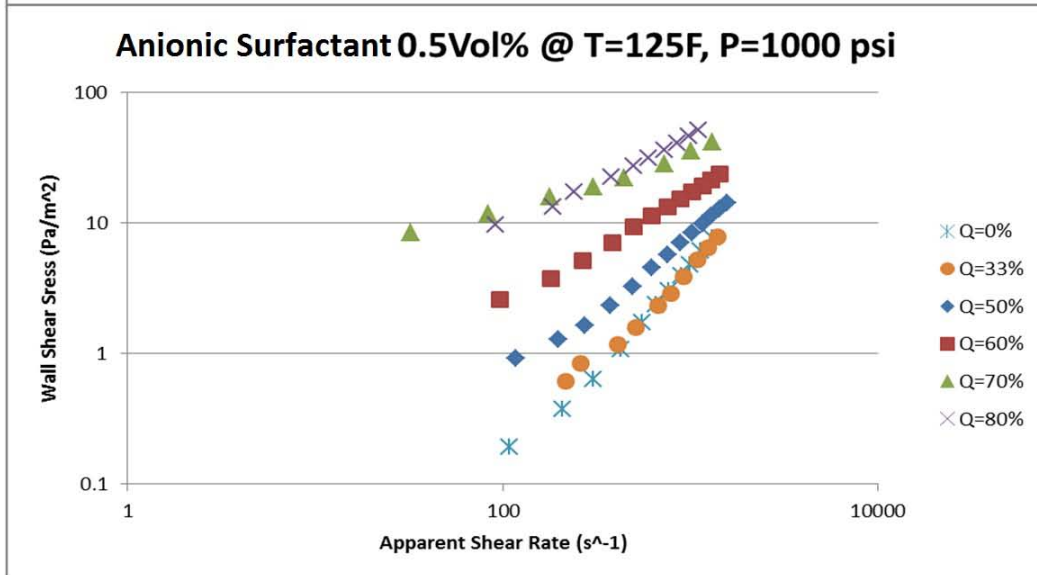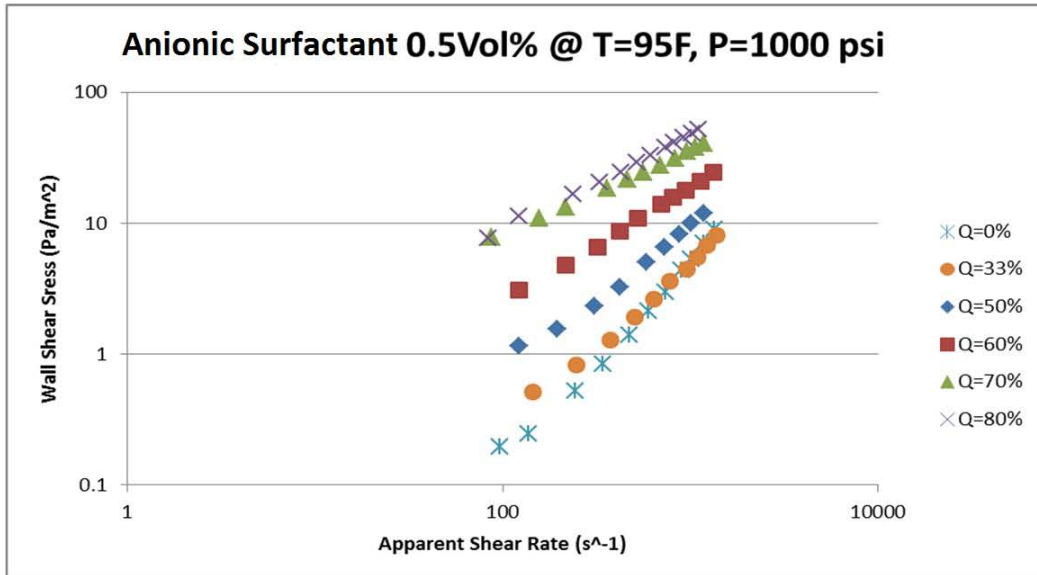
Anionic Surfactant 0.5Vol% @ T=95F, P=1000 psi

Anionic Surfactant 0.5Vol% @ T=125F, P=1000 psi

Anionic Surfactant 0.5Vol% @ T=155F, P=1000 psi

Shear Rate Effect

In Figure 64, the apparent viscosities at different qualities are plotted against the shear rate.
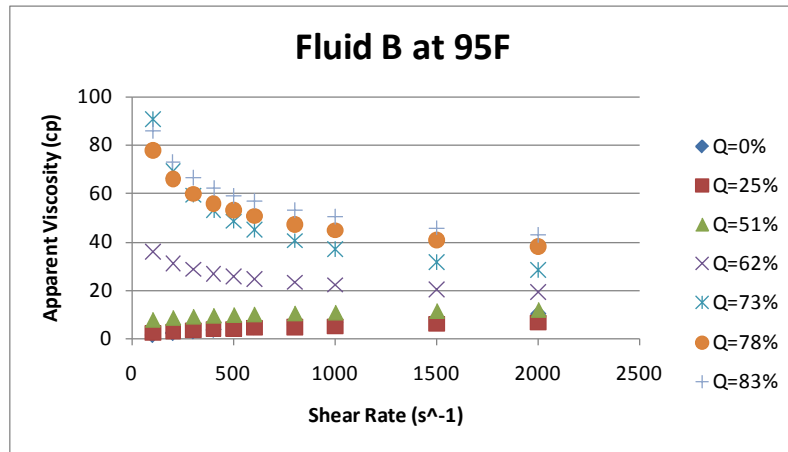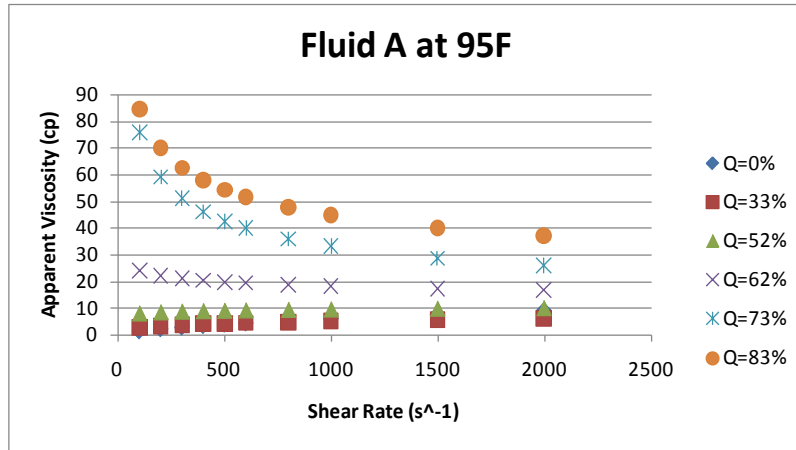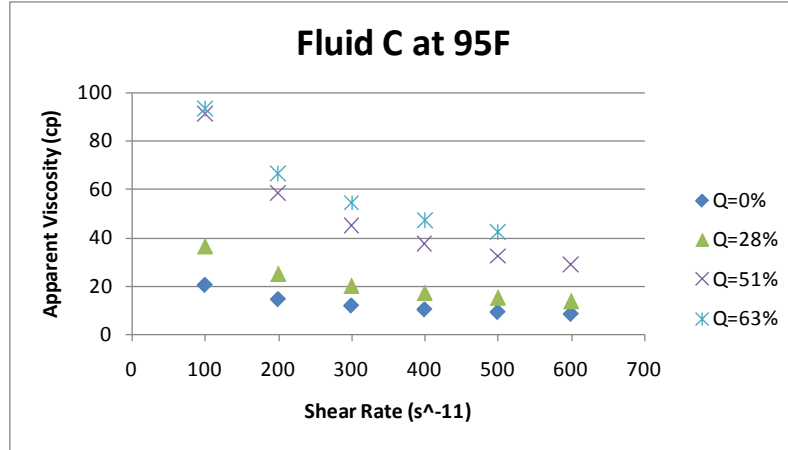
Figure 64. Apparent viscosity vs. shear rate for three fluids

For fluids A and B, the foams behave like a shear thinning fluid only at a quality above 50%, while, for fluid C, its foams always have the viscosity decrease with the shear rate increasing. And for all three fluids, the shear thinning effect becomes larger as the foam quality goes high. It is found that the low quality foams (< 50%) generated from fluid A and B possess higher viscosities at low shear rate and lower viscosities at high shear rate, compared with their base fluids (Figure 65). This is a good property for the fracturing fluid, because when doing fracturing a low friction loss in the tubing facility (high shear rate zone) and a high viscosity in fractures (low shear rate zone) are always preferred.
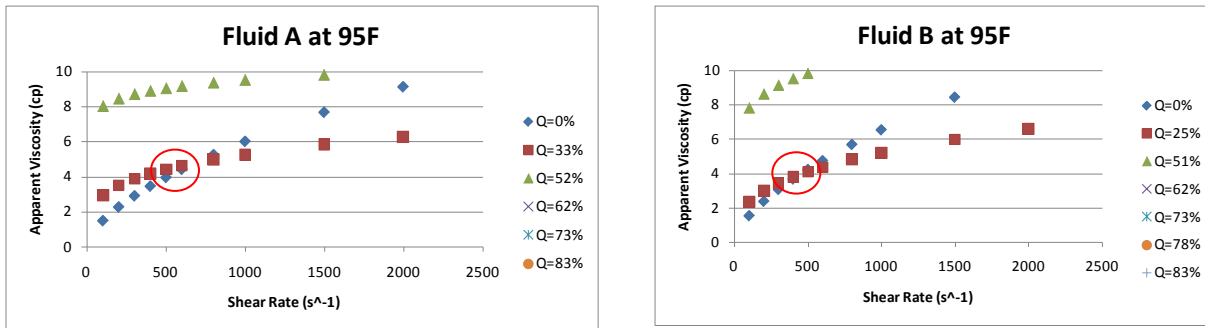
Figure 65. Apparent viscosity vs. shear rate for three fluids at low qualities

93

(Red circle represents the crossover of two fluids)

Quality Effect

Figure 66 shows the effect of the foam quality and shear rate on the foam stability.
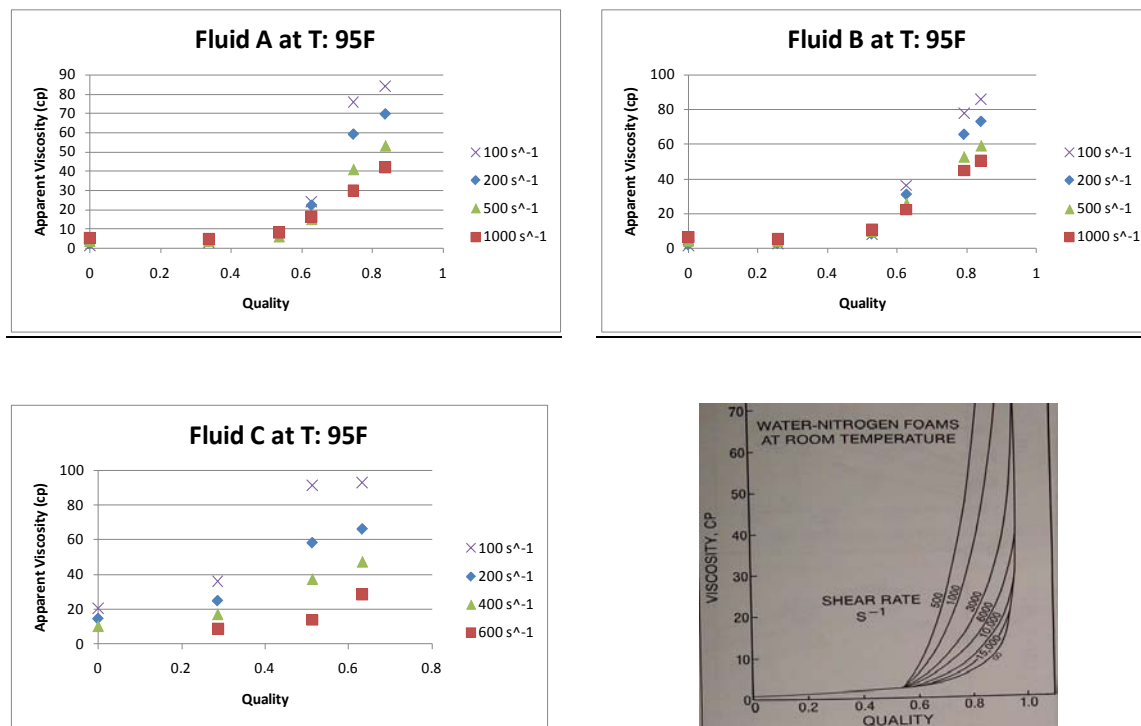
Figure 66. Apparent viscosity vs. quality at different shear rates for three fluids and the

reference data

The last picture in Figure 66 shows the literature values for the water-nitrogen foam viscosities measured at the room temperature [Mitchell, 1970]. Both our results and the reference results show that at qualities above 50%, the viscosity suddenly increases and varies exponentially with quality attributed to the closely packed bubble interactions. It should be noted that the viscosity at quality of 80% was measured lower than the value predicted from an exponential trend. One explanation can be that our pump cannot mix such high quality, high viscous foams uniformly because of its horsepower limit.

Temperature effect

In Figure 67, the apparent viscosities at the typical shear rate in fractures (500 s^{-1}) are plotted against temperatures for different quality foams generated from fluids A, B and C.
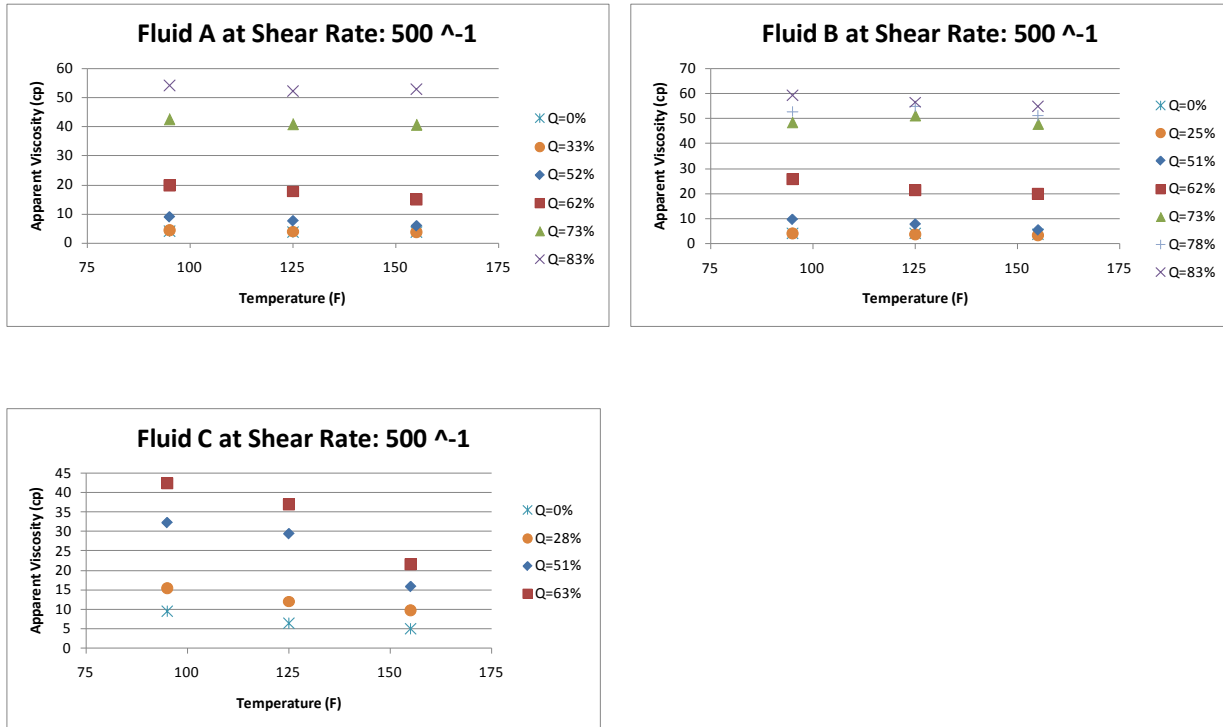
Figure 67. Apparent viscosity vs. temperature for foams of varied qualities of fluids A, B and

C

Generally the viscosity decreases with the increasing temperature. According to Figure 67, the temperature effects are more significant for high quality foams. One of the reasons is that increasing temperature causes destabilization of the foams by accelerating the liquid drainage in the lamellae and reducing the surfactant stability and solubility. Besides, the high temperature leads to the degradation of the wormlike micelles formed by the VES, which make the viscosity of the VES foams decrease more than the viscosity of the regular surfactant foams at high temperature.

Pressure Effect

Figure 68 shows the pressure effect on the foam rheology test. The foams made from fluid B are measured under back pressures of 500 psi and 1000 psi, respectively. There is no big difference between the results measured under two back pressures until the quality goes above 60%.
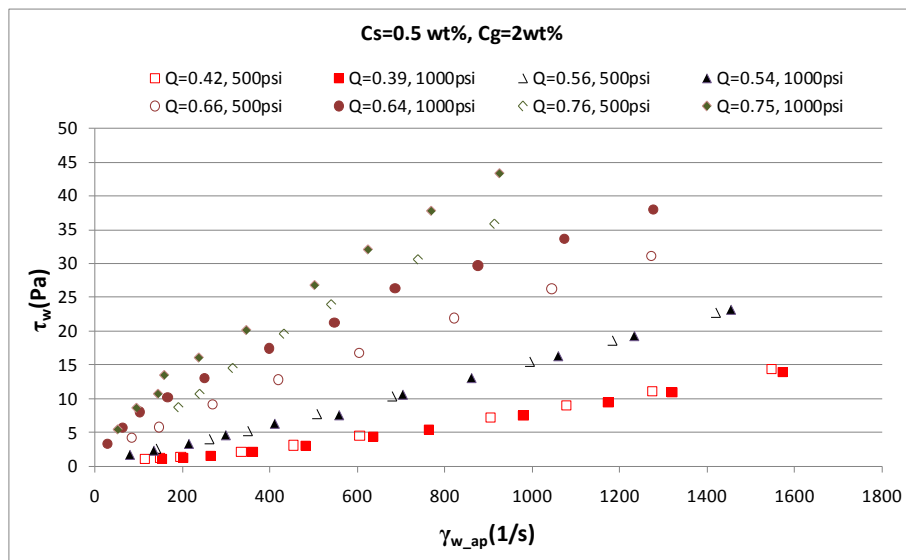
Figure 68. Wall shear stress vs. apparent shear rate measured at different pressures for fluid B

Furthermore, a test was conducted for the same foam with a quality of 50% under pressures of 200, 400, 600, 1000 psi. This test shows the effect pressure. The results are shown in the table below.

Table 10. Power Law Parameters for 50% Quality Foams of Fluid B at Varied Pressures

	200 psi	400 psi	600 psi	800 psi	1000 psi	Max. Relative Difference

						MAX($|(a_{pi}-a_{pj})/a_{pj}|$)
n'	1.159752	1.237649	1.241419	1.250094	1.234549	7.22%
K'	-2.56567	-2.7675	-2.76069	-2.79877	-2.72958	8.33%
R^2	0.99886	0.996406	0.999094	0.999858	0.999845	-

For the foams with a quality of 50%, the flow consistency index K' decreases and the flow behavior index n' increases slightly as the pressure increases from 200 psi to 1000 psi. The changes are both limited within 10%. It is reasonable to believe that the change could be less for lower quality foams.

Liquid Composition Effect

Figure 69 shows apparent viscosities of foams produced from different surfactant fluids. The shear rate is kept constant at a typical fracturing shear rate of 200 s^{-1}. The measurement is conducted at 1000 psi and 95 F.
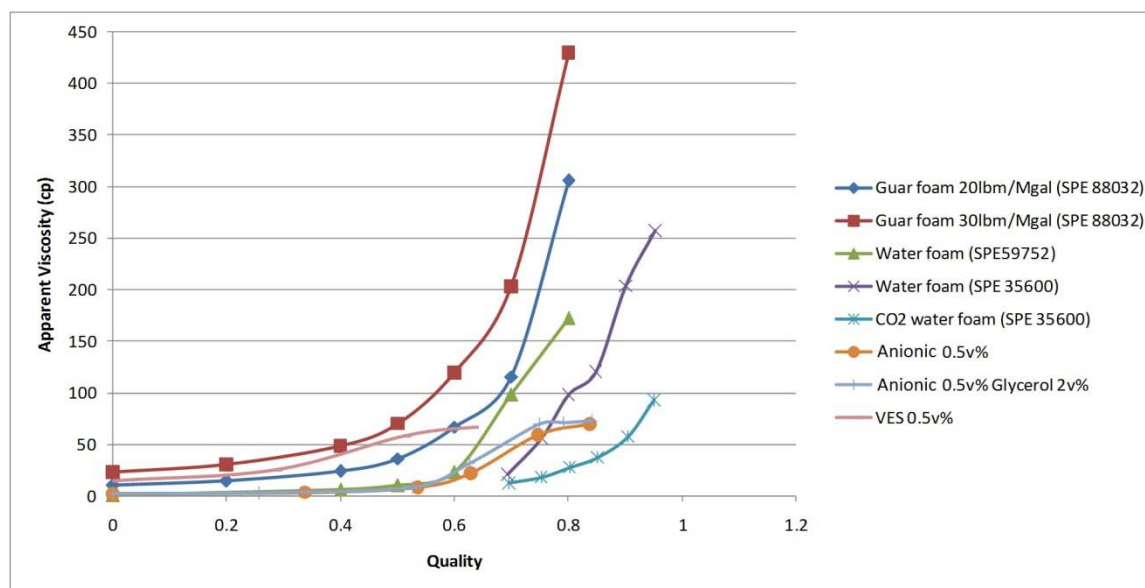
Figure 69. Apparent viscosity vs. quality for different foam base fluids

Our gel-free water foams have viscosities similar to those in the literature (Bonilla et al. 2000) at qualities below 0.5. At qualities above 0.5, viscosities are smaller for our experiments. One reason for the deviation at high quality range could be the nonuniformity in texture. According to the water foam results, increasing the surfactant concentration can increase the foam viscosity, especially at high qualities. It is because that the increased surfactant concentration not only increases the liquid phase viscosity of the foams, but also increases the stabilization of the foam structure. Adding glycerol can also increase the foam viscosity, but not as much as that increased by the increasing surfactant concentration. Compared with Guar foams (SPE 88032), the aqueous foams A and B are both less viscous than 20 lbm/Mgal guar foams, while the VES foam C has an apparent viscosity similar to that of guar foams with 20 lbm/Mgal to 30 lbm/Mgal guar foams.

Proppant Transport Test

After the rheology test, the fluid samples are circulated out of the loop and into a fracture slot. The proppants are also added at the inlet of the slot. A video camera is used to record the transport of the proppant in the slot.

b

c

Figure 70. Photographs of the transport experiment (a. foam samples, b. proppant samples, c. screenshot of the transport process through fracturing slot)

The foam samples used in the proppant transport test are 50% quality foams made from fluid A. Figure 70 (a) is a photograph of foams collected at the outlet of the foam loop, from which we can see the foam has a fine, uniform texture. The proppant samples we added to the foams are mixtures of sands, ULW proppants (Figure 70 (b)). Figure 70 (c) is a picture of the proppants during the transport through the slot. The slot was initially filled with water. Then the foam carrying the proppants was injected in the slot at a flow rate of 2 LPM (320 s^{-1}). The back pressure of the whole system is 14.7 psi. From Figure 70 (c), we can see most proppants stayed within the foam and the water at the bottom was almost clear with no proppants. During the test,

the water foams presented good suspension and transport capacities for all the proppants we tested.

Fracture Propagation Simulator Validation

Our numerical simulator for fracture propagation was validated by comparing the fracture width distribution along the fracture length after 30 minutes of water injection with an analytical solution. The comparison between analytical results and numeric results (no leak off, Newtonian fluid) is plotted in Figure 71. The numerical solutions agree well with the analytical ones. The change of the length step dx and time step dt do not affect the numerical results implying that the step sizes are adequate.
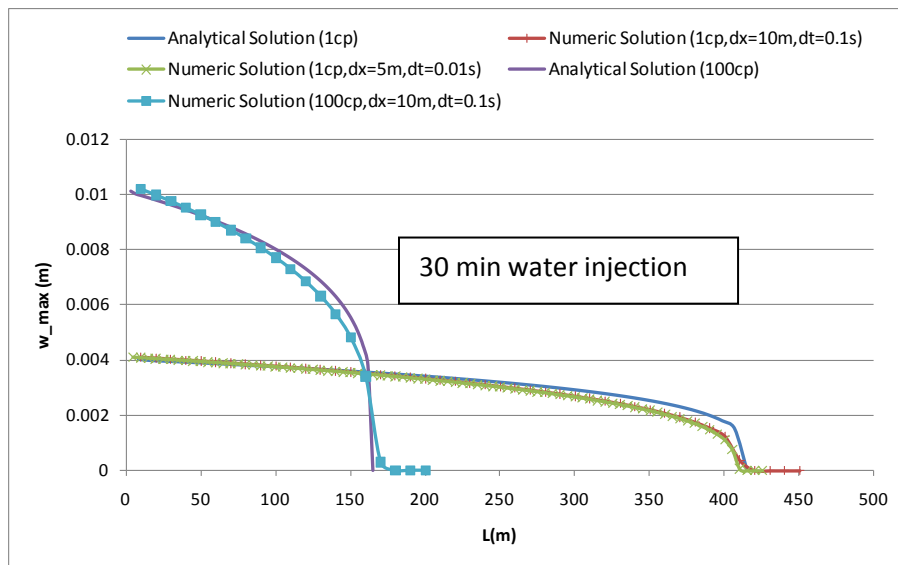
Figure 71. Comparison between analytical solutions and numeric solutions

Base Case (History Matching Case)

After validating our simulator, a field case is history matched by our simulation. The field data is obtained from an older single well in Barnett [Franz et al., 2005]. Figure 72 shows the cumulative gas production and gas rate of the fractured well.
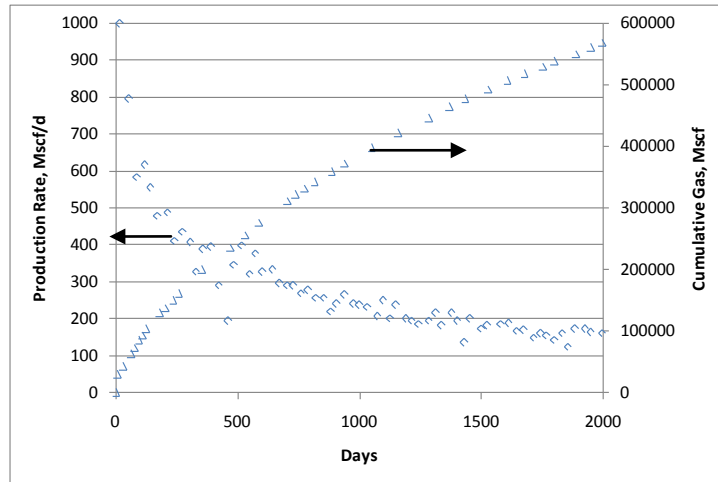
Figure 72. 2000 days of cumulative production and gas rate from a single fractured well

Reservoir Pressure	3750 psia
Matrix Gas Porosity	4%
Shale Thickness	300 ft
Gas Desorption	Vl=88scf/ton, Pl=440psi
Matrix Permeability	0.0001 md
Natural Fracture Permeability	0.001 md
Natural Fracture Porosity	0.1%
Natural Fracture Spacing	20 ft orthogonal when used

Table 11. Reservoir parameters for the history matching case

Injection rate of slurry = 0.05 m3/s
10 minutes initial water pad injection

10 minutes water-sand slurry injection
Injected sand concentration = 20vol%
Propped fracture Length = 170 m
Constant well pressure constraint = 500 psi

Table 12. Injection schedule

The reservoir parameters used for simulation are listed in Table 11. The parameters adjusted for matching the simulations with the field data are listed in Table 12. The first step in this history match is running the fracture propagation simulator to obtain the fracture geometry and the proppant concentration distribution, which is shown in Figure 73.
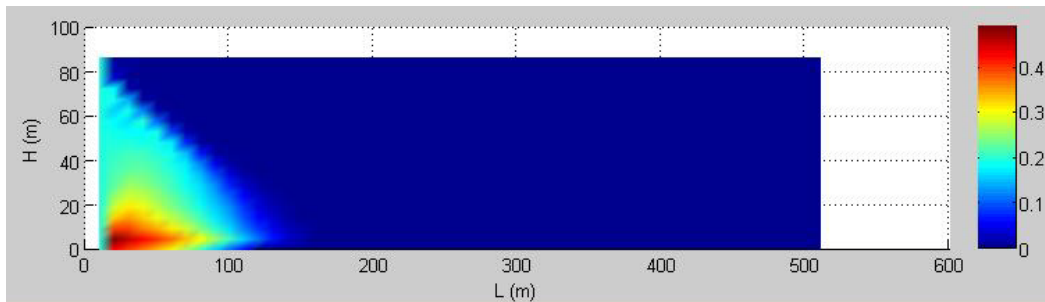
Figure 73. Proppant concentration distribution from the Frac Simulator

The second step is converting the proppant concentration to the fracture conductivity distribution and importing it into the CMG reservoir simulator as shown in Figure 74.
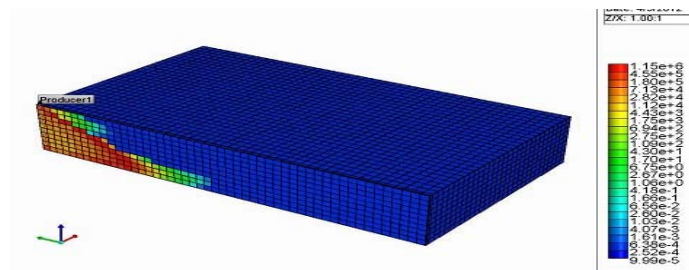
Figure 74. Conductivity distribution from the CMG

The gas production estimated (dashed lines) from the CMG simulator is compared in Figure 75 with the field data (dots). The simulation results can match the field data very well by adjusting the parameter values. This field case is taken as the reference case or base case for the following studies.
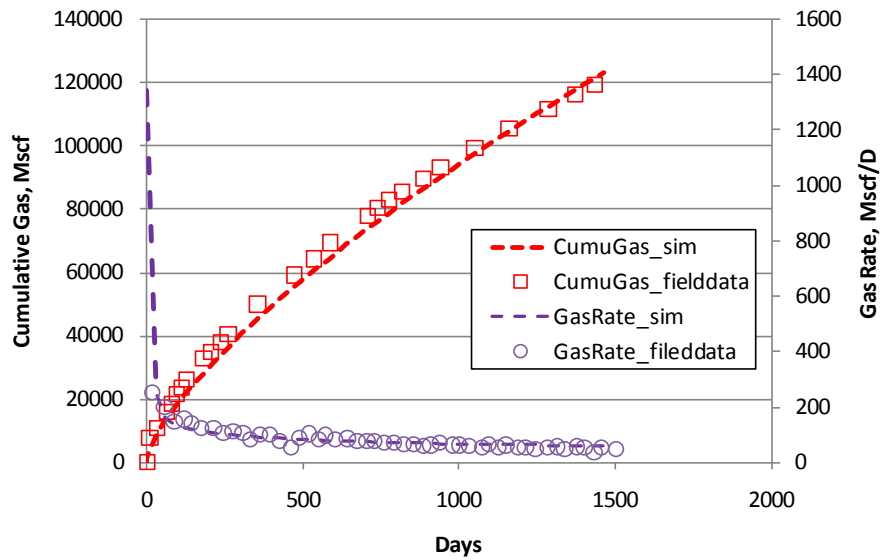
Figure 75. History match results

Impact of Proppant on Production
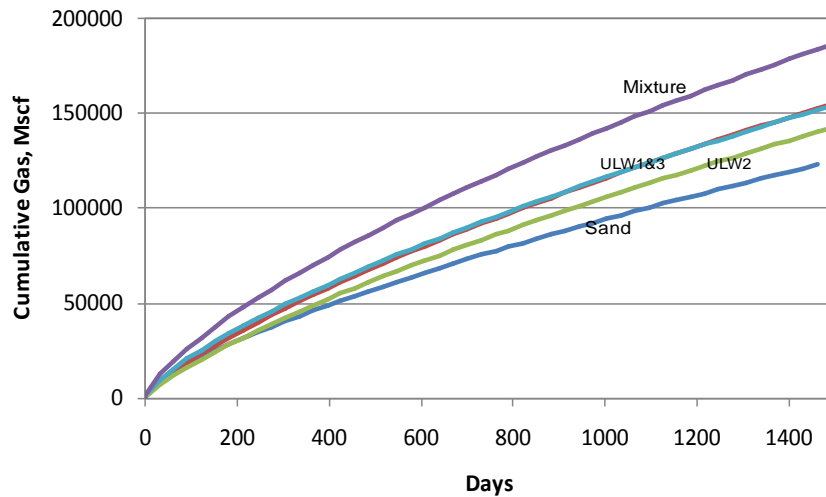
Figure 76. Cumulative production of 5 years for different proppants

In this study, all the parameters are the same as the base case except the proppants. Water is injected as the initial pad for 10 minutes and as the proppant laden fluid for another 10 minutes. ULW1 Polymer, ULW2 Resin-Walnut, ULW3 Resin-Ceramic and the mixture (25% each of ULW1 Polymer, ULW2 Resin-Walnut, ULW3 Resin-Ceramic and sand), are chosen as the proppants. The final production results are compared with the base case in Figure 76.

According to the results above, the proppant mixture gives the best production. ULW1 Polymer and ULW3 Resin-Ceramic are the second best with a similar production results. ULW2 Resin-Walnut is the third best and the sand is the worst. The conductivity distributions of these fractures are shown in Figure 77.

Sand

ULW1 Polymer

ULW2 Resin-Walnut

ULW3 Resin-Ceramic

Mixture

Figure 77. Conductivity distribution for each proppant

The sand and ULW3 Resin-Ceramic have the much larger conductivities than ULW1 Polymer and ULW2 Resin-Walnut at the same concentrations. But ULW1 Polymer and ULW2 Resin-Walnut can be placed more uniformly by water in the fracture than ULW3 Resin-Ceramic and sand due to their smaller specific gravities. The reason that the mixture is the best is that the ULW1 Polymer, ULW2 Resin-Walnut proppants retard the settling of the sand and ULW3 Resin-Ceramic to make them travel farther and be distributed more uniformly, and at the same time exhibit a large conductivity value due to the presence of sand and ULW3 Resin-Ceramic. Overall, the mixture combines the advantage of good distribution of ULW1 Polymer, ULW2 Resin-Walnut with the advantage of high conductivity of ULW3 Resin-Ceramic and sand.

Figure 78. Production performance of 10 years for different ULW1 Polymer/sand ratios

To further study the ULW proppants impact on the sand distribution and the final production performance, ULW1 Polymer is added to sand at different ratios. The 10 year cumulative productions of cases with different ULW1 Polymer/sand ratios are compared in Figure 78. Increasing the sand volume from 20% to 30% does not help the production, while adding a small (1%) amount of ULW1 Polymer proppant in the sand can greatly improve the production. As the ULW1 Polymer concentration increases, the improvement of the production slows down, which is shown in Figure 79.
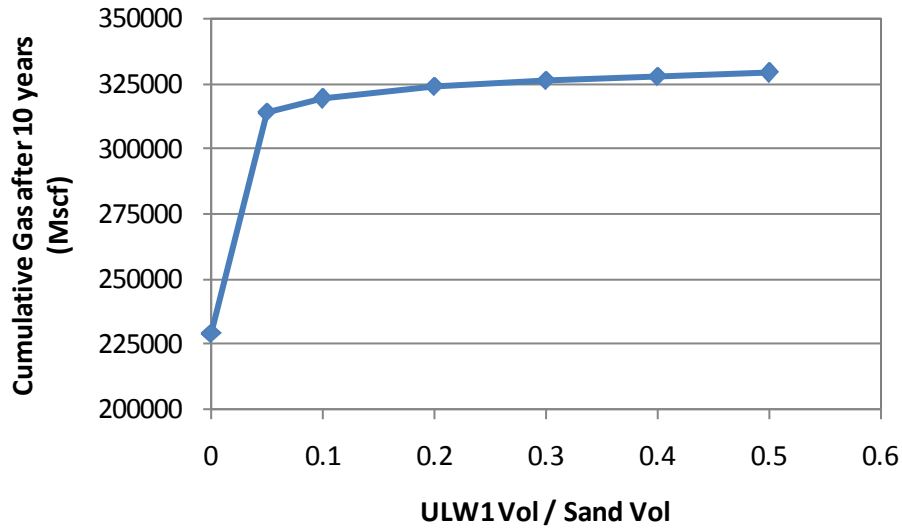
Figure 79. Production after 10 years vs. ULW/sand ratio

Impact of Foam on Production

In this study, all the parameters are the same as the base case except for the fracturing fluid. Water and a 60% quality foam chosen as the fracturing fluids. The total injection volume of both water and foam are the same (10 minute initial pad injection followed by 10 minute slurry injection). Figure 80 shows that although the sand can be placed uniformly by foams, but the fracture length opened by foams is shorter than that created by water because of the much larger viscosity of foams than that of water. It should be noted that the fracture length and the conductivity distribution are both important to fracture production.
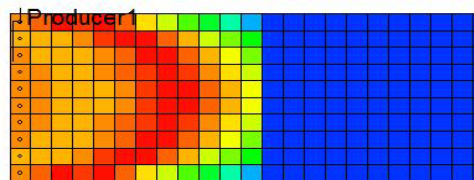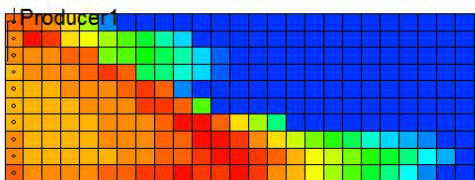
10 min water/sand injection (L_{frac}=240m)   10 min foam/sand injection(L_{frac}=120m)

Figure 80. Conductivity distribution for water/sand slurry and foam/sand slurry

Figure 81 compares the foam fracturing performance and the water fracturing performance under different circumstances. For the base case, water is better than foam. As the injection time increases, the foam gradually outperforms water. Besides, for a higher permeable reservoir, the foam also can be a better fracturing fluid than water. The reason is that the fracture length is most critical to production for low permeability reservoirs while the fracture conductivity is more critical for high permeability reservoirs.
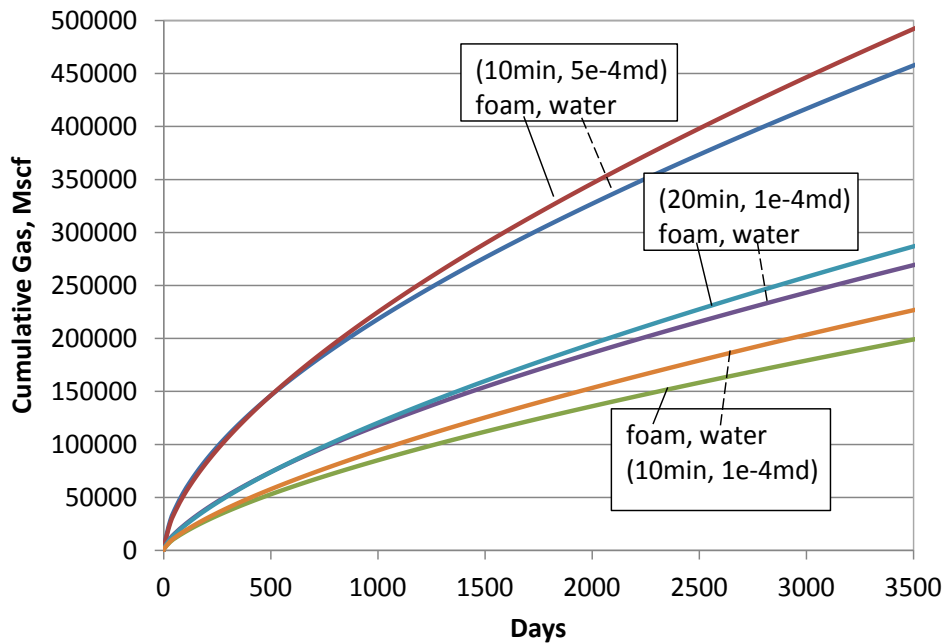
Figure 81. Production trend along 10 years for different cases.

Impact of Proppant Injection Strategy on Production

Other than proppants and fluids, the injection strategy is another important parameter affecting the production performance. There are 6 cases, with different injection schedules and strategies, studied in this section. The injection schedule for each case is listed in Table 13. For

all the cases, the water is injected as the initial pad for 10 minutes. Following that, the slurry is injected for another 10 minutes.

Case1	**water/sand** slurry
Case2	**foam/sand** slurry
Case3	**water/sand** slurry followed by **water/ULW1 Polymer** slurry
Case4	**water/ULW1 Polymer** slurry followed by **foam/sand** slurry
Case5	**water/ULW1 Polymer** slurry followed by **water/sand** slurry
Case6	**water/mixture(ULW1 Polymer+sand)** slurry

Table 13. Injection schedule variations

To make a fair comparison, the total injected slurry volume and proppants amount are kept the same for all 6 cases. The production after 10 years is shown in Figure 82. Compared with the base case, all other injection schedules improve the fractured well productivity. The production is the highest for water-sand/ULW1 Polymer mixture (case 6) and water-ULW1 Polymer slurry followed by water-sand slurry (case 5). For case 6, ULW1 Polymer injected along with the sand can enhance the sand distribution and optimize the conductivity distribution. For case 5, The ULW1 Polymer is injected in the first stage to maximize the propped fracture length. The sand injected in the second stage can form a high conductive conduit in the near-wellbore part. This is also an ideal conductivity distribution for production. As illustrated in Figure 83, the gas flow (V_cum) decreases along the fracture as the distance from the wellbore

(x) increases. Pressure drop (DP) between the fracture pressure and the well bore pressure increases with x. So a higher proppant conductivity is needed for the fracture near the well bore, while a much smaller conductivity is sufficient for the fracture away from the well bore.
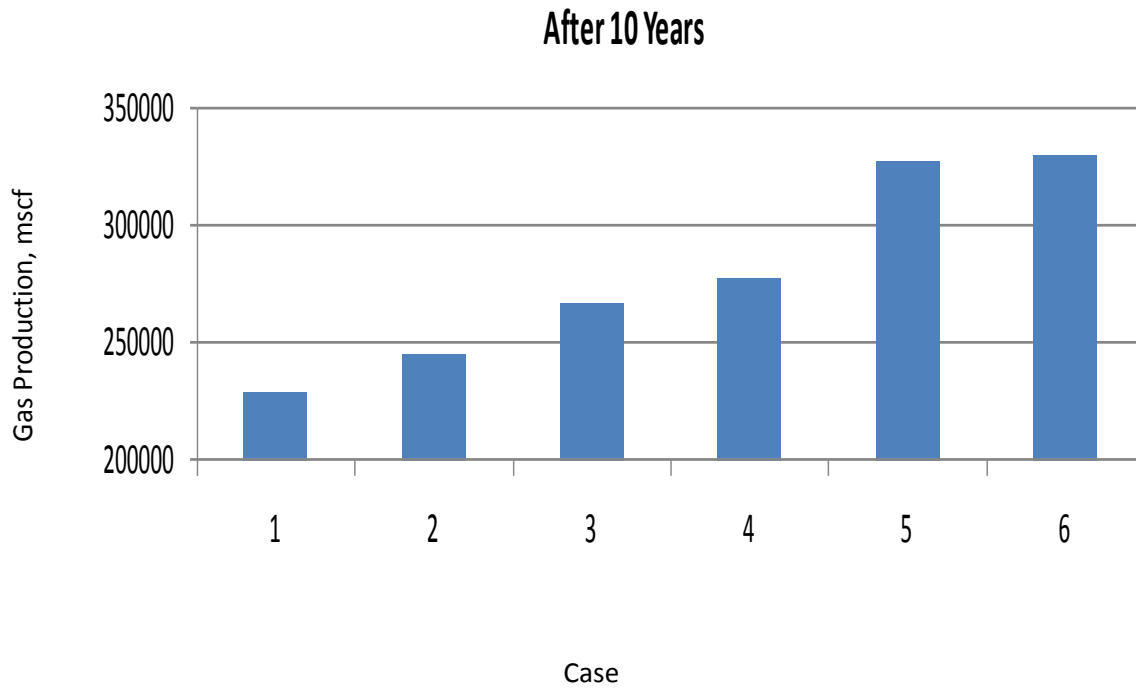
After 10 Years

Figure 82. Production after 10 years for 6 cases
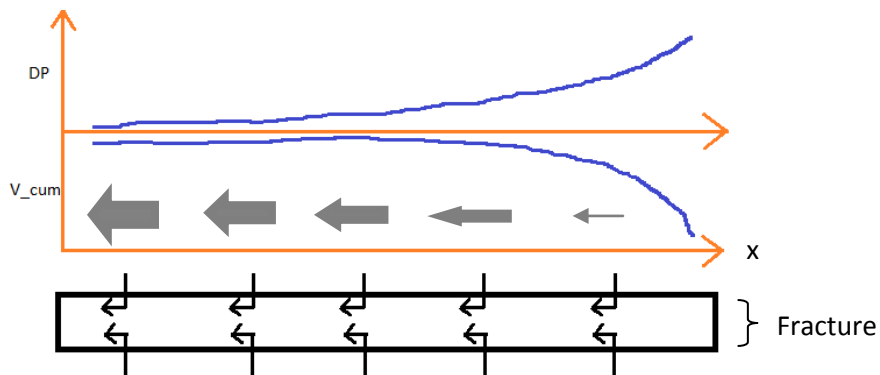
Figure 83. Pressure difference and cumulative flow rate distributions along the fracture

Impact of Fracturing Fluid Leakoff

In the previous study, the leakoff effect was not considered. In this study, we consider this impact by adding a leakoff term in the differential equation below,

$$-\frac{G}{64(1-v)h}\frac{d}{dx}\left[\frac{\partial(w_{max}{}^4)}{\mu\partial x}\right]+\boxed{\frac{C_{leakoff}}{\sqrt{t-\tau}}}+\frac{dw_{max}}{dt}=0$$

The leakoff coefficient is calculated to be 5.67E-7 $m/s^{1/2}$ for the water and 1E-7 $m/s^{1/2}$ for the foam. Figure 84 compares the simulation results from the model with and without leakoff terms.
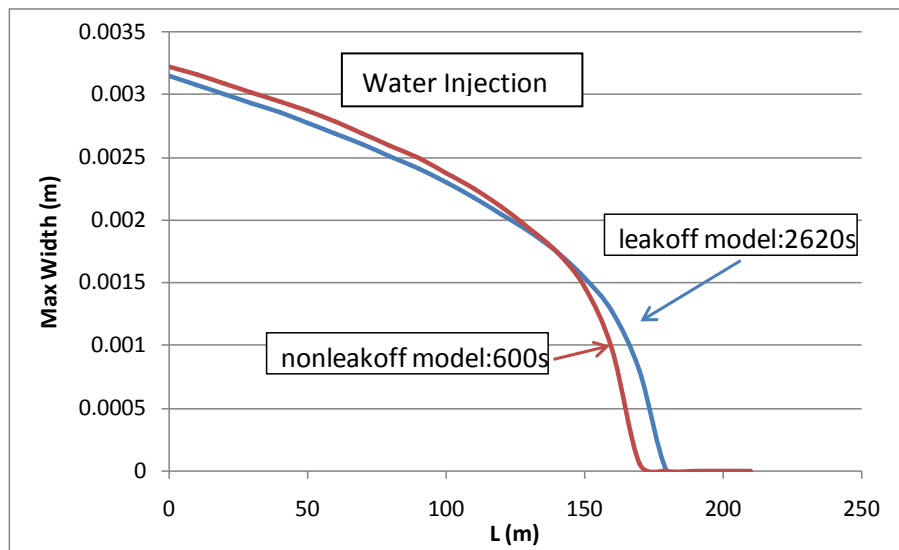
Figure 84. Fracture width calculated from leakoff and non-leakoff models.

The inclusion of leakoff increases the time spent to create the same length of the fracture. In this case, the fracturing time is four times larger with the leakoff model (43.67 min to open a fracture of length 170-180m) compared to the non-leakoff model (10 min). Figure 85 compares the production results calculated from both the leakoff model and the non-leakoff model for different slurry injection schedules outlined in Table 14.
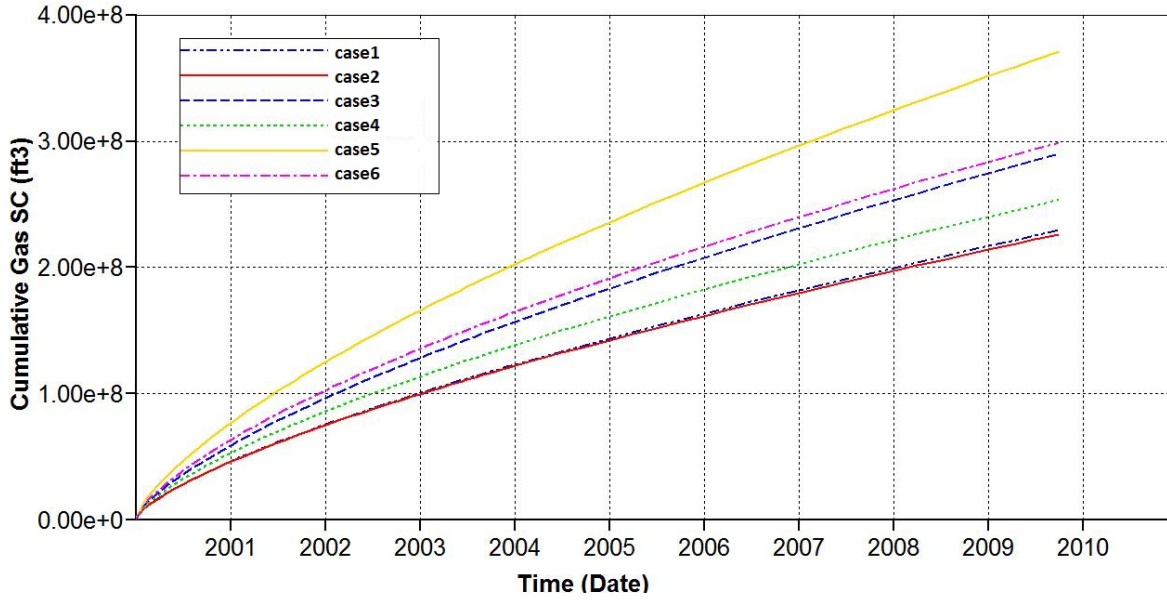
Figure 85. Ten years production trends from leakoff and nonleakoff models.

All the cases show that the production decreases when the leak-off is included. This is because the proppant settle down in a shorter length when the leakoff occurs, which can be observed by comparing the conductivity distributions with and without the leak off in Figure 86.

Case1	No leakoff	10min waterpad + 10min water-sand slurry
Case2	Leakoff	40min waterpad + 10min water-sand slurry
Case3	No leakoff	10min waterpad + 20min water-sand slurry
Case4	Leakoff	40min waterpad + 20min water-sand slurry
Case5	No leakoff	10min waterpad + 30min water-sand slurry

Case6	Leakoff	40min waterpad + 30min water-sand slurry

Table 14. Injection schedule for 6 cases
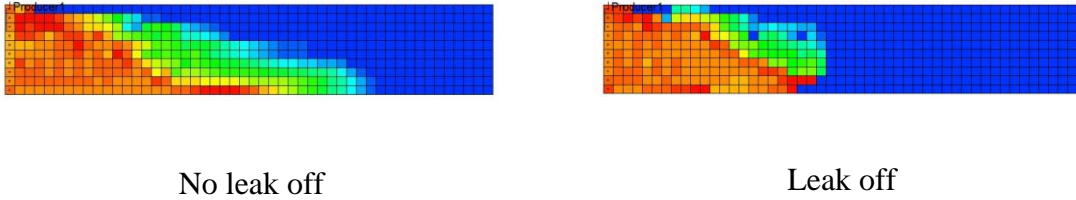
No leak off   Leak off

Figure 86. Conductivity distributions by injecting 30 min slurry from leakoff and non-leakoff models.

The leakoff decreases the water horizontal velocity; the fracture width is smaller when there is leakoff, which leads to a higher wall retardation effect on proppant flow. Another important conclusion from Figure 85 is that the leakoff impact becomes larger as the injection time increases.

By using the new simulator updated with the leakoff model, the foam effect is re-studied. The detail information of three cases are listed below,

Case1	Leakoff	43.67min water pad + 30min water/sand slurry
Case2	Leakoff	10min foam pad +30 min foam/sand slurry
Case3	Leakoff	43.67min water pad +30 min foam /sand slurry

Table 15. Three cases injection schedules
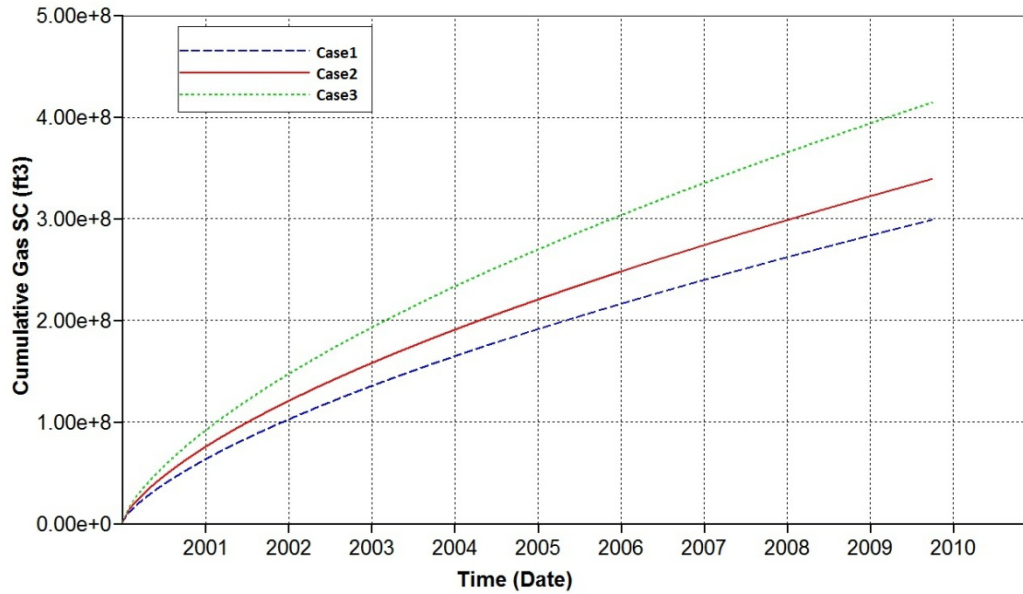
Figure 87. Ten years production comparison of water and foam treatment by considering leakoff

The 10 years production results for three cases are plotted in Figure 87. The foam performs better than water because it leaks off much slower than water. The design of water as the initial pad and foam as the proppant carrying fluid is the optimum design outperforming the other two designs, because it not only increases the fracture length by initializing fracture with low viscosity water but also has better proppant placement due to lower leakoff and high viscosity of foams.

Impact to Producers

This project made developments in two areas: use of lightweight proppants and foam fracturing fluids. The simulation of the fracturing process showed that mixing a small amout of ULW1 Polymer proppant with the sand can increase the propped fracture length in slick water fracturing and increase the productivity of the reservoir. This idea needs to be field tested. The tests also showed that gel-free foam can carry sand further into the fracture and improve the fracture conductivity. Again the idea needs to be field tested. Field testing of these ideas are very expensive now-a-days because the wells have multiple fractures. All the fractures need to be created using the same process; otherwise the process cannot to be evaluated.

Technology Transfer Efforts

Presentations:

Mohanty, K.K., "Modeling Fracturing Process: Effect of Fracturing Fluid," NSF Workshop on Hydraulic Shale Fracturing, Arlington, VA, May 14-15, 2012.

Gu, Ming, "Foams for Shale Fracturing," Presented at the RPSEA Conference on Unconventional Gas, Pittsburgh, April 17-18, 2012.

Gu, Ming, "Improved Fluids for Shale Fracturing," Presented at the RPSEA Conference for Small Producers, Lawrence, November 7-8, 2011.

Mohanty, K. K., "Light Weight Proppants for Shale Fracturing," Presented at the RPSEA Conference on Unconventional Gas, Denver, April 19-20, 2011.

Gaurav, A., "Ultra-Lightweight Proppants in Shale Gas Fracturing," SPE 138319, SPE Tight Gas Completions Conf., San Antonio, November 2-3, 2010.

Mohanty, K. K., "Improvement of Fracturing for Gas Shales," Presented at the RPSEA Conference on Unconventional Gas, Denver, April 19-20, 2011.

Publications:

Gaurav, A., Dao, E. & Mohanty, K. K., "Evaluation of Ultra-Lightweight Proppants for Shale Fracturing," *J. Petrol. Sci. & Engg.*, accepted for publication (2012).

Gaurav, A., Dao, E. & Mohanty, K.K., "Ultra-Lightweight Proppants in Shale Gas Fracturing," SPE 138319, Proceedings of the SPE Tight Gas Completions Conf., San Antonio, November 2-3, 2010.

Reports:

Topical Progress Report-1, RPSEA, November, 2009.

Topical Progress Report-2, RPSEA, July, 2010.

Topical Progress Report-3, RPSEA, November, 2010.

Topical Progress Report-4, RPSEA, November, 2011.

Topical Progress Report-5, RPSEA, August, 2012.

Conclusions

- ULW-1 is spherical, ULW-2 is slightly angular and UlW-3 is highly angular.

- Bulk density of ULW-1 is the least (0.6 gm/ml); that of ULW-3 is the highest (1.2 gm/ml). ULW-2 pack has an intermediate density (0.8 gm/ml).

- Of the three proppants tested, ULW-1 is the most deformable and ULW-3 is the most brittle. ULW-2 is fairly deformable. Measurement of fracture conductivity would determine whether the permeability loss due to deformation is small enough to make them useful in Barnett shale applications.

- ULW-1 and ULW-2 lose small amounts of proppants due to crushing of the proppant pack, whereas ULW-3 loses a significant amount due to formation of fines. After failure, ULW-3 leaves fine broken pieces, which can plug up the pores on the fracture surface.

- Of the three proppants tested, two of them, namely ULW-1 and ULW-2 were significantly strong to be able to endure the stresses expected in the Barnett shale conditions as individual particles. The failure points of ULW-3 particles tested lied marginally above the expected stresses in Barnett shale.

- Proppant pack conductivity decreases as the confining stress increases. The decrease is a little lower for partial monolayers. This decrease is also lower for ULW 3 because it is more rigid.

- Conductivity is an increasing function of proppant concentration for ULW 3. For ULW1 Polymer and ULW2 Resin-Walnut, the conductivity has a minimum at about 0.1-0.4 lbm/ft^2; the partial monolayer conductivity is not much lower than that of multilayer packs.

- The proppant conductivity is low (of the order of 1-10 mD-ft) at 6000 psi confining stress.

- The foam stability depends on the surfactant used. Of the surfactants studied, the anionic surfactant Anionic 1 had best foam stability, while the nonionic surfactant Nonionic NP30 had the worst foam stability. The half-life for the Anionic 1 surfactant was a lot higher than one hour (thus greater than the time needed to put one hydraulic fracture in these wells).

- The addition of the stabilizer glycerol to a nonionic surfactant solution can improve the foam stability. The addition of the amphoteric surfactant, Amphoteric 1, to cationic surfactant solutions did not change their foam generation capability, but slightly enhanced their stability. The addition of an anionic surfactant to the eight cationic surfactants improved foam generation. Use of longer hydrophilic groups in the nonionic surfactant improved foam stability in most cases.

- Increasing the surfactant concentration causes an increase in foam stability, for the reason that the more surfactant molecules could be absorbed on the surface of the liquid film to make the film stronger.

- High temperature reduces the stability of foams.

- The bubble size affects foam stability. The foam column with a larger bubble size has a lower stability.

- Proppants follow Happel equation for settling velocity in water. Proppants hardly fall in foams tested.

- The three kinds of water foams (A: 0.5 vol% regular anionic surfactant fluid, B: Fluid A + 2 vol% glycerol, C: 0.5 vol% viscoelastic surfactant fluid) all exhibited rheological behavior analogous to a power-law fluid.

- The regular surfactant water foams showed shear thinning behavior at qualities above 0.5 and shear thickening below 0.5. The VES foams showed shear thickening at qualities from 0 to 60%.

- Temperature lowers the viscosity of low quality foams, while pressure increases the viscosity of the high quality foams.

- Compared with water, the low quality foams made by fluid A and B are more viscous at a low shear rate range, but at a high shear rate range they appear less viscous because water flow is turbulent and foam flow is laminar. This property is good for reducing pump pressure head while keeping the enough viscous force for proppant transport in fractures.

- The aqueous foams A and B are both less viscous than 20 lbm/Mgal guar foams, while the VES foam C has an apparent viscosity similar to that of guar foams with 20 to 30 lbm/Mgal.

- The 50% quality foams made from fluid A were injected into a fracturing slot for the proppant transport study. Good proppant suspension and transport were observed.

- By adjusting the injection time of initial pad and slurry, the proppants injection concentration, the simulations can match the field data well.

- The ULW proppants gave better gas production than sand, but the mixture of ULW and sand can be the best choice.

- Adding small amount of ULW1 Polymer can highly improve the sand performance by improving the sand placement. More ULW1 Polymer addition is not necessary because of its decreasing production improvement efficiency with increasing concentration.

- Foam can be a better choice than water for highly permeable reservoirs or longer injection schedules.

- Different injection strategies can highly impact the fractured well performance. By using our simulation techniques, the injection strategy can be easily optimized for maximum production results. In this single well case (Barnett), injecting water/mixture of sand and ULW1 Polymer slurry after the initial water pad injection can be the best design choice.

- Leakoff also affects the production results, especially for a long injection schedule. The single-phase leakoff coefficient can be calculated from the Darcy's law. The leakoff rate of foam is assumed to be 1/5 of that of water. Foam performs better than water because of its low leakoff rate and high proppant transport capacity.

Recommendations

- Field test mixtures of lightweight proppants and sand to improve the transport of sand proppants and the propped fracture conductivity.

- Field test foams as the fracturing fluid to improve sand transport and the propped fracture conductivity.

Acknowledgements

References

Aboud, R. S., and Melo, R. C. B., "Past Technologies Emerge Due to Lightweight Proppant Technology: Case Histories Applied on Mature Fields", SPE 107184, presented at the 2007 SPE Latin American and Carribean Petroleum Engineering Conference held in Buenos Aires, Argentina, 15-18 April 2007.

Agrawal, R.G., Carter, R.D., and Pollock, C.B., "Evaluation and Performance Prediction of Low-Permeability Gas Wells Stimulated by Massive Hydraulic Fracturing," JPT, 362-372, 1979.

Asmolov, E. S., "The inertial lift on a small particle in weak-shear parabolic flow", Physics of Fluids, v. 14, No. 1, pp. 15, 2002.

Brannon, H. D., Malone, M. R., Rickards, A. R., Wood, W. D., Edgeman J. R., and Bryant, J. L., "Maximizing Fracture Conductivity with Proppant Partial Monolayers: Theoretical Curiosity or Highly Productive Reality?", SPE 90698, presented at the SPE Annual Technical Conference and Exhibition held in Houston, Texas, U.S.A., 26-29 September 2004.

Bonilla, L. F. et al.: "Experimental Investigation on the Rheology of Foams", SPE 59752 (2000).

Brannon, H. D., and Starks, T. R., "Maximizing Return on Fracturing Investment by Using Ultra-Lightweight Proppants to Optimize Effective Fracture Area: Can Less Really Deliver More?", SPE 119385, presented at the 2009 Hydraulic Fracturing Technology Conference held in The Woodlands, Texas, USA, 19-21 January 2009.

Cinco-Ley, H., Samaniego-V., F., and Dominguez-A., N.: "Transient Pressure Behavior for a Well With Finite-Conductivity Vertical Fracture, "Soc. Pet. Eng. J. (Aug 1978) 253-264.

Darin, S.R. and Huitt, J.L.: "Effect of a Partial Monolayer of Propping Agent on Fracture Flow Capacity", SPE 1291-G, presented at the Annual Fall Meeting of SPE, Dallas, October 4-7, 1959.

Frantz, J.H., Williamson, J.R., Sawyer, Johnston, D. "Evaluating Barnett Shale Production Performance-Using an Integrated Approach", SPE 96917, 2005.

Gadde, P.B., Liu, Y., Norman, J., Bonnecaze, R., and Sharma, M.M., "Modeling Proppant Settling in Water Fracs," SPE 89875, Presented at the SPE ATCE, Houston, 26-29 September, 2004.

Gidley, J. L. et al.: "Recent Advances in Hydraulic Fracturing", SPE Monograph 12 (1989).

Harris,P.C.: "High-Temperature Rheological Study of Foam Fracturing Fluids", SPE 13177 (1987).

Harris, P.C.: "Effects of Texture on Rheology of Foam Fracturing FLuids", SPE 14257 (1989).

Harris, P.C.: "A Comparison of Mixed-Gas Foams with N2 and CO2 Foam Fracturing Fluids on a Foam-Loop Viscometer", SPE 20642 (1995).

Harris, P.C. et al.: "High-Quality Foam Fracturing Fluids", SPE 35600 (1996).

Harris, P.C. et al.: "Rheology of Crosslinked Foams", SPE 28512 (1996).

Harris, P.C. et al.: "Measurement of Proppant Transport of Frac Fluids", SPE 95287 (2005).

Howard, G. C., Fast, C. R.: "*Monograph 2 – Hydraulic Fracturing",* AIME, Millet the Printer, Dallas, TX (1970).

Hutchins, R. D.: "A Circulating Foam Loop for Evaluating Foam at Conditions of Use", SPE 80242 (2003).

International Standard, "Procedures for measuring the long-term conductivity of proppants", ISO 13503-5.

Liu, W. "Settling and Hydrodynamic Retardation of Proppants in Hydraulic Fractures", Ph.D. Dissertation, UT Austin, 2006.

Mcguire, W. J., and Sikora, V. J.,: "The Effect of Vertical Fractures on Well Productivity," *Trans*., AIME (1960) **219**, 401-03.

Mitchell, B.J.: "Viscosity of Foam", PhD dissertation, U. of Oklahoma, Norman (1970).

Palisch, T. T., Vincent, M. C., and Handren, P. J., "Slickwater Fracturing: Food for Thought", SPE 115766, presented at the 2008 SPE Annual Technical Conference and Exhibition held in Denver, Colorado, USA, 21-24 September, 2008.

Reidenbach, V.G., Harris, P.C.: "Rheological Study of Foam Fracturing Fluids Using Nitrogen and Carbon Dioxide" SPE12026 (1986).

Rickards, A. R., Brannon, H. R., Wood, W, D., and Stephenson, C. J., "High Strength, Ultralightweight Proppant Lends New Dimensions to Hydraulic Fracturing Applications", SPE 84308, presented at the 2003 SPE Annual Technical Conference and Exhibition, Denver, 5-8 October, 2003.

Sani, A.M., at al.: "Experiment Investigation of Xanthan Foam Rheology", SPE 67263 (2001).

Schein, Gary. W., "The Application and Technology of Slickwater Fracturing", SPE 108807, SPE Distinguished Lecture, 2005.

Sudhakar, D. K.: "New Empirical Friction Loss Correlation for Foam Fluids in Coiled Tubing", SPE 74810 (2002).

Sudhakar, D. K.: "New Rheological Correlations for Guar Foam Fluids", SPE 88032 (2004).

Terracina, J. M., Turner, J. M., Collins, D. H., and Spillars, S. E., "Proppant Selection and Its Effect on the Results of Fracturing Treatments Performed in Shale Formations", SPE 135502-MS, presented at the SPE Annual Technical Conference and Exhibition, Florence, Italy, 19-22 September, 2010.

Tinsley, J. M. *et al.*: "Vertical Fracture Height-Its Effect on Steady-State Production Increase," *JPT* (May 1969) 633-38; *Trans*., AIME, **246.**

Wang, F., "Production Fairway: Speed Rails in Gas Shale," Presented at the 7th Annual Gas Shale Summit, Dallas, Texas, 6-7 May, 2008.

Analysis of Fracturing Treatments Using Light Weight Proppant

By

Ali Daneshy

Daneshy Consultants Int'l

Introduction

The production increase resulting from a hydraulic fracture depends on the length of the created fracture, and its permeability. Based on reservoir engineering analysis, one can show that increasing the length of the permeable fracture will improve the production results. Because of its higher density (relative to water) the proppant gradually settles inside the fracture and can accumulate at its bottom. The main mechanism for slowing proppant settlement has been increasing fluid viscosity. While high flow velocity can also carry the proppant, the fluid velocity inside the fracture drops rapidly away from the wellbore and is not sufficient to carry the proppant.

The oil and gas industry has established that economical production from very low permeability reservoirs requires creating long fractures, in the order of several hundred to over 1000 feet. These require injection of large volumes of fluid, in the order of several hundred thousand to millions of gallons per well. Viscosifying these large volumes of fluid requires large amounts of expensive additives which increase the cost of the treatment. The production rates from low permeability reservoirs often are not sufficient to justify these costs. The industry response has been to use lower cost fluids for hydraulic fracturing of these reservoirs. The most common fluid is a mixture of water plus friction reducer, which is commonly called "slick

water". The disadvantage of slick water is that its low viscosity is not sufficient to carry the proppant deep inside the fracture. Thus, the proppant pumped with slick water is expected to rapidly settle inside the fracture, resulting in a short fracture length.

Study of fracture permeability has shown two general systems for creating permeability. In one system one tries to fill the fracture with large amounts of proppant, thus creating a wide permeable fracture. In this system the fluid flows through the packed proppant body. The other system is known as partial mono-layer, which requires much smaller amounts of proppant. In this approach the proppant covers only a part of the fracture. Its main role is to keep the fracture open. Reservoir fluid flows around the proppant and through the sections kept open by it. In this system the proppant serves the role of a pillar that keeps the fracture open for flow around the pillar.

The appeal of the light weight proppant relates to the expectation that because of its lower density it can travel deeper inside the fracture, thus creating a longer propped (and permeable) fracture length. However, since these proppants are usually more expensive than sand (the most common type of proppant), the industry can not afford these for low permeability and productivity reservoirs. Thus, a possible solution to the dilemma has been to try to build the proppant in a partial mono-layer form.

As is the case with many new products, the oil and gas industry is trying to establish the optimum method for use of the light weight proppants by the trial and error technique. To this end, several different techniques of injecting this proppant inside the fracture have been experimented in different wells. Below we present a few example cases of these trials together with the rationale for their design. In addition, we will try to highlight some of the operational results of using ultra light weight proppant. In each case sufficient well information will be

presented to give the reader a sense of the well condition, its completion, and some general observations specific to each fracturing treatment. At the end of this presentation we will offer comments regarding the productivity of these wells and general observations regarding the use of light weight proppants. The following pertain to all the example cases report here.

The fracturing fluid was "slick water". The initial injected volume is commonly called "pad volume" and it does not contain any proppant. The purpose of pad volume is to establish ability to inject into the well with acceptable pressures and rates, and create a fracture capable of receiving the subsequent slurry mix. In addition, in most treatments HCl acid is pumped into the well at the beginning of pumping in order to clean the perforations and lower the breakdown pressure of the formation. Following the injection of pad volume, a slurry consisting of proppant and fluid is injected into the well. Initially this slurry contains a small concentration of proppant. Gradually as more slurry is pumped into the well the concentration of proppant is increased. Pumping continues until the planned volume of fluid and proppant weight is injected inside the fracture.

Chart Specifications

All the fracturing charts presented in this section have the following common characteristics;

X-axis depicts the elapsed pumping time

Pressure is shown in dark blue color and its scale is on the y-axis on the left-hand side of the graph

Injection rate is shown in color pink and its scale is on the y-axis on the right-hand side of the graph

Proppant concentration is shown in dark brown and its scale is also on the y-axis on the right hand side of the graph. Because the numerical value of proppant concentration is much lower than the injection rate, the scale for it is in 0.1 #/gal or 0.01 #/gal.

Treatment #1. This well is located in the Barnett formation and is drilled to a vertical depth of 7,620 ft, with measured depth of 10,748 ft. The well was completed with a 5 ½ in. cemented casing. The temperature at the bottom of the well was 178 $^{\circ}$F. This well was fractured in 8 stages. The examples shown here are from the fractures in stages 2 and 7 of this well.

Stage 2. The perforated interval in this stage extended from 10,040 – 10,253 ft. There were 38 perforations covering 213 feet of this interval. Perforation diameters were 0.42 in.

The pumping data for this treatment was as follows. The pad volume was 43,500 gal plus 2,500 gal of 15% hydrochloric acid (HCl). The injected slurry volume was 653,000 gal. Proppant weights and types were; 137,500 lbs 100 mesh sand, 40,000 lbs 20/40 mesh sand, and 18,000 lbs 14/40 mesh ULW1 Polymer proppant. It should be noted that because of its low specific gravity, the ULW1 Polymer proppant occupies a larger volume than sand with the same weight.
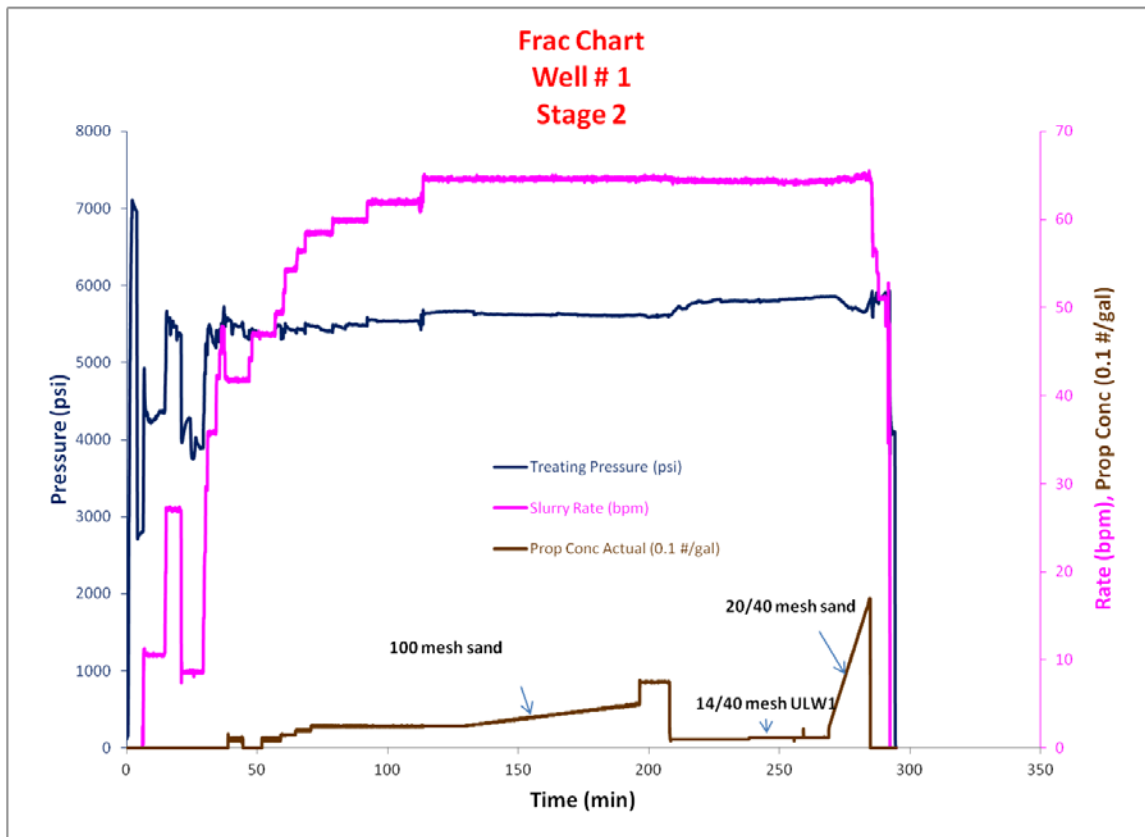
Fig. A1. Fracturing treatment chart for Well #1, Stage 2 fracture

During the early injection period the rate was gradually increased such that the pumping pressure was within the safe range (Figure A1).

The initial proppant was 100 mesh sand and its concentration was 0.1 #/gal. This concentration was gradually increased in small steps to 0.15, 0.2, and 0.25 #/gal. The reason for the small sand concentration increments was to allow fracture growth create an open path for slurry movement inside the fracture. Next, the proppant concentration was slowly ramped from 0.25 to 0.5# gal. The 100 mesh sand concentration was then increased to 0.75#/gal. By this time the planned weight of 100 mesh sand was pumped inside the fracture.

Injection of the 14/40 mesh ULW1 Polymer proppant started at a concentration of 0.1 #/gal and later increased to 0.12 #/gal. The logic behind pumping this proppant at this time is to

let it move over the 100 mesh sand which has been deposited at the bottom of the fracture and travel deeper inside the formation. This was expected to result in a longer permeable fracture, which is one of the requirements for higher production increase.

The final injected slurry contained 20/40 mesh sand in concentrations increasing from 0.25 #/gal to 2.0 #/gal. The intent of this proppant was to create higher permeability and conductivity near the wellbore. The larger proppant size and higher concentration both yield higher fracture conductivity. The need for higher near wellbore conductivity stems from the fact that all of the produced fluid converges towards the wellbore and so this part of the fracture has to transmit the highest flow rate during production. Another reason is that the flow near the wellbore is radial and fracture needs higher permeability to avoid turbulent flow.

Stage 7. Figure A2 shows the treatment chart for stage 7 fracture. One of the differences between this treatment and the earlier stage is the slower rate of increase in injection rate. This was in response to higher pressures encountered in this well. Also, the maximum rate in this stage was higher. It was reduced to the same level as in stage 2 while pumping the ULW1 Polymer proppant. The reduction in rate was not due to use of ULW1 Polymer.
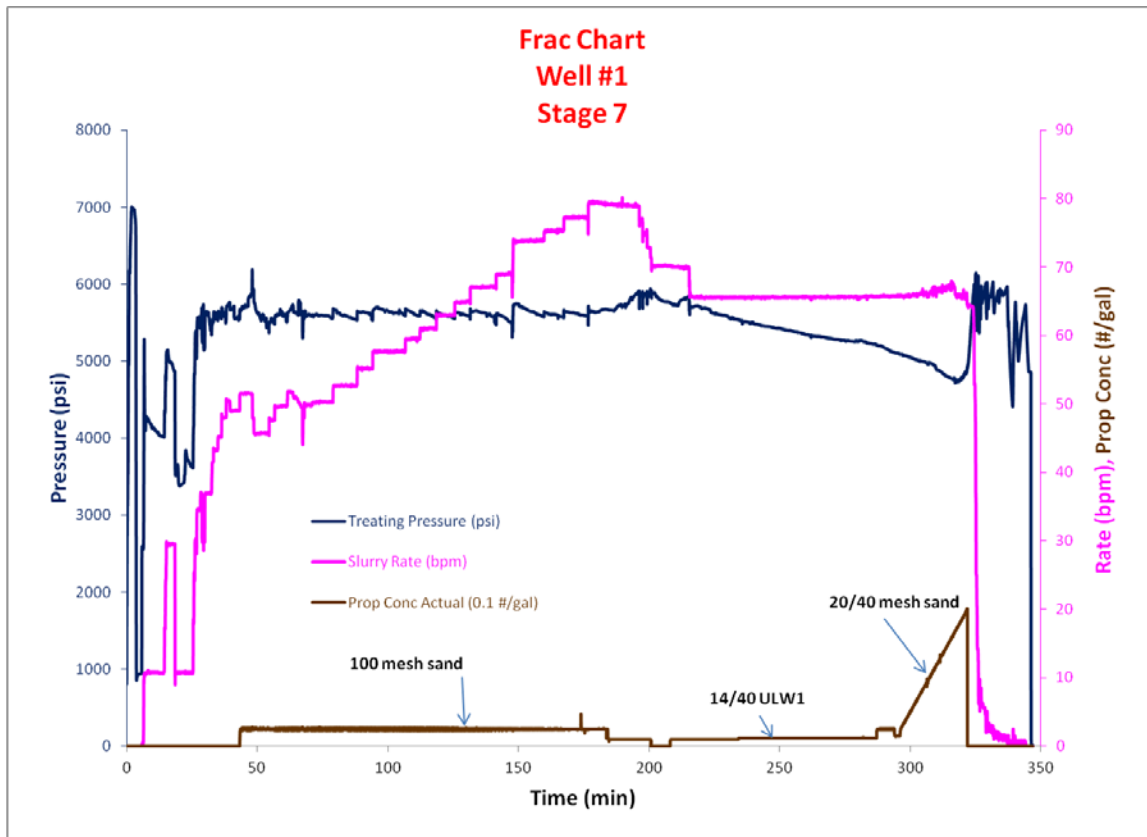
Fig. A2. Treatment chart for the fracture created in Stage 7

The sharp pressure increase at the end of this stage indicates imminent screen-out. This is usually associated with near wellbore filling of the fracture with proppant. Fortunately in this fracture all of the proppant had already been pumped inside the wellbore, although not displaced inside the fracture. The low injection rate at the end of this treatment was necessitated by high wellbore pressure. This injection was intended to displace the sand remaining inside the wellbore into the fracture.

The design philosophy in this well was to initially fill the fracture with sand, and then let the low density proppant move over it deeper inside the formation. If sand was not pumped at the beginning, some of the light weight proppant would have been carried with the fracturing fluid to

the bottom of the fracture and then covered with sand. This would have neutralized its beneficial effect.

Well #2

This well was also drilled in the Barnett formation. It was drilled to a vertical depth of 7,722 ft. Total measured depth was 11,924. It was completed with a cemented 5 ½ in. liner and fractured in 10 stages. For each fracture stage the well was perforated with 48 shots over a four foot interval. Perforation diameter was 0.42 in. The proppant used was ULW2 Resin-Walnut, which has slightly higher density than ULW1 Polymer. Below we present the treatment results for two of the 10 stages.

Stage 1. The fracturing treatment chart for this stage is presented in Figure A3, below. The perforated interval was 11,850 – 11,854 feet. The total injected fluid volume was 861,500 gal. The proppant used consisted of 273,000 lbs 40/70 mesh sand, 190,000 lbs of 100 mesh sand, and 1260 lbs of 45/65 mesh ULW2 Resin-Walnut proppant.
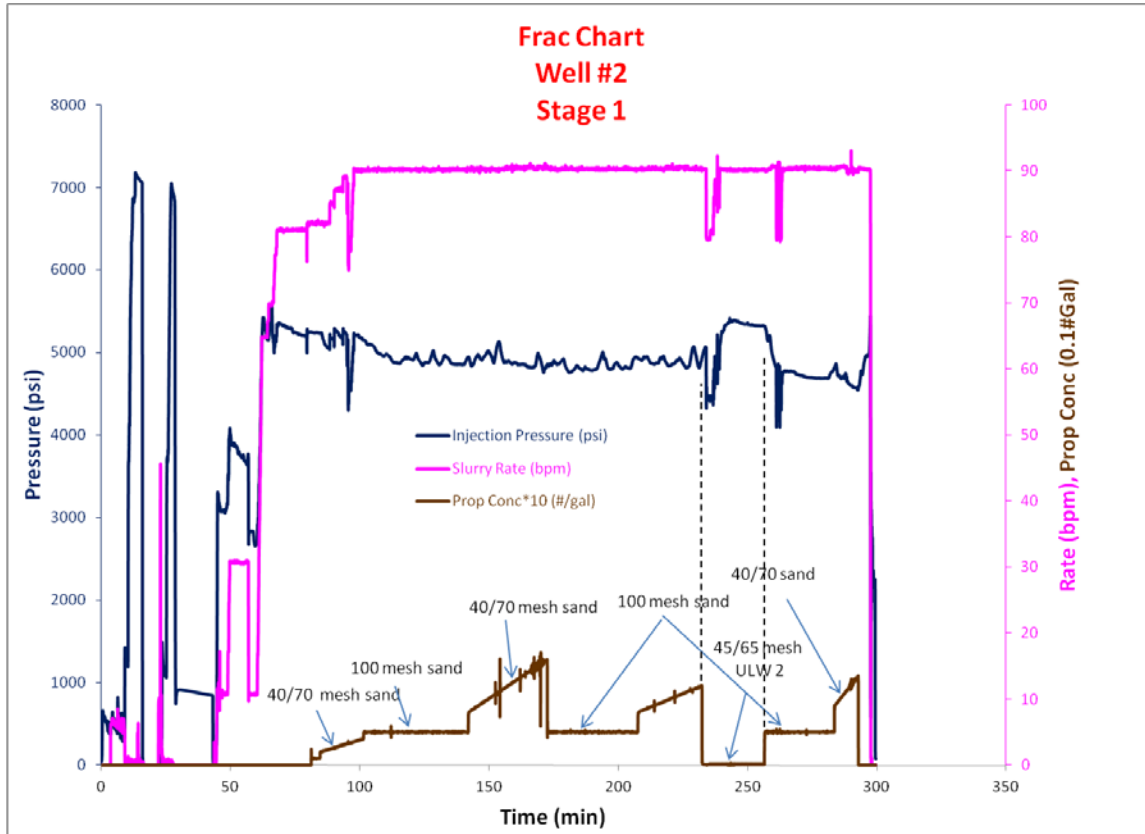
Fig. A3. Fracturing treatment chart for stage 1, Well #2

As seen on this chart, the proppant pumping schedule in this well was different than in Well #1. Here, the injected proppant schedule consisted of several sequences of 40/70 and 100 mesh sand. The ULW2 Resin-Walnut proppant was pumped in a very small amount (1,260 lbs) at a concentration of 0.014 #/gal and close to the end of the treatment. Again, the intent in using the light weight proppant was to place it farther inside the formation to allow gas flow from a larger fracture surface area. The combination of higher injection rate (90 bpm) and light weight proppant will both help the proppant travel deeper inside the fracture. At the same time the lower density proppant created a lower hydrostatic head, which in turn caused an increase in surface injection pressure, as shown by dashed lines in Figure A3.

Stage 5. The graph in Figure A4 shows another example of treatment with ULW2 Resin-Walnut in the same well. The perforated interval covered 10,110 – 10,114 ft. Total of 48 perforations with diameter of 0.42 in. were shot in this interval. The injected slurry volume was 780,000 gal. The proppants used were 251,000 lbs 40/70 mesh sand, 170,000 lbs 100 mesh sand, and 1,120 lbs 45/65 ULW2 Resin-Walnut. The concentration of ULW2 Resin-Walnut was 0.014 #/gal.
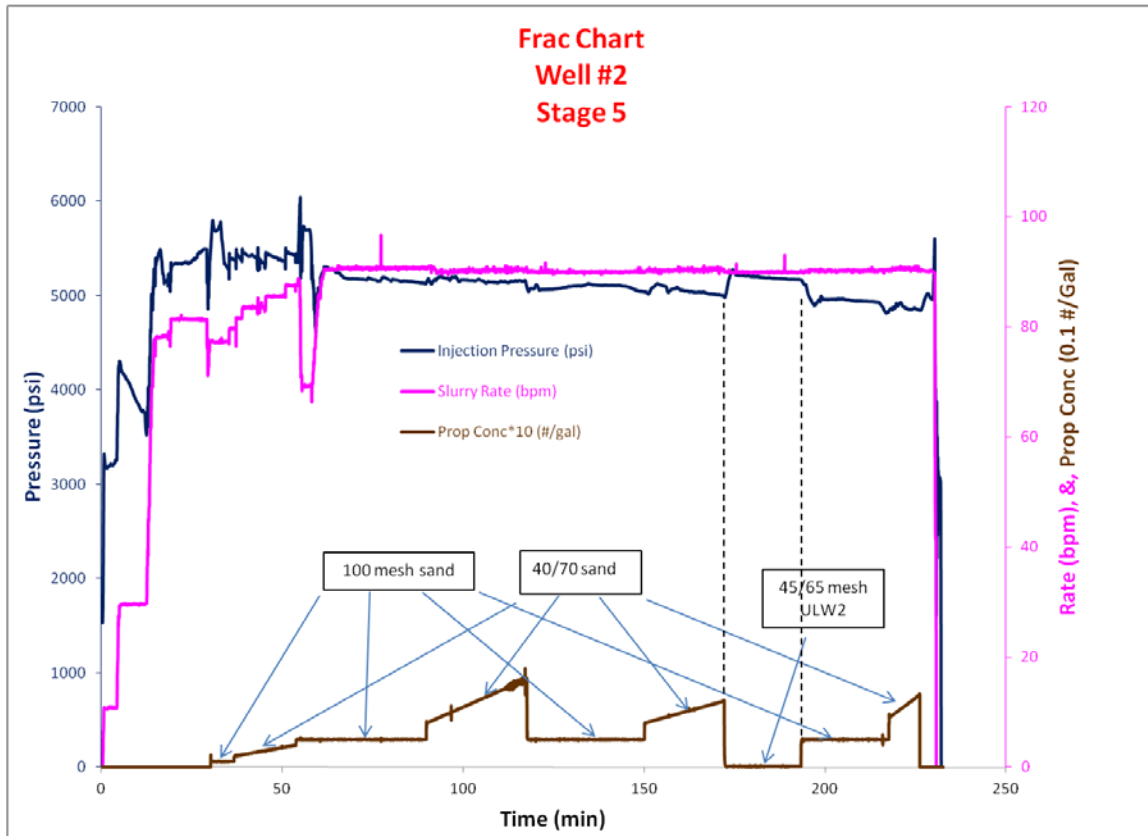
Fig. A4. Fracturing treatment chart for stage 5 fracture in Well #2

Again, the increase in surface pressure while pumping the light weight proppant was due to lower hydrostatic head.

Well #3

This well was also drilled in the Barnett shale. Its vertical depth was 7,200 ft and drilled to a depth of 10,940 ft. It was completed with cemented 5½ in. casing. The fracturing treatments were pumped through the casing. The well was fractured in 8 stages. The details of two stages of these will be discussed here.

Stage 1. The fractured interval during this stage was 10,600 – 10,804 ft. There were 50 perforations in this interval with a diameter of 0.57 in. The total slurry volume pumped in this stage was 450,000 gal. In addition 5000 gal of 15% HCl was also pumped into this well at the start of injection.

The proppant schedule in this stage consisted of 7,500 lbs 100 mesh sand pumped at a concentration of 0.25#/gal followed by 7,000 lbs 30/80 mesh ULW1 Polymer at a concentration of 0.02 #/gal. The treatment chart for this stage is presented in Figure A5, below.
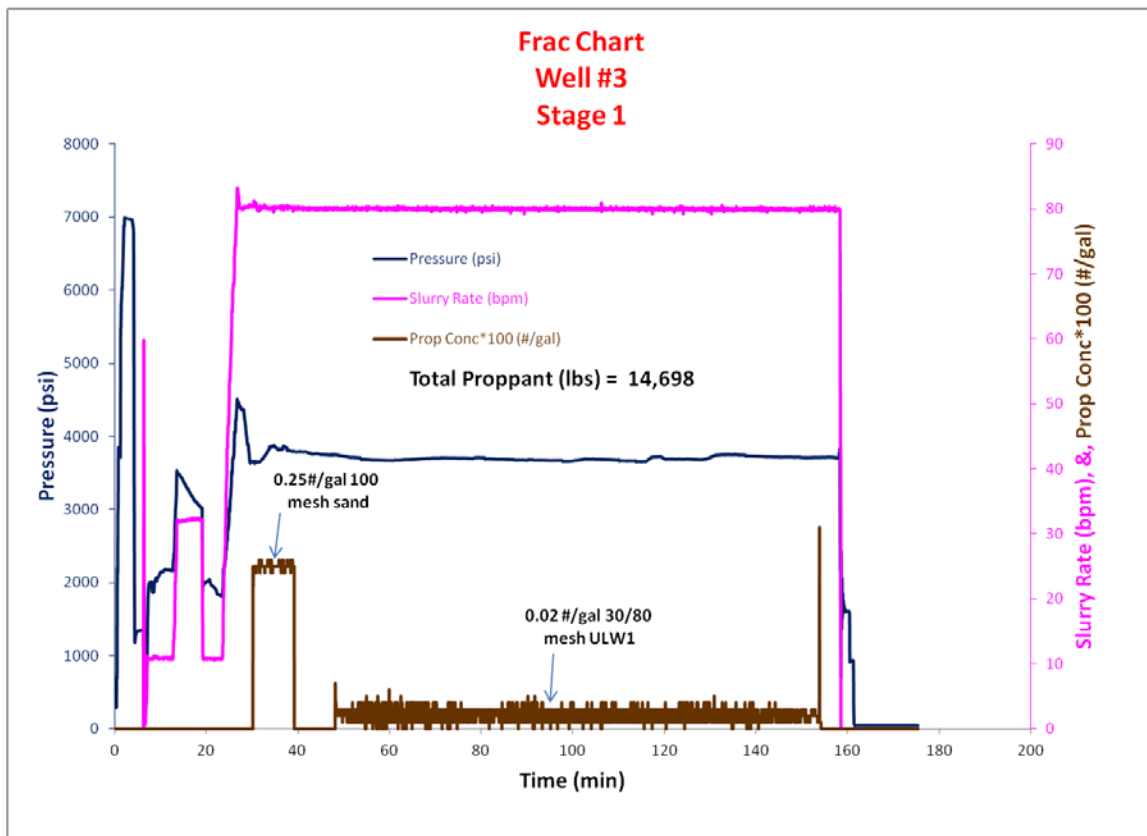
Fig. A5. Fracturing treatment chart for Well #3, stage 1

This well has a very different proppant pumping plan than the previous two wells. Here, the light weight proppant is the main means of creating fracture conductivity. It was pumped at very low concentration (0.02 #/gal) for around 100 minutes of pumping. The design philosophy in this well was to spread a "partial mono-layer" proppant throughout the fracture. In this system the role of proppant is to keep the fracture open and allow the proppant to flow around it through the thin open fracture. Even though the open fracture width will be very small, since the flowing fluid is gas (with very low viscosity) and flow rate is small, the open fracture will have sufficient conductivity to transmit the gas.

Stage 8. The data for stage 8 of the fractures in this well is shown in Figure A6. The perforated interval was 354 ft (7,650 – 8,004 ft). The number of perforations was 50 and their diameter was 0.57 in. The total slurry volume was 462,000 gal. Hydrochloric acid (HCl) at a concentration of 15% was injected during the early pumping. The injected proppant consisted of 7, 500 lbs 100 mesh sand plus 7,000 lbs 30/80 ULW1 Polymer proppant.
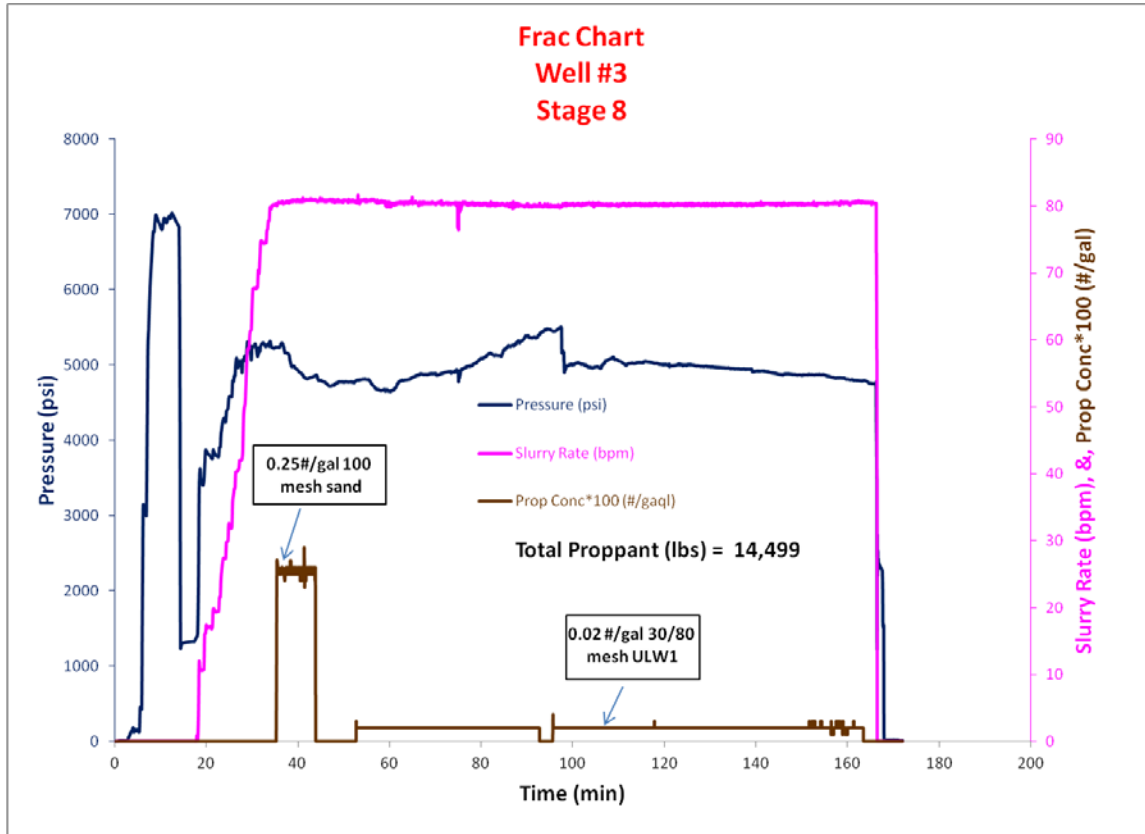
Fig. A6. Fracturing treatment chart for Well #3, stage 10

Once again, the fracturing philosophy in this well was to place the proppant in a partial mono-layer along the fracture face.

Well #4

This well was also drilled in the Barnett shale. Its vertical depth was 7,421 ft and total depth was 10,701 ft. It was completed with a cemented 5½ in. casing. It was fractured in eight stages.

Stage 1. The treatment in this stage consisted of pumping 1,010,000 gal of fluid containing 310,000 lbs 40/70 mesh sand, 230,000 lbs 100 mesh sand, and 1,540 lbs of 30/80 mesh ULW1 Polymer proppant. The perforated interval covered 4 ft (10,630 – 10,634). The 48 perforations

shot in this interval had a diameter of 0.42 in. The treatment chart for this stage is presented in Figure A7 below.

The design philosophy in this well was to use sand for near wellbore fracture conductivity and light weight proppant for points deep inside the fracture. One of the reasons for using high injection rate is to carry sand by high fluid velocity inside the fracture. The concentration of ULW1 Polymer proppant was 0.014 #/gal. As the graph shows, because of the lower density of light weight proppant which creates lower hydrostatic head the surface injection pressure increased when this proppant was injected into the well.
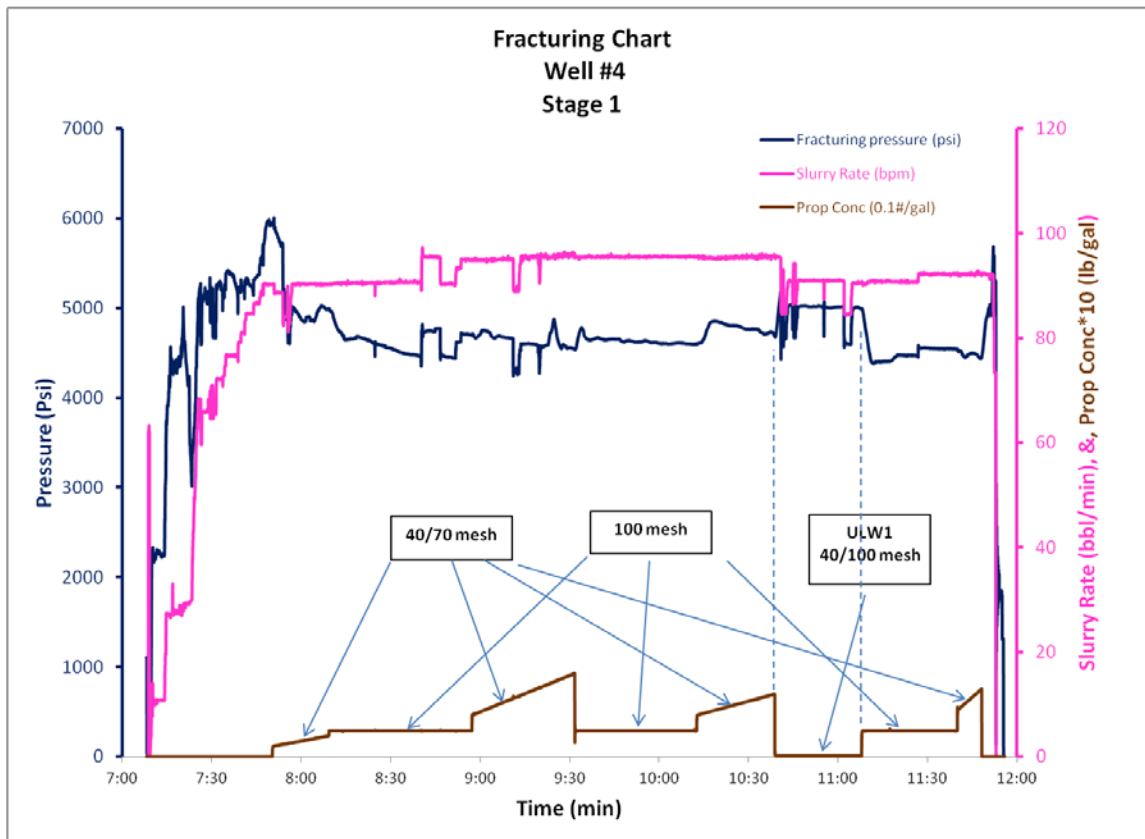
Fig. A7. Fracturing treatment chart for Well #4, stage 1

Stage 8. The treatment chart for the last stage of fracturing in this well is presented in Figure A8. The perforated interval was 7,830 – 7,834 ft. Total number of perforations in this interval was 48 and they had a diameter of 0.42 in. Injected slurry fluid volume was 988,000 gal. The proppant consisted of 310,000 lbs 40/70 mesh sand, 220,000 lbs 100 mesh sand, and 1,540 lbs ULW1 Polymer proppant which was mixed at a concentration of 0.014 #/gal. Treatment chart for this stage is presented in Figure A8.

The reduction in surface pressure while pumping the light weight proppant is not seen in this chart. The reason is that other variables were creating larger pressure variations than created by change in hydrostatic head. This treatment also appears to have been on the verge of screen-out at the end of pumping. This is unlikely to have been caused by the use of light weight proppant.
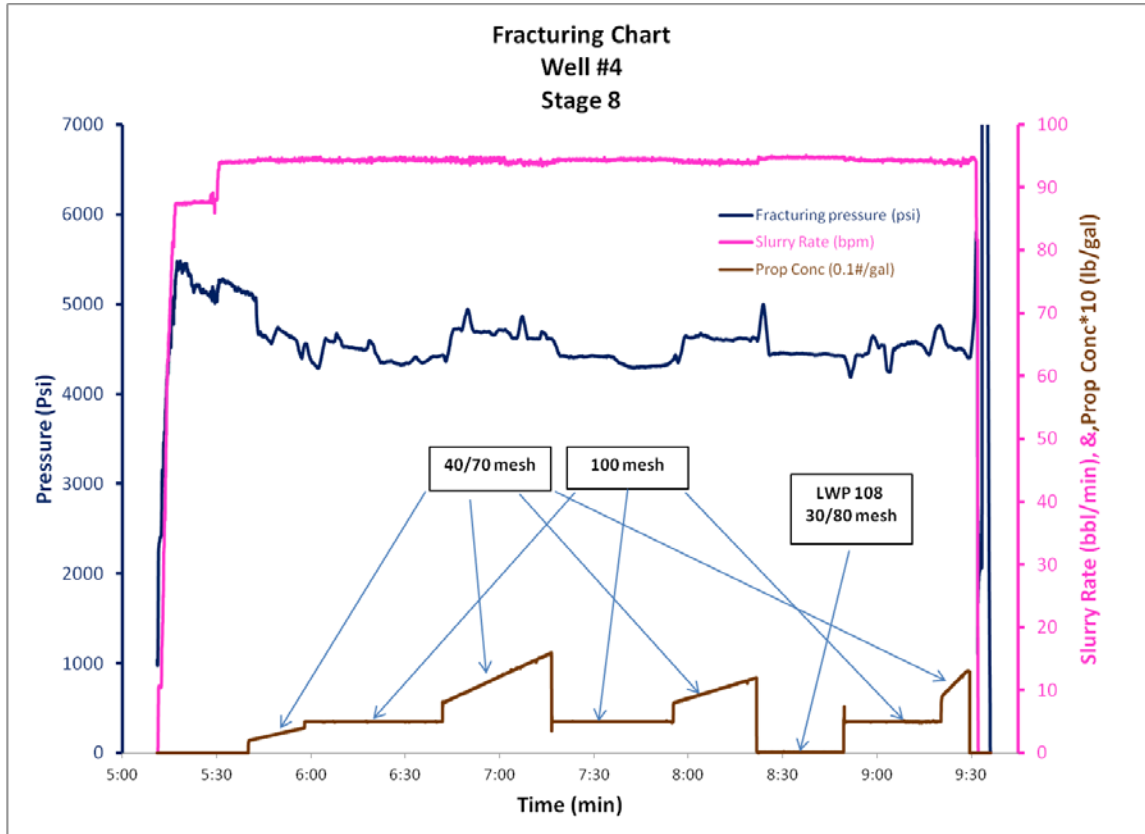
Fig. A8. Fracturing treatment chart for Well #4, stage 8

General Observations

As these examples show, no specific design philosophy and procedure has yet emerged regarding the most effective way of using these proppants. One of the limiting factors in this regard has been the high cost of the light weight proppants (compared with other types). One of the concerns with the use of light weight proppant had been its flowback after the treatment. The fear was that the fluid returning after the fracturing treatment can easily flow the proppant back. This has not generally been observed in actual field cases.

Proppant metering. The common method of adding proppant is to mix it in the blender with water and other fracturing additives. In this case the proppant is fed into the blender through a feed screw. Changing the speed of the feed screw allows controlling the weight of added

proppant. Proppant concentration is computed by measuring the flowing fluid density with a densitometer along the flow path. Knowing the density of the fluid and proppant, one can easily compute the concentration of the proppant in the slurry. Because of their low density and very low concentrations one can not use this technique with light weight proppants. The concentration is usually regulated during the mixing process. In some cases the proppant is blended similar to a dry additive. The concentration is adjusted by setting the rpm of the feed screw into the blender. The signal from the feed screw is used for data display and reporting. In some other applications, such as in foam fracturing treatments where proppant can not be added to the blender, it is mixed in a slurry (for example with a surfactant) and added to the system similar to any other additive.

Production Results

Using the standard industry practice, the production results of wells fractured with low density proppant have been compared with adjacent offset wells in all of the examples cited above. Unfortunately the results have been inconclusive. The production differences between comparison wells have generally been within normal ranges.